5G Channel Model for bands up to 100 GHz

Annex A: Summary of channel sounding, simulations and measurement data

(March 2016)

Contributors:

Aalto University	**Nokia**
AT&T	**NTT DOCOMO**
BUPT	**New York University**
CMCC	**Qualcomm**
Ericsson	**Samsung**
Huawei	**University of Bristol**
INTEL	**University of Southern California**
KT Corporation	

Contents

# Annex A: Summary of channel sounding, simulations and measured data

Annex A summarizes channel sounding and simulation campaigns performed by the partners.

A.1   Urban microcellular scenarios – street canyon

A.1.1 Aalto University

A.1.1.1   Channel sounder

The channel sounder is based on a vector network analyzer (VNA) with a range extension option using RF-over-fiber solution as shown in Fig. A1.1.1-1. The sounder is capable of measuring 15, 30 and 60 GHz bands by changing the up- and down-converters at the transmit and receive sides. In indoor scenarios, each band covers 14-16, 27-29, and 61-65 GHz RF for the measurements, while the first two bands are reduced to 14-14.9 and 27-27.9 GHz in outdoor scenarios due to the radio license. The RF signal is produced by mixing the signals from the VNA and the local oscillator. The transmit power fed to the antenna port is 17 dBm in the 15 and 60-GHz bands and 2 dBm in the 28-GHz band. On the receive side of the channel sounder, an electromechanical rotator was installed to rotate horn antennas for directional channel sounding. The rotator works in synchronization with the VNA for data acquisition. Two different horn antennas are used for vertical and horizontal polarization measurements; both have 19 dBi gain with the half-gain beamwidth of 10o in azimuth and 40o in elevation. In a channel sounding of a single link, the directional scanning is performed twice with the horn antennas having different polarizations. The transmit antenna is an omni-directional biconical antenna with maximum 2 dBi gain. The VNA sweeps over the frequency band of interest to measure channel transfer functions. The number of frequency points in the sweep and the IF bandwidth determines the noise level of the sounder. They are set to 10001 points and 40 kHz, respectively. A back-to-back calibration measurement that connects the transmit and receive sides through a 20-dB attenuator is always performed before and after the channel sounding to obtain channel transfer functions of the sounder.
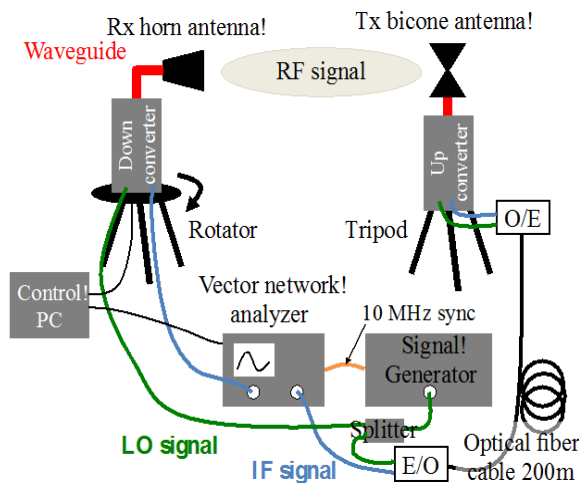
Figure A1.1.1-1: Aalto's channel sounder architecture.

A.1.1.2   Channel sounding

The channel sounding was performed in a campus area of the Aalto University School of Electrical Engineering, Espoo, Finland. As described in Fig. A1.1.2-1, the measurement was performed between two 200-m long buildings. The buildings have three floors and are 25 m high. The receive antenna was fixed at one side of the street, while the transmit antenna was placed at 11 locations. Four of the transmit antenna locations were behind a building at the end of the street canyon and hence non-line-of-sight channels, while the other 7

channels had line-of-sight. The longest separation distance between the transmit and receive antennas was about 124 m. Both the transmit and receive antennas were set at 2.77 m above the ground. The directional horn antenna at the receive side was rotated over azimuth angles with 5 deg azimuth steps towards horizontal directions to measure power azimuth angular spectra. The measurements were performed at 15, 28 and 60 GHz in July, June and November 2015, respectively. The measurement site has obvious differences for the three frequencies due to moving objects such as cars. There were trees at the end of the street canyon, whose amount of leaves differs for the summer and winter seasons. However, the effects of vegetation were expected to be insignificant because of the low antenna height.

(a) Photo of the sounding site.
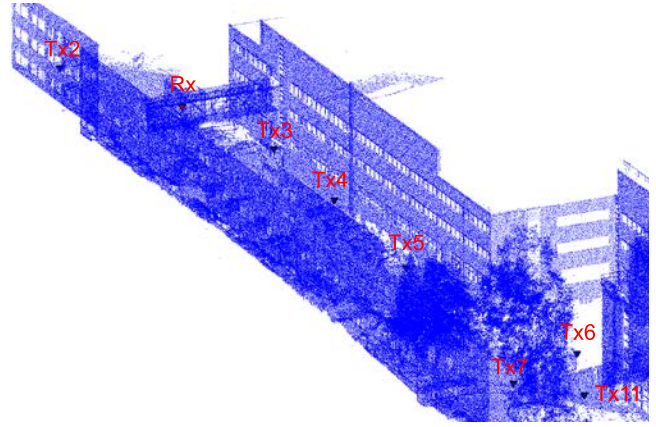
(b) Point cloud environmental description of the sounding site.

Figure A1.1.2-1: Aalto's channel sounding in a street canyon.

A.1.1.3   Channel simulations

A ray-based channel simulation tool calibrated by the measurements is used to acquire more channel data for parameterization of channel models. We use a point cloud, which is obtained from a laser scanning of a physical environment where the channel sounding takes place, for this purpose. The point cloud offers detailed description of the environment with a typical accuracy of 5 cm, which is crucial in high frequency channel simulations. The recorded point cloud of the street canyon is illustrated in Figure A1.1.2-1. The prediction method simulates a specular reflection from the points 0 and uses a single-lobe directive scattering model [DEFV+07] to calculate the diffuse backscattering from each point. We assume that the field consists of a line-of-sight (LOS) path along with single- and double-bounce reflections and scattering from the points [JaHa14]. The effect of shadowing caused by blocking objects in the environment such as walls, furniture and human body is modeled properly by searching for points that fall into the first Fresnel zone for each path; if points are found, additional attenuation of 30 dB is added to the path. The reflection and scattering losses are optimized so that the simulated channel resembles the measured power delay and angular-delay profiles. With the optimized channel simulation tool, it is possible to have channel responses when the antennas are in the area where the channel sounding is performed.

A.1.1.4   Findings and observations

A.1.1.4.1 Frequency dependence of specular peaks and pathloss is marginal at 15, 28 and 60 GHz line-of-sight channels other than the Friis' free space loss.

Figure A1.1.4.1-1(a) shows power delay profiles of 15, 28 and 60 GHz omni-directional line-of-sight channels measured at the same transmit and receive antenna locations. Despite significant difference of the noise floor due to the difference in RF components of the sounder and measurement bandwidth in the different bands, it is

possible to see from the figure that strong specular components represented by peaks appear at the same delays. Furthermore, the diffuse scattering, which appears as exponential decay of the power as delay goes longer, is present at all frequencies. Only the difference is their relative power levels attributed to smaller antenna gains, as the frequency is higher. Figure A1.1.4.1-1(b) shows omni-directional pathloss [HNJP16], showing that the pathloss of line-of-sight channels is mostly close to the free space loss. The pathloss of non-line-of-sight channels have 10 to 25 dB excess loss compared to the free space loss. The higher frequency tends to show greater excess loss.
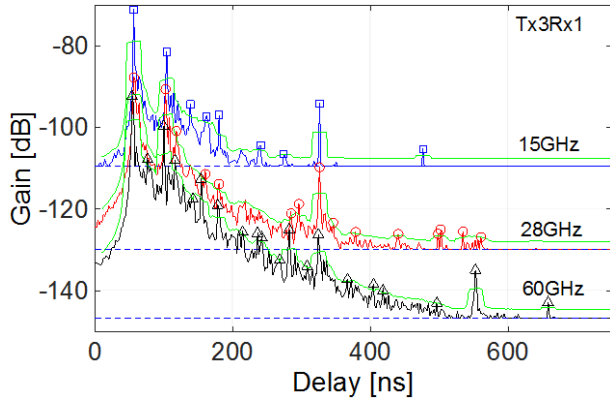
(a) Power delay profiles.
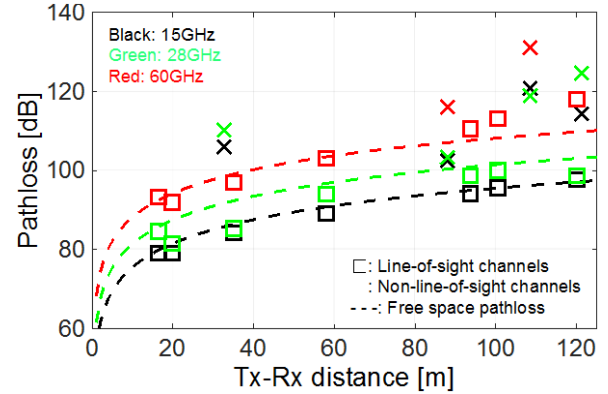
(b) Omni-directional pathloss.

Figure A1.1.4.1-1: Comparison of 15, 28 and 60 GHz channels in a campus street canyon scenario.

A.1.2 China Mobile (CMCC) & Beijing University of Posts and Telecommunications (BUPT)

A.1.2.1   Channel sounder

The channel sounder PropSound CS is developed by Elektrobit of Finland. PropSound CS is working based on the pseudo-noise sequence sliding correlating principal and supports MIMO channel sounding by Time Domain Multiplexing (TDM) with high speed electrical switching. The sounder is capable of measuring 2.35/3.5/4.9/6/8GHz bands with a maximum bandwidth of 200MHz. In our measurement campaign, the center frequency to 3.5GHz and 6GHz with 100 MHz bandwidth.

The specifications of antenna arrays and the system parameter during this measurement are showed in Fig. A1.2.1-1, Fig. A1.2.1-2 and Table A1.2.1-1.

Figure A1.2.1-1. Omni-directional antenna array (ODA) at left (receiver), Uniform planar antenna array (UPA) at right (transmitter)

Table A1.2.1-1: The specifications of antenna arrays and system configuration

Parameter		value	
Antenna type		ODA	UPA
Center frequency		3.5/6 GHz	3.5/6 GHz
Antenna ports number		56	32
Antenna elements number		28 dual polarized	16 dual polarized
Antenna elements distribution		Cylinder	Planar
Gain		6 dBi typical	6 dBi typical
Polarization		+/- 45 deg	+/- 45 deg
Front to back ratio		N/A	30 dB typical
Spacing		0.5 wavelength	0.5 wavelength
Angle range	Azimuth	-180°~ 180°	-70°~ 70°
	Elevation	-55° ~ 90°	-70°~ 70°
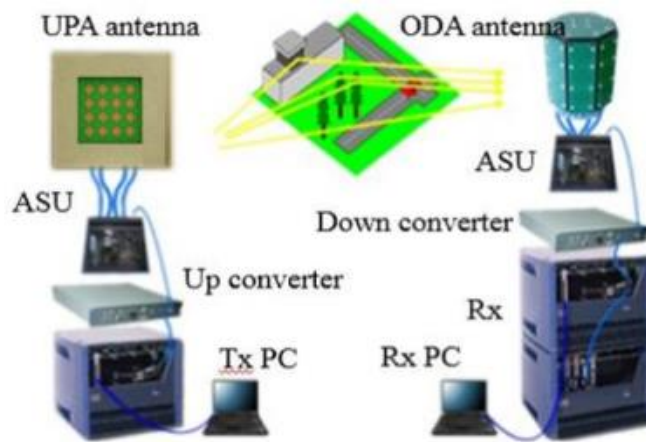
Figure A1.2.1-2: CMCC's channel sounder architecture.

A.1.2.2   Channel sounding

The channel sounding was performed in a campus area of Beijing University of Posts and Telecommunications, which is a typical UMi scenario. The base station (as the transmitter) was set up on the top of a 3-floor office building. The base station antenna height is 13m. Surrounding buildings were relatively much higher than the base station. Moderate traffic and people were on the surrounding main roads. The measurement routes were mainly planned on the roads around, as showed in Fig. 2.1.2-1. Some of the routes are LoS, while others are NLoS. The receiver was placed on the trolley of 1.7m height. The trolley was moved at pedestrian speed about 3km/h. Fig. 2.1.2-1 is a top view of the measurement scenario. Table A1.2.2-1 shows the parameters of measurement.
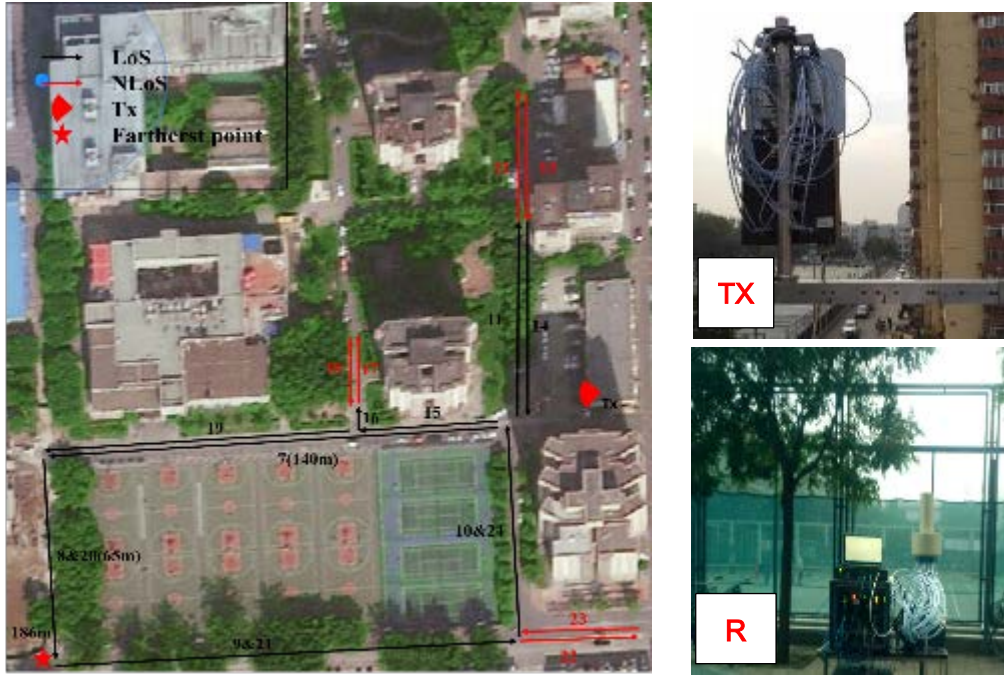
Figure A1.2.2-1: UMi Measurement scenario.

Table A1.2.2-1: Parameters of measurement.

Item	Value
Tx height	14.4 m
Rx height	1.8 m
Length of PN sequence	127
Time of one chip	10 ns
Time of one cycle	2.32 ms
Transmitting power (fed to the Tx)	23 dBm

A.1.2.3   Findings and observations

A.1.2.3.1 EoA and EoD follows the Laplacian distribution in LoS and NLoS at 3.5 GHz and 6 GHz

Fig. A1.2.3.1-1shows the EoD and EoA distribution in UMa LoS and NLoS from field channel measurement results. Laplace distribution is considered for elevation angle distribution. In Figure A1.2.3.1-1, the mean value of EoD/EoA is normalized to 0. Laplacian distribution is used to model EoD and EoA.
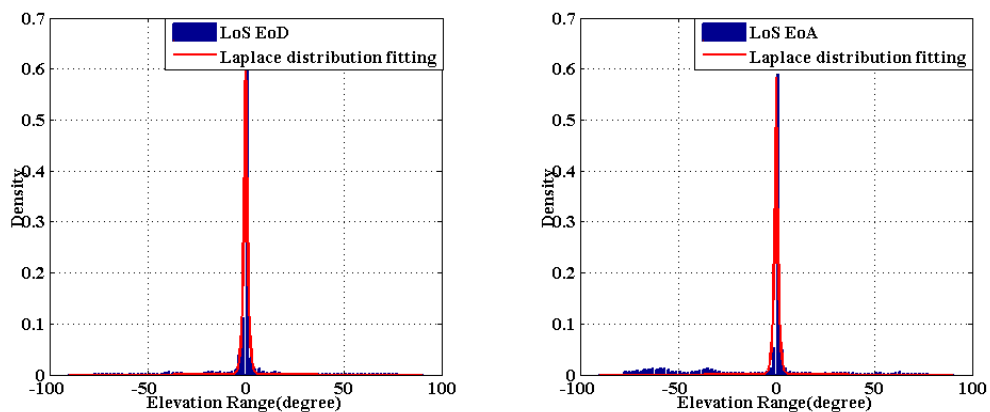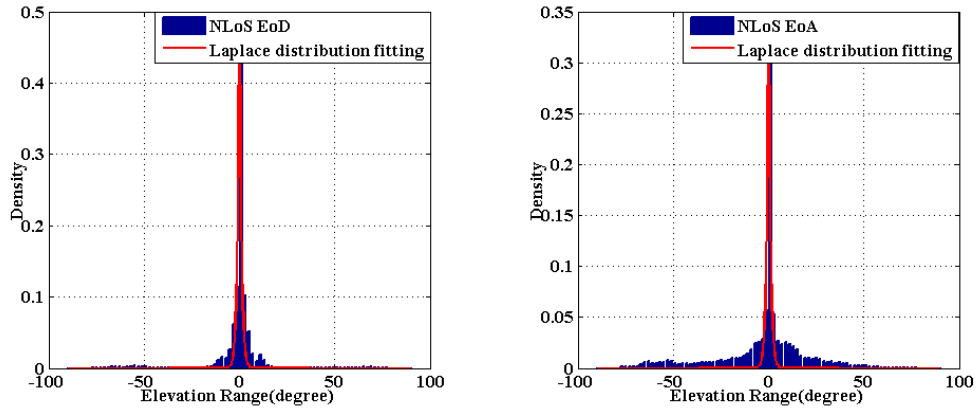
Figure A1.2.3.1-1 The EoD and EoA distribution in UMi LoS and NLoS

The Laplace distribution fits the EoD and EoA well. The multi-path energy concentrates on a specified angel in the LoS situation, while is dispersed over different angles in the NLoS situation.

A.1.2.3.2 ESA, ESD, ASA, and ASD follow the log-normal distribution. Angular spread in 6 GHz is smaller than that in 3.5 GHz in LoS.

Table. A1.2.3.2-1shows the ESD, ESA, ASD and ASA (RMS azimuth angle spread of arrival) distribution in UMa LoS and NLoS from field channel measurement results. A larger angle dispersion can be observed for 6 GHz compared with 3.5 GHz.

Table A1.2.3.2-1: ESD, ESA, ASA and ASD in UMi LoS/NLoS

Frequency		3.5GHz		6 GHz	
Situation		LoS	NLoS	LoS	NLoS
ESD[*]	μ	1.14	1.26	1.28	1.23
log10 ([degree])	σ	0.50	0.59	0.29	0.44
ESA[*]	μ	0.6	0.88	1.38	1.36
log10 ([degree])	σ	0.16	0.16	0.13	0.21
ASD[*]	μ	1.2	1.41	1.4	1.46
log10 ([degree])	σ	0.43	0.17	0.25	0.27
ASA[*]	μ	1.75	1.84	1.71	1.78
log10 ([degree])	σ	0.19	0.15	0.12	0.15

[*] The values of ESA, ASD and ASA in 3.5GHz are referred to 3GPP TR 36.873. The values of ESD are refer to 3GPP TSG-RAN WG1 #74 R1-133525.

Table A1.2.3.3-1: Cross-correlation with other LS parameters in UMi LOS/NLOS

Frequency	3.5GHz		6 GHz	
Situation	LoS	NLoS	LoS	NLoS
ASD VS DS	0.5	0	0.07	-0.17
ASA VS DS	0.8	0.4	-0.17	0.31
ASD VS ASA	0.4	0	0.29	0.42
ASD VS K	-0.2	N/A	-0.27	N/A
ASA VS K	-0.3	N/A	-0.29	N/A
DS VS K	-0.7	N/A	-0.25	N/A
ESD VS K	0	N/A	-0.26	N/A
ESA VS K	0	N/A	-0.3	N/A
ESD VS DS	0	-0.5	-0.26	0.12
ESA VS DS	0.2	0	-0.06	0
ESD VS ASD	0.5	0.5	0.72	0.73
ESA VS ASD	0.3	0.5	0.2	0.42
ESD VS ASA	0	0	-0.38	0.41
ESA VS ASA	0	0.2	0.57	0.40
ESD VS ESA	0	0	0.21	0.75

A.1.3 Ericsson

A.1.3.1   Real-time MIMO channel sounding at 15 GHz

A.1.3.1.1 Measurement equipment

In this scenario, basic propagation properties at 15 GHz are assessed through radio channel measurements using a 5G radio access prototype; the prototype consisting of two terminal platforms (TPs) and one mobile terminal. TPs are installed on the walls of two office buildings at heights 8.5 m (TP1) and 12 m (TP2), respectively. TPs are separated with a distance of approximately 80 m; see Figure A1.3.1.1-1.

Figure A1.3.1.1-1: Ericsson 'Urban microcellular scenario – Open square.

For open square outdoor measurements, terminal's antenna is installed on top of a van at a height 2.9 m; see Figure A1.3.1.1-2(a); for outdoor blocking measurements, terminal is carried on an electrical scooter with a typical antenna height of 1.5 m; see Figure A1.3.1.1-2(b).

(a) Mobile antenna location (van).   (b) Mobile antenna location (scooter),

Figure A1.3.1.1-2: Ericsson 'Urban microcellular scenario – test mobile antenna location.

Total transmit power from each TP over the 200 MHz bandwidth is 1 W. Each antenna element at the TPs has a maximum gain of 15 dBi, azimuth half power beam width (HPBW) of 90°, and elevation HPBW of 8.6°. Mobile terminal antenna element is roughly omni-directional with -3 dBi gain and 4 dB feeder loss.

The radio interface is OFDM with a subcarrier spacing of 75 kHz, a symbol length of 13.3 µs, and a 0.94 µs cyclic prefix. Reference symbols are transmitted from the TP to facilitate phase and amplitude measurements for all 16 (4x4) MIMO transmit-receive antenna pairs between the mobile terminal and the TP. Measurement resolution is 5 ms in time (corresponding to 200 Hz sampling rate) and 1 MHz in frequency. Channel estimates for the downlink transmissions are logged in the form of both complex channel gains for the 4x4 MIMO channel and the total received signal strength on the 4 receive antennas over each 100 MHz band.

A.1.3.1.2 Measurements

Ericsson's urban microcellular measurements were conducted in an open square area in Kista, Stockholm, Sweden, surrounded mainly by 4-8 floor office buildings. Main test areas are typically located 10-65 m from corresponding antennas, and are in LoS apart from local blocking, by e.g. signs, trees and vehicles, causing smaller local areas to be in NLoS. Mobile terminal (antenna) was driven around the square and some nearby streets up to 250 m away including NLoS areas with a typical speed of 0-30 km/h. Measurements were conducted during business hours, meaning that pedestrians, cars, trucks, public transportation, etc. were present in the area.

A.1.3.1.3 Findings and observations

A.1.3.1.3.1 Outdoor coverage areas are primary in LoS and reflections to e.g. building facades considered important to achieved coverage in non-LoS areas.

Given described test system setup, we see that primary coverage areas are in LoS to any of the TPs. In the enclosed square and along adjacent streets within LoS, coverage is quite good with received signal strength above -65 dBm. In non-LOS conditions, coverage disappears as received signal strength quickly decreases towards the noise floor with the present configuration of the test system. In practice, coverage is achieved along streets in TP antenna directions and on the TP-side of a corner, see Figure A1.3.1.3.1-1.
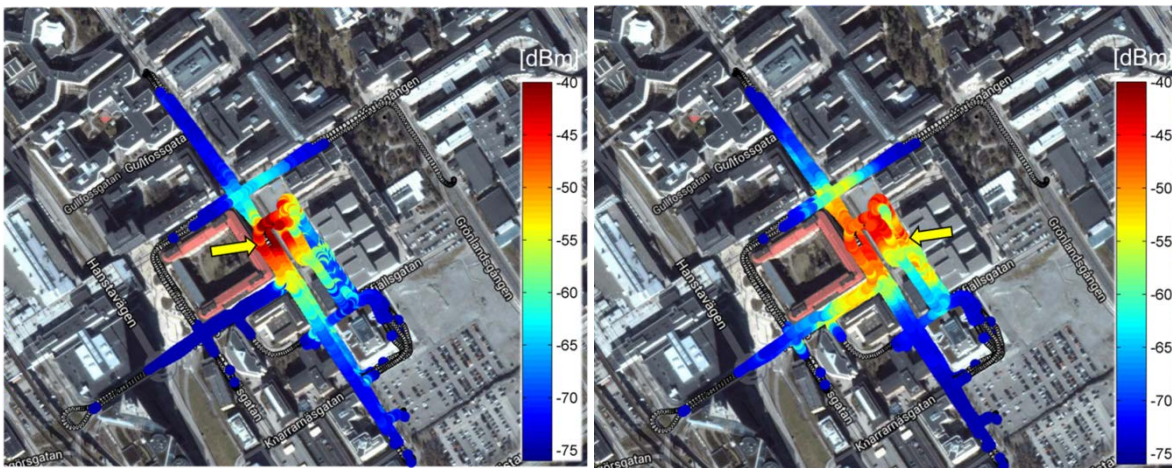
(a) Coverage area for TP 1   (b) Coverage area for TP2

Figure A1.3.1.3.1-1: Ericsson 'Urban microcellular scenario – coverage areas.

### A.1.3.1.3.2 Observed corner loss and propagation along street do not deviate significantly from what is assumed for lower frequency bands. No indications on significant LOS propagation difference at 15 GHz.

Figure A1.3.1.3.2-1 shows the LOS/NLoS transition when turning around a building corner. Observed additional loss after the corner is around 20 dB, see Figure A1.3.1.3.2-1(b); observed loss does not deviate significantly from what is assumed for lower frequency bands. The rather steep loss slope is also observed in corresponding coverage map in Figure A1.3.3.3.2-1(a).
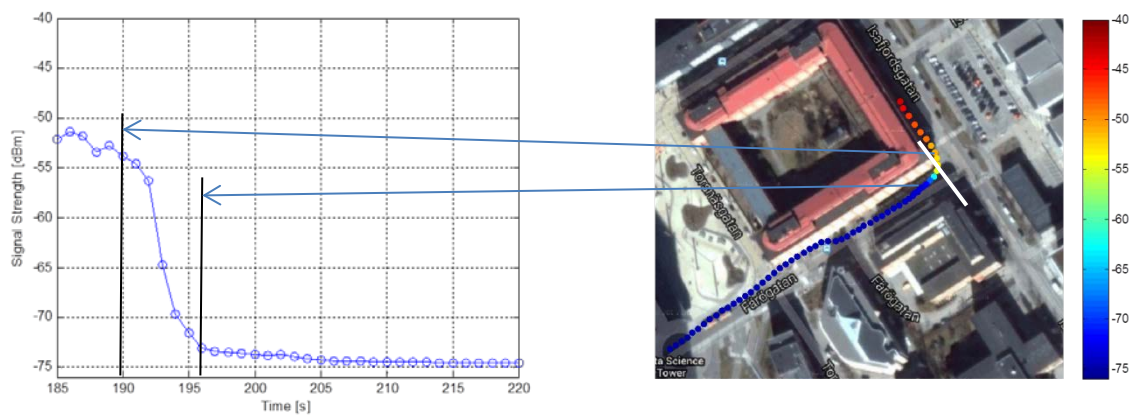
(a) Signal strength vs. position along route in time   (b) Map positioning overview

Figure A1.3.1.3.2-1: Ericsson 'Urban microcellular scenario – corner loss.

Figure A1.3.1.3.2-2(a) shows signal strength as a function of distance between mobile antenna and the transmit antenna. Blue markers correspond to all samples illustrated Figure A1.3.1.3.2-2(b). Free space propagation is indicated with the black line; excess loss compared to the free space reference is caused by the antenna pattern and by shadowing and blocking. Red markers in Figure A1.3.1.3.2-2(a) represent samples from the street right in front of the antenna and driving south-east in LoS. The red line is according to the empirical two-slope model based on measurements at 900 MHz along streets reported in [BeBL92]; used model parameters mimicking assessed street are; x_0=1 (first slope propagation constant 2), m=4 (second slope propagation constant 4) and x_L=120 (i.e. a break point at 120 m). Model parameters matching measurement data from the 15 GHz LoS street

(red markers) do not deviate from the 900 MHz parameters in [BeBL92], indicating no significant LoS propagation difference at 15 GHz.
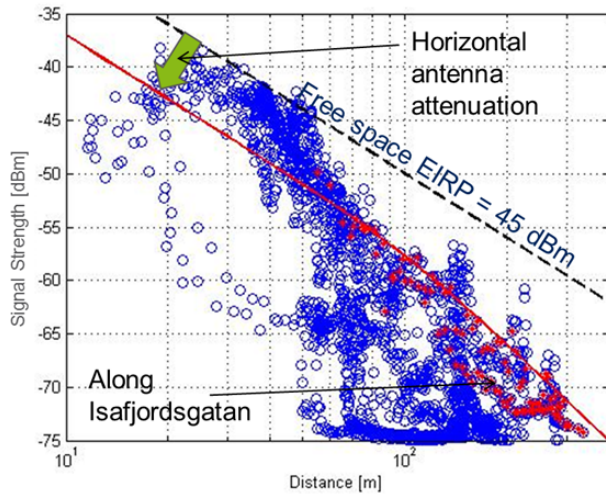
(a) Signal strength vs. distance
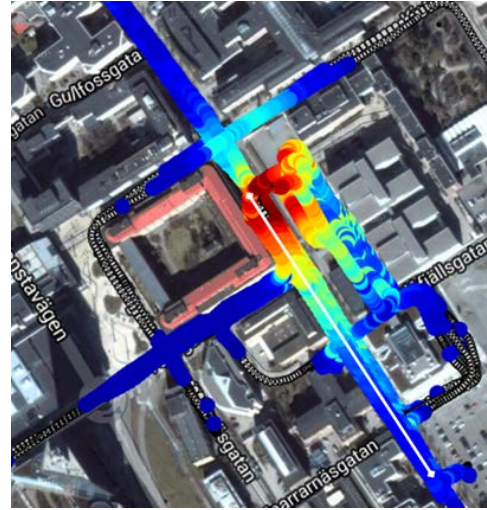
(b) Map overview, white line corresponds to safjordsgatan-samples as in figure (a)

Figure A1.3.1.3.2-2: Ericsson 'Urban microcellular scenario – corner loss.

A.1.3.1.3.3   No apparent difference of delay spread was observed at 15 GHz compared to the values in the 3GPP 3D UMi LoS.

Delay spread statistics for the outdoor area described in Figure A1.3.1.3.3-1 for the 4x4 complex channel estimates with 1 MHz and 5 ms resolution (as further described in section A.1.3.1.1) is achieved via a transformation from frequency to delay domain using windowed IFFT and averaging over all RX-Tx antenna combinations and a thresholding of 6dB over noise level and 30 dB below peak level, calculate RMS delay spread based on power density profiles with > 20 dB SNR.
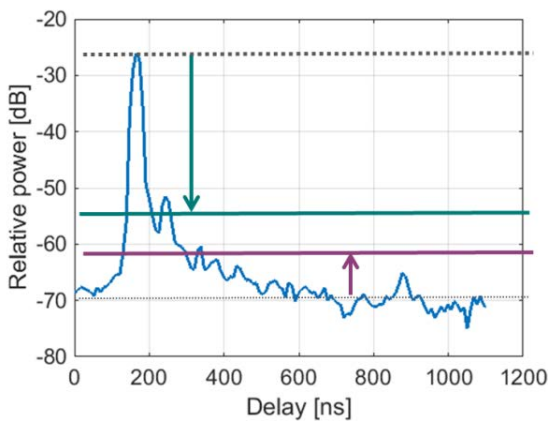
(a) Double thresholding
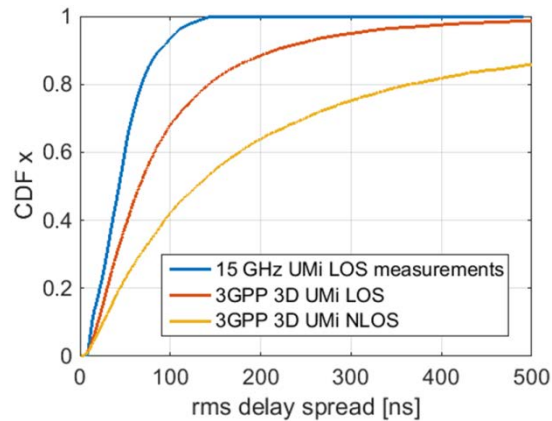
(b) RMS Delay spread for 15 GHz UMi

Figure A1.3.1.3.3-1: Ericsson 'Urban microcellular scenario – RMS delay spread.

Somewhat lower delay spread than 3GPP 3D UMi LoS is observed, which is within expected range of variability of a single measurement campaign compared to a model. Based on these results we cannot conclude that RMS delay spread reduces with increasing frequency.

A.1.3.2 Multi-frequency measurements

A.1.3.2.1 Channel sounder

The channel sounder setup is based on a vector network analyzer (VNA) from Keysight (10 MHz – 43.5 GHz). In order to allow long-range measurements, antenna remoting using an optical fiber extension of the transmit RF cable is employed as shown in Fig. A1.3.2.1-1. The measurements have been performed at 2.44, 14.8 and 58.68 GHz carrier frequencies using 80, 200, and 2000 MHz bandwidth, respectively. The VNA supports operating frequencies of up to 43.5 GHz. Hence, to achieve 58.68 GHz transmission over the air, the VNA RF signal which is swept between 2 and 4 is up-converted in the transmitter (TX) and down-converted in the receiver (RX) as shown in Fig. A1.3.2.1-2. For this purpose the local oscillator signal of frequency 15 GHz is distributed to the TX end over optical fiber. The transmit power fed to the antenna port is around 10 dBm in all the frequency bands. Two identical vertically polarized dipole antennas are used at both TX and RX; both have 2 dBi gain. The VNA sweeps over the frequency band of interest to measure channel transfer functions. The number of frequency points in the sweep and the IF bandwidth determines the noise signal to level of the measured impulse responses. The number of frequency points is set to 1601 for 2.44 and 14.8 GHz measurements and to 8001 for 58.68 GHz measurements. The IF bandwidth is set to 10 kHz in all measurements and has been reduced to 300 Hz for better noise suppression at some measurement points. A calibration measurement at short distances is always performed before and after the channel sounding to obtain reference line-of-sight (LoS) measurement. More details on the measurement setup in 60 GHz can be found in [MeAB15].
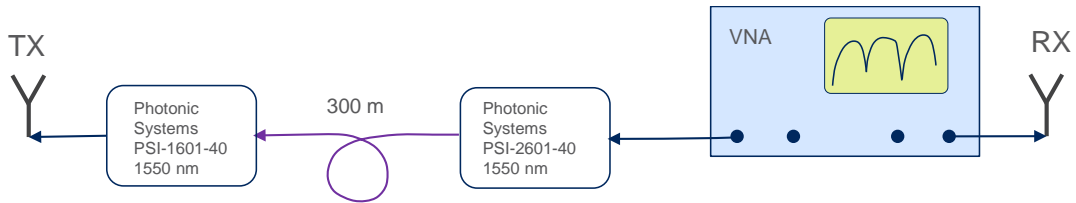
FIGURE A1.3.2.1-1: MEASUREMENT SETUP FOR 2.44 AND 14.8 GHz.
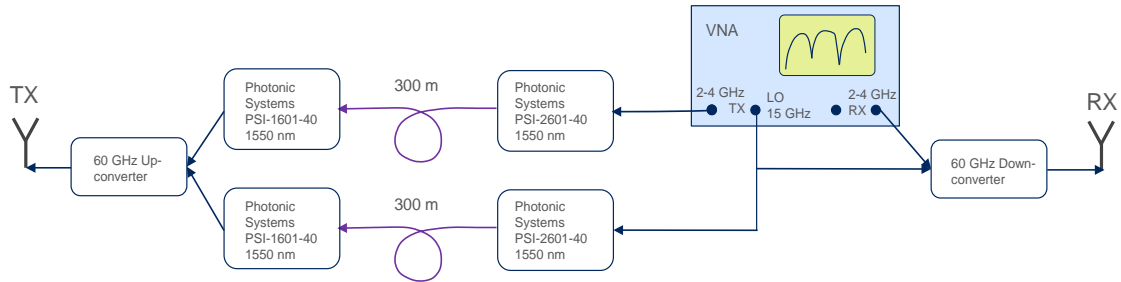
FIGURE A1.3.2.1-2: MEASUREMENT SETUP FOR 58.68 GHz.

A.1.3.2.2 Channel sounding

The channel sounding was performed around Ericsson Research building in Kista, Stockholm, Sweden, which is a suburban area with 4-6 floors office buildings. Two measurement campaigns were performed, each around one corner of the building as depicted in Fig. A1.3.2.2-1 (left). The measurement campaign along the green path is denoted as campaign 1 and the one along the red path is denoted as campaign 2. Both TX and RX antennas are installed at 1.5 m height above the ground. The building has 5 floors and is 27 m high. At each measurement campaign, the RX antenna was fixed close to one corner of the building, shown in Fig. A1.3.2.2-1 as RX1 for campaign 1 and RX2 for campaign 2, while the TX antenna was placed at 16 locations. In campaign 1, RX1 is

located on top of a bridge at a height 5 m above the street where the TX is located as shown in Fig. A1.3.2.2-1 (upper right). TX and RX2 in campaign 2 are, however, at the same street level as shown in Fig. A1.3.2.2-1 (lower right). Moreover, a few locations in each measurement campaign are in LoS with the corresponding RX, while the rest of the locations are behind the corner and hence in non-LoS (NLoS). The measurements were performed during June, July, and August 2015. There were changes in the environment for each measurement campaign due to moving and fixed objects locations such as cars passing by and parked cars. There were also a few closely-spaced trees along LoS part of the measurement route in campaign 2, while there were sparsely distributed trees along both LoS and NLoS segment of the measurement route in camping 1.

Figure A1.3.2.2-1: Measurement scenario around Ericsson Research building.

A.1.3.2.3 Findings and observations
Findings and observations are summarized in R1-160846 available at:
ftp://ftp.3gpp.org/TSG_RAN/WG1_RL1/TSGR1_84/Docs/R1-160846.zip.

A.1.4 Electronics and Telecommunications Research Institute (ETRI)
A.1.4.1   Channel sounder
To explore the spatio-temporal characteristics of a wireless channel including the path loss, ETRI developed a wideband channel sounder. This channel sounder is designed for performing a field measurement campaign and collecting measured data by transmitting and receiving signals with a 500 MHz bandwidth at carrier frequencies of 28 and 38 GHz [KwKC15]. Note that the channel sounder can be operated as a transmitter (TX) or receiver (RX) depending on the settings.
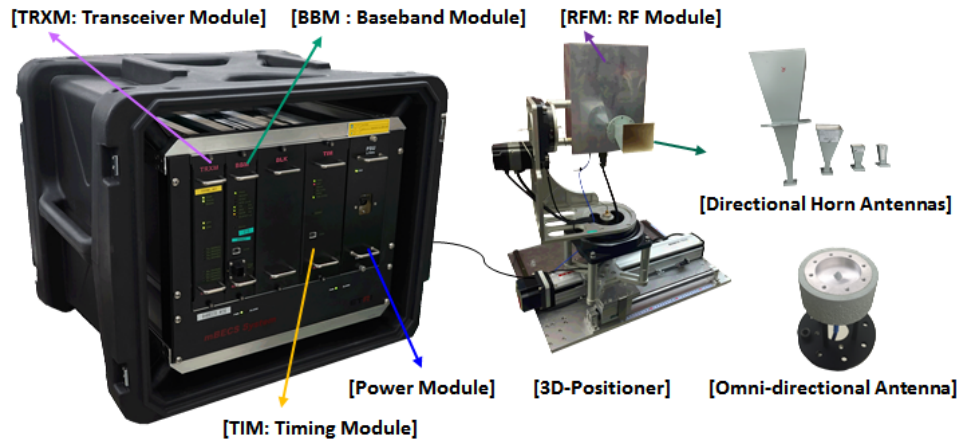
Figure A1.4.1-1: ETRI Channel Sounder.

As shown in Figure A1.4.1-1, the sounder is composed of a baseband module (BBM), a transceiver module (TRXM), a timing module (TIM), a 28-GHz or 38-GHz RF module (RFM), and antennas (directional horn antennas and an omnidirectional antenna). The 3D-Positioner includes a RFM and an antenna servo unit that generates servo signals for stepping motors to control the orientation of the horn antenna with 1° accuracy (horizontally and vertically). The rubidium oscillator of timing module provides the reference clock maintaining stable time synchronization between TX and RX. Table A1.4.1-1 describes detailed specifications of the channel sounder. The dynamic range of the sounder is sufficient to measure a path loss of up to 170 dB. The temporal resolution for multipath analysis is 2 ns. It is noted that, to remove the system impairment from measured channels, a calibration process is carried out prior to actual measurements by directly connecting between TX and RX.

Table A1.4.1-1: Specifications of ETRI channel sounder.

System parameters		Specifications
Center frequency		28 / 38 GHz
Channel Bandwidth		500 MHz
PN code length of probing signal		4095 chips
Maximum power of TX (w/o antenna)	28 GHz	29 dBm
	38 GHz	21 dBm
Automatic gain control range of RX		60 dB
Multipath resolution		2 ns
HPBW of pyramidal horn antenna and gain	28 GHz	10º(24.4 dBi), 30º(15.4 dBi), 60º(9.9 dBi)
	38 GHz	10º(24.6 dBi), 30º(16.4 dBi)), 40º(12.6 dBi)
Gain of omnidirectional antenna	28 GHz	5 dBi
	38 GHz	6 dBi

A.1.4.2   Channel sounding

The outdoor measurements were conducted in Dunsan-dong site (located in Daejeon) in Korea, which were selected to represent typical dense urban environment. It is a downtown area inhabited by 7-11 story buildings (20-35 m height) with 24-35 m wide streets between buildings.

Note that the measurement site is composed of rectangular flat street grids. Figure A.1.4.2-1 depicts a detailed measurement scenario, on which the locations of TX and RX of the sounder are marked for line-of-sight (LoS) and non-LoS (NLoS) situations. To emulate typical urban microcellular scenarios (street canyon), we installed the TX antennas at a height of 10 m and the RX antenna at 1.5 m (pedestrian level) as illustrated in Figure A.1.4.2-1.

To expand the communication range between TX and RX of the sounder, a 30º Half-Power-Beam-Width (HPBW) horn antenna is used for TX. At the RX side, an omnidirectional antenna or 10º HPBW horn antenna is used separately according to channel parameters that can be analyzed. For example, measured data from omnidirectional antenna are used to derive a path loss model. For the case of directional horn antenna, we rotated the boresight of the RX antenna in small steps to measure signals from all azimuthal directions, while keeping the TX boresight fixed with a wider HPBW antenna to cover the entire range of interest. The rotation step size was 10º in the azimuthal direction ranging from 0° to 360º. The measured data from this directional horn antenna are used to derive multi-path characteristics such as delay and angular spread. The measurement campaigns were taken during daytime and outside of normal rush hours. Furthermore, traffic was light and ran at about 30 km/h, with few people on sidewalks.
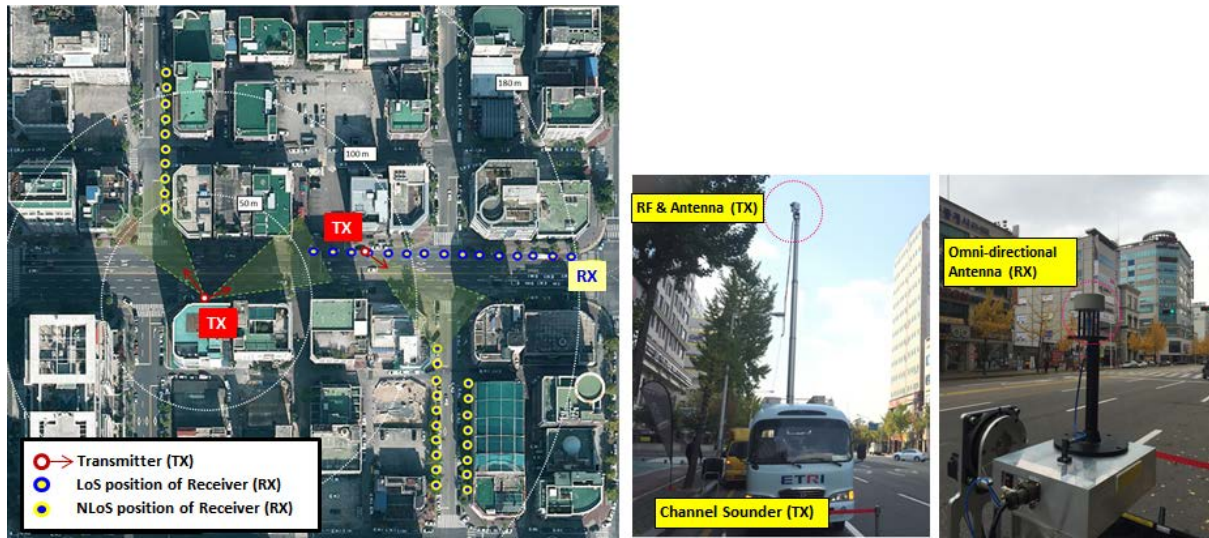
Figure A1.4.2-1: Measurement scenario (left) and campaign at Dunsan-dong site (right).

A.1.4.3   Findings and observations

A.1.4.3.1 Path loss exponent of CI model tends to be similar at 28 and 38 GHz

In order to overcome considerable path loss in the high frequency bands above 6 GHz, high-gain directional antennas have been typically used to measure propagation channel characteristics. However, synthesizing omnidirectional characteristics by scanning these directional antenna measurements may cause erroneous results due to improper selections of the antenna beam-width and the rotation step size. Thus, we use an omnidirectional antenna at the receiver side to obtain path loss characteristics by limiting distance range up to 200 m.

There are two popular path loss models: the alpha-beta-gamma (ABG) model [SRRT+16] and the close-in (CI) free space reference distance model [RMCS+15]. The below figures show scattered plots of the measured path loss data along with the CI model predictions in an Urban Micro-cell (UMi) scenario at 28 and 38 GHz in LoS and NLoS environments, respectively. The path loss exponent (PLE) of the CI model is 2.1 for both frequencies in LoS, which agree with the free space PLE of 2. In NLOS, the PLE of the CI model is 3.0 for both frequencies. Therefore, we can observe that the PLE of the CI model tends to be similar at both frequencies in LoS and NLoS environments. The standard deviation of the shadow fading differs by only a fraction of a dB in LoS. In NLoS environments, the difference is about 1.6 dB.

(a) LoS   (b) NLoS
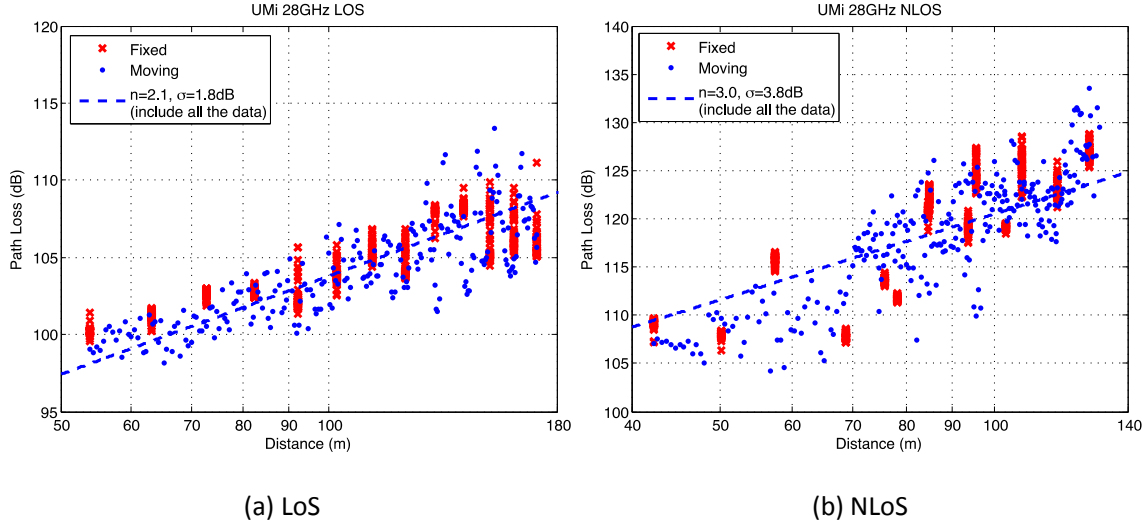
Figure A1.4.3.1-1: Measured path loss at 28 GHz in UMi scenario.

(a) LoS   (b) NLoS
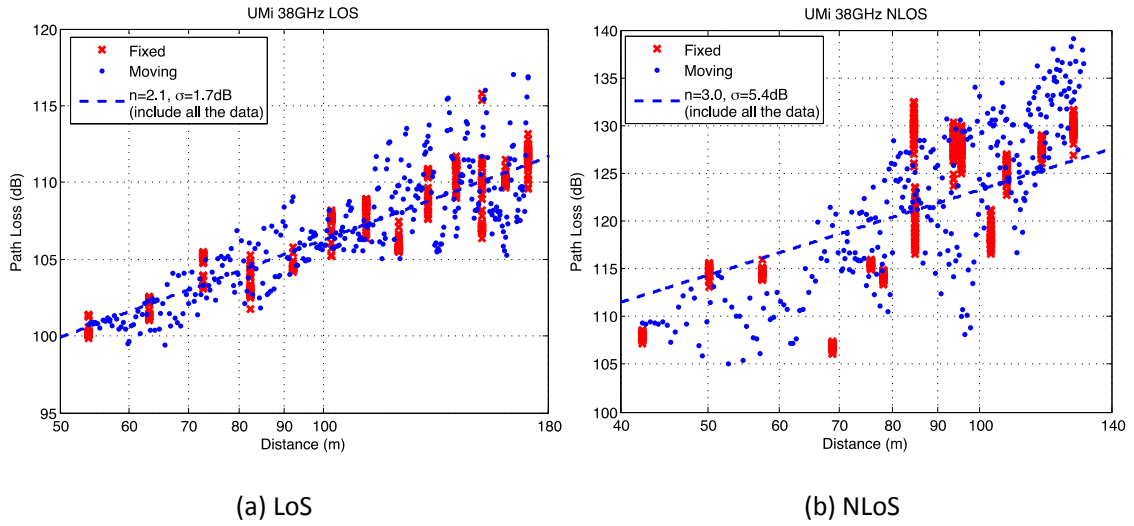
Figure A1.4.3.1-2: Measured path loss at 38 GHz in UMi scenario.

Table A1.4.3.1-1 summarizes the path loss parameters in the ABG and CI models in UMi scenario.

Table A1.4.3.1-1: Parameters in the ABG and CI path loss model in UMi scenario

Scenario	Environment	Distance [m]	Model	Frequency [GHz]	PLE/α	β [dB]	γ	σ [dB]
UMi	LoS	50-180	CI	28	2.1	-	-	1.8
				38	2.1	-	-	1.7
			ABG	28-38	1.9	40.6	1.8	1.7
	NLoS	40-140	CI	28	3.0	-	-	3.8
				38	3.0	-	-	5.4
			ABG	28-38	4.5	3.1	2.0	4.3

A.1.4.3.2 Delay and angular spread

In order to understand spatio-temporal characteristics of 28 and 38 GHz channel, high-resolution parameter estimation algorithm, Space-Alternating Generalized Expectation- maximization (SAGE) [FTHD+99, WZWG+15] was adopted to extract multipath components (MPCs) from the measurements data. For the calculation of delay

and angular spread, MPCs are cut out which power is 25 dB lower than the strongest MPC. Cumulative distribution functions of delay spread (DS) and angular spread (AS) are in the below figures and table.
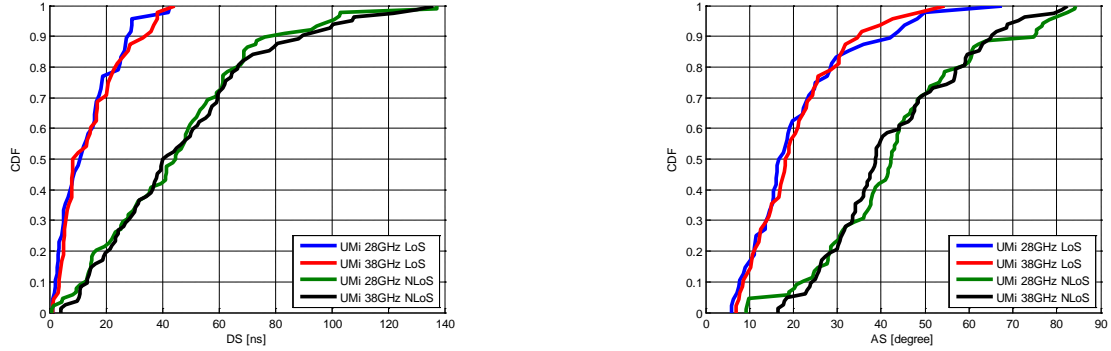
Figure A1.4.3.2-1: CDF of DS (left) and AS (right).

Table A1.4.3.2-1: Percentiles of DS and AS.

		Delay spread [nsec]		Angular spread [degree]	
		28 GHz	38 GHz	28 GHz	38 GHz
LOS	10%	2.2	3.5	7.8	8.6
	50%	10.8	8.4	16.8	18.2
	95%	29.2	37.8	47.1	41.5
NLOS	10%	12.6	13.4	22.0	24.2
	50%	44.6	40.0	42.2	38.7
	95%	99.4	106.6	77.7	71.0

A.1.4.3.3 Cluster parameters

For cluster-wise analysis, the K-PowerMeans algorithm [CCSB+06] is utilized for clustering of estimated MPCs from SAGE. Cumulative distribution functions of cluster parameters are in the below figures and table.
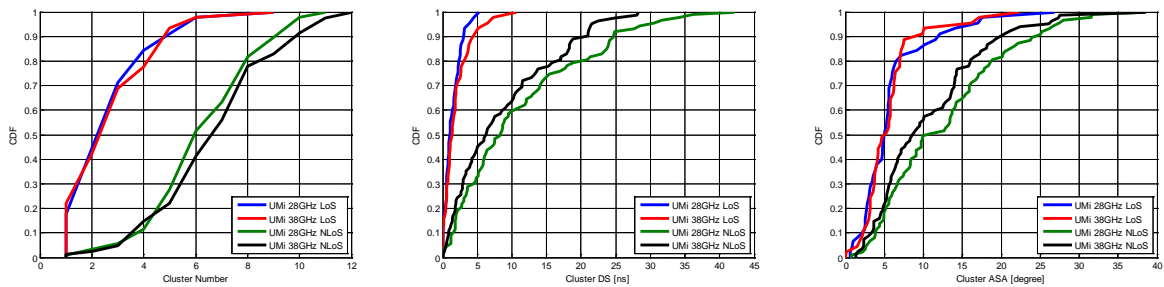
Figure A1.4.3.3-1: CDF of cluster number, DS and AS.

Table A1.4.3.3-1: Percentiles of cluster number, DS and AS

		Cluster number		Cluster DS [nsec]		Cluster AS [degree]	
		28 GHz	38 GHz	28 GHz	38 GHz	28 GHz	38 GHz
LOS	10%	1.0	1.0	0.0	0.0	2.1	2.3
	50%	2.2	2.3	1.1	1.3	5.0	5.0
	95%	5.6	5.4	3.7	6.1	16.3	14.7
NLOS	10%	3.7	3.5	1.5	0.9	3.8	3.3
	50%	5.9	6.6	8.3	6.3	10.5	8.6
	95%	9.7	10.6	29.8	21.5	27.2	25.8

A.1.4.3.4 Channel model parameters

In summary, we embraced a popular channel model framework, e.g. the existing 3GPP 3D channel model for a geometry-based stochastic channel modeling. Based on the framework, we extended the applicable frequency range of the channel model for an UMi - street canyon scenario by seeking parameters at 28 and 38 GHz as shown in the Table A1.4.3.4-1 [PLLK16].

Table A1.4.3.4-1: Channel model parameters for UMi – street canyon scenario.

Parameters		28 GHz		38 GHz	
		LOS	NLOS	LOS	NLOS
Delay spread (σ_{DS})	μ_{DS}	-8.1	-7.5	-8.0	-7.4
$\log_{10}$(seconds)	ε_{DS}	0.4	0.4	0.4	0.3
AoA spread (σ_{ASA})	μ_{ASA}	1.3	1.6	1.3	1.6
$\log_{10}$ (degrees)	ε_{ASA}	0.3	0.2	0.2	0.2
K-factor [dB]	μ_K	11	N/A	9	N/A
	ε_K	2	N/A	1	N/A
Cross-Correlations	ASA vs DS	0.6	-0.2	0.8	0.2
	ASA vs SF	0	0.1	-0.4	0.2
	DS vs SF	-0.5	-0.2	-0.2	-0.3
	ASA vs K	-0.2	N/A	0.1	N/A
	DS vs K	-0.4	N/A	-0.4	N/A
	SF vs K	-0.1	N/A	-0.2	N/A
Delay scaling factor rτ		1.3	0.9	1.2	0.9
Ave. number of cluster		3.0	6.7	3.0	7.1
Cluster DS (nsec)		1.4	11.2	2.0	8.7
Cluster ASA (degrees)		6.1	12.7	5.8	10.8

A.1.5 Huawei Technologies

A.1.5.1 Channel sounder

A dual-band ultra wideband channel sounder is designed to measure the 28G and E-band channel model. The sounder systems base on a vector network analyzer (VNA) from Rohde & Schwarz, which provides an intermediate frequency (IF) signal and sampling receive IF signal from down converter.

In our configuration, the frequency increases linearly in the measurement bandwidth with an increment of 10MHz. A local oscillator (LO) frequency is generated by an integrated frequency synthesizer of Agilent. The LO frequency is then sextupled to around 73GHz by a frequency converter for E-band. Meanwhile, the LO frequency is doubled for 28G. After that, the measurement sequence of IF signals generated by the VNA is mixed with the LO signal one by one to generate a RF signal ranging from 72GHz to 74GHz for E-band and 27GHz to 29GHz for

28G, which is then received by the Rx. When the measurements for the whole bandwidth at some posture finish, the azimuth and elevation angles or the location of Rx is changed. And the process mentioned repeats to acquire the data for other positions. Vertically polarized horn antennas with 25dBi gain and 10° half power beam width are used for E-band and 28GHz in this measurement. The dual-band UWB sounder systems are calibrated with a back-to-back measurement which connects the transmitter and receiver through 50 dB attenuator. A channel sounder system for measurement is demonstrated as figure A1.5.1-1.

Figure A1.5.1-1: Huawei channel sounder.

A.1.5.2   Channel sounding

Huawei's channel measurement result for Street Canyon scenario was implemented at TianQuan Road in Hi-tech Western District of Chengdu in China. The measurement includes more than 80 Tx-Rx positions for LOS scenario and 50 positions for NLOS scenario. The height of Tx antenna is about 6m while the Rx is setup to about 1.8m for the UMI case. The cable driven by rubidium clock helps to synchronize the Tx and Rx. The whole measurement campaign composes of a main street and three crossed streets. The locations of Tx and Rx are shown in Figure A1.5.2-1for LOS and NLOS scenarios respectively. Location of Tx is configured at end of the street to acquire a maximum length about 150m. The Tx for LOS scenario was placed in the middle of the street (marked with a blue triangle) and the positions of Rx (marked with green point) were located at the straight line by the street. In NLOS scenario, the Tx was chosen at the corner of the first crossed street (marked with a red triangle) to ensure that the LOS path was obstructed and the Rx (marked with red five-pointed stars) were placed randomly at the NLOS area.

Table A1.5.2-1: Channel Sounder System parameters.

Configuration	Street canyon	
	LOS	NLOS
Tx Height	6 m	6 m
Rx Height	1.8m	1.8m
TX Ant Gain	10dB	10dB
Rx Ant Gain	25dB	25dB
Tx Antenna	Horn Ant of 55°	Horn Ant of 55°
Rx Antenna	Horn Ant of 10°	Horn Ant of 10°
Polarization	Vertically	Vertically
Central Frequency	28G/73 GHz	28G/73 GHz
Sweep point	2001	2001

Bandwidth	2 GHz	2 GHz
Tx Locations	1	1
Rx Locations	80	50
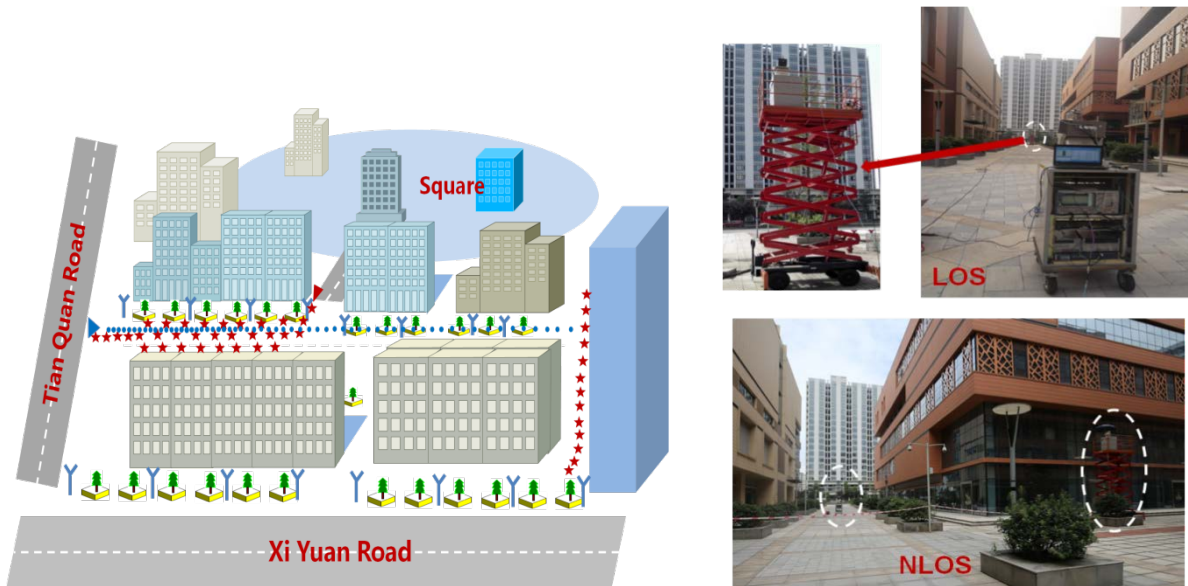
Figure A1.5.2-1: Huawei channel sounding in Street Canyon.

A.1.5.3   Findings and observations

A.1.5.3.1 Multi zone pathloss modeling

It is not quite accuracy to predict the propagation loss with all sample in a single linear fitting approach. With limited complexity increasing, such as, sector/zone grouping, the model predict accuracy can be increased significantly. 72GHz and 28GHz large-scale pathloss were measured and analyzed for Canyon scenario. Multi Zone model was investigated. At least two zones can be observed for the measured distance range. The std. deviation and the prediction error can be adopted as model evaluation criteria.
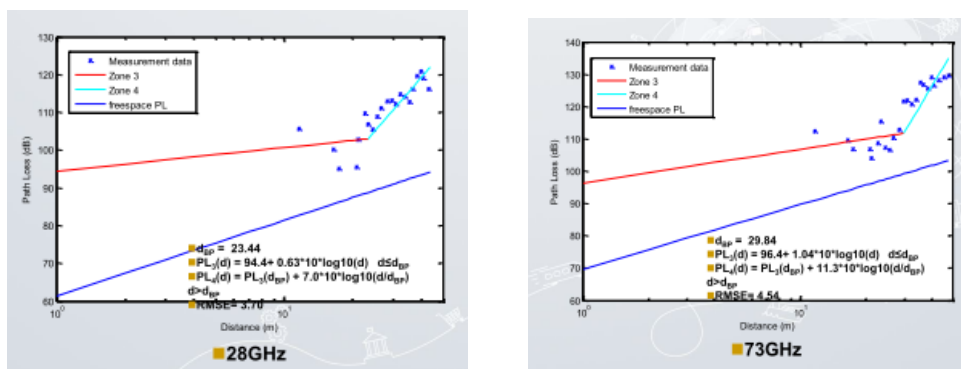
Figure A.1.5.3.1-1

A.1.5.3.2 Impact of measurement bandwidth on large-scale parameters

From Figure A.1.5.3.2-1(a) show delay spread shrinks with increased bandwidth. Minor difference between 28GHz and 73GHz at each bandwidth. The delay spread trends to a constant beyond 400MHz. Figure A.1.5.3.2-1(b) show AoA spread keeps almost stable with increased bandwidth. 2. Minor difference between 28GHz and 73GHz at each bandwidth. From figure A.1.5.3.2-1(c) show ZoA spread keeps almost stable with increased bandwidth. Minor difference between 28GHz and 73GHz at each bandwidth.

(a)   (b)   (c)
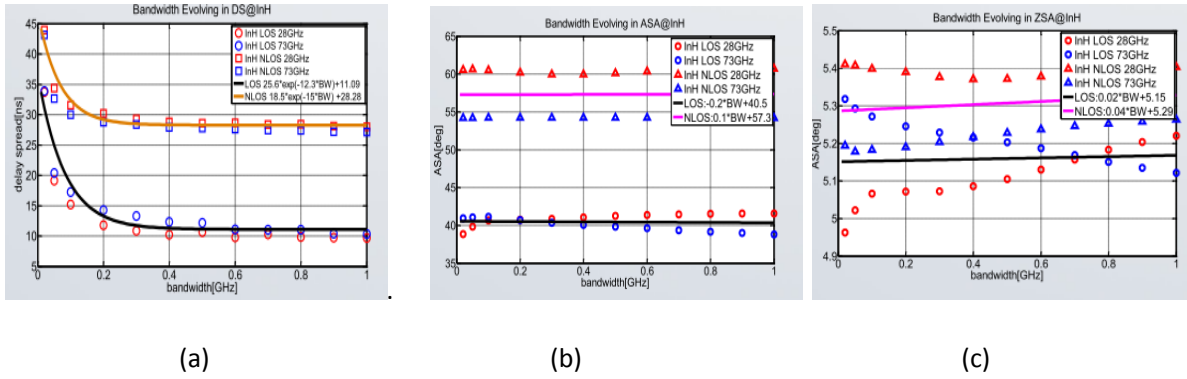
Figure A.1.5.3.2-1

A.1.6 Intel/Fraunhofer HHI

A.1.6.1 Channel measurements

The channel sounding is conducted in city center and residential areas in Berlin. The table below summarizes the channel sounder parameters:

Table A1.6.1-1: Channel sounder parameters.

Parameter	Value
Antenna setup (# of simultaneously supported TX and RX at BS and MS)	1 TX station and 1 RX station
Maximum number of simultaneously supported frequency bands	2
Coverable frequency bands	3.7 and 28 GHz
Bandwidth (maximum)	250 MHz @ 10 GHz and 60 GHz
Multipath time resolution	approx. 1 ns
Waveform	Optimized multi-tone sequence
TX power	30 dBm max, 36 dBm EIRP max
Measurement repetition rate	≥ 1 kHz
System processing gain (without further post-processing)	≥ 60 dB (≥ 100 dB expected for static scenarios with channel coherence time in the order of 1 s)
Antenna characteristics at TX / RX	omnidirectional / omnidirectional
Antenna gain at TX / RX	approx. 2 dBi
Antenna azimuth 3 dB beam width	omnidirectional
Antenna elevation 3 dB beam width	approx. 80 deg.
Antenna polarization at TX / RX	vertical / vertical

A.1.6.2   Findings and observations

Figure A1.6.2-1 and Figure A1.6.2-2 show the NLOS path Loss data for street canyon scenario in a residential area. The path loss parameters based on CI model and ABG model are summarized in Table 1.
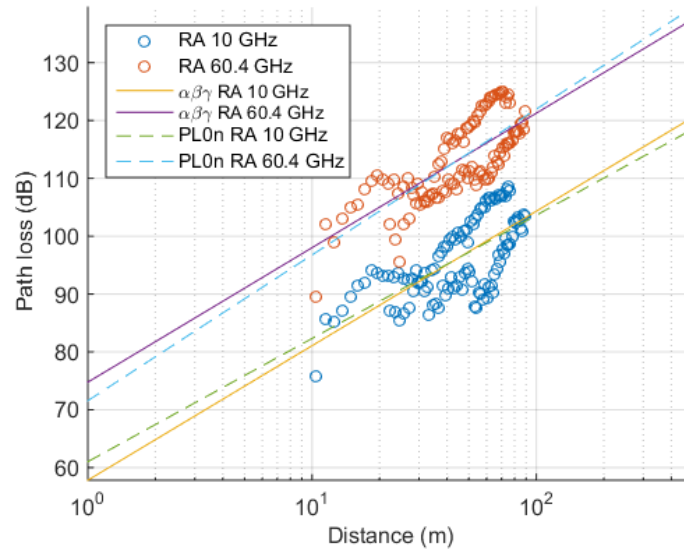
FIGURE A1.6.2-1: NLOS PATH LOSS DATA FOR STREET CANYON IN RESIDENTIAL AREA (10 GHZ AND 60.4 GHZ), AROUND ONE CORNER.
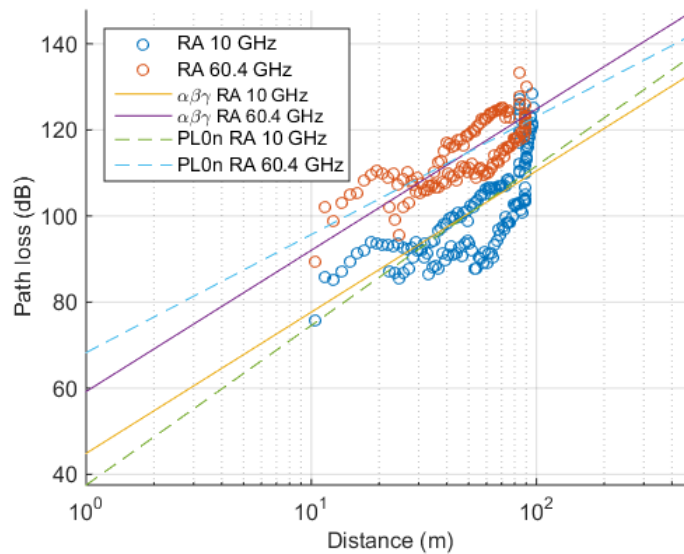
FIGURE A1.6.2-2: NLOS PATH LOSS DATA FOR STREET CANYON IN RESIDENTIAL AREA (10 GHZ AND 60.4 GHZ), AROUND ONE AND TWO CORNERS.

TABLE A1.6.2-1: PATH LOSS PARAMETERS.

Scenario	Environment	Distance [m]	Model	Frequency [GHz]	PLE/α	β [dB]	γ	σ [dB]
UMi	NLoS (one corner)	10-100	CI	10	2.13	-	-	-
				60	2.52	-	-	-
			ABG	10, 60	2.33	36.1	2.17	-
	NLoS (one and two	10-100	CI	10	3.71	-	-	-
				60	2.74	-	-	-

corners)		ABG	10, 60	3.28	26.5	1.84	-

Figure A1.6.2-3 shows the RMS delay spread of the measured locations at 10 GHz and 60 GHz. A higher delay spread is observed at 10 GHz. The delay spread tends to increase as Tx-Rx distance increases.
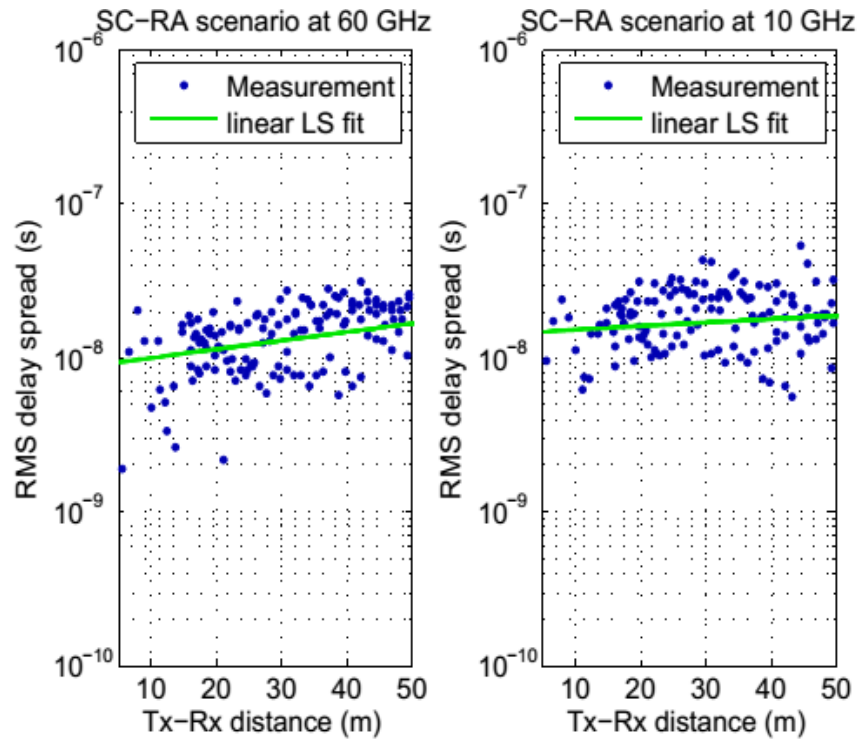
FIGURE A1.6.2-3: RMS DELAY SPREAD DATA FOR STREET CANYON IN RESIDENTIAL AREA (10 GHZ AND 60.4 GHZ).

A.1.7 NTT DOCOMO, INC.

A.1.7.1 Measurement system

Table A1.7.1-1 shows specifications of measurement equipment. Transmitter sends continuous wave (CW) and received power is recorded at receiver.

Table A1.7.1-1: Specifications of measurement equipment and parameters.

Parameters	Values, Types
Frequency	0.81 GHz, 2.2 GHz, 4.7 GHz, 26.4 GHz, 37.1 GHz
Transmission power	43 dBm (0.81 GHz, 2.2 GHz), 40 dBm (4.7 GHz, 26.4 GHz), 37 dBm (37.1 GHz)
Transmission signal	CW
BS antenna height	1.5 m, 6 m, 10 m
Tx antenna (BS)	Sleeve
MS antenna height	2.5 m
Rx antenna (MS)	Sleeve
Distance between BS -MS	30 to 676 m (LOS), 56 m to 959 m (NLOS)

A.1.7.2   Measurement campaign

Path loss measurements were carried out in a dense urban area in Tokyo [KITO+15]. Figure A1.7.2-1 shows picture of measurement site and Tx antenna setting. In the measurement site, the average building height is 18 m, the average road width is 29 m and buildings occupy 46 % of the area. Table A1.7.1-1 gives the measurement parameters. Continuous wave (CW) is transmitted from a BS antenna, and the received power level is recorded at the MS while the MS is moving. The BS antenna height is set to 10 m. The MS antenna is established on a measurement vehicle and the height of the antenna is 2.5 m. The antennas used for the BS and MS are sleeve antennas. The measured frequencies are 0.81 GHz, 2.2 GHz, 4.7 GHz, 26.4 GHz, and 37.1 GHz. The distance between the BS and the MS was between 30 m to 676 m in LOS case, and between 56 m to 959 m in NLOS case. Path loss is obtained every meter by taking median value of received power levels within 10 m (before and after 5 m).

Figure A1.7.2-1: Measurement site and setting of Tx antenna.

A.1.7.3   Findings and observations

Figure A1.7.3-1 shows path loss over distance from the BS to MS at 4.7, 26.4 and 37.1 GHz for LOS and NLOS cases. Moreover, regression analysis is applied to the measurement data by using CI and ABG models. Summary of these regression results is shown in Table A1.7.3-1.

CI model is expressed as

$$PL(d) = 10 n \log_{10}(d) + \mathsf{FSPL}(f_C, 1) + \chi_\sigma \qquad \text{(A1.7.3-1)}$$

$$\mathsf{FSPL}(f_C, d) = 32.44 + 20\log(f_C) + 20\log(d) \qquad \text{(A1.7.3-2)}$$

where *PL* is path loss in dB, *d* is distance from BS to MS in meters, f_c is frequency in GHz, and χ_σ is shadow fading factor in dB, which is log-normal distribution with standard variation of σ_{SF}.

ABG model is expressed as

$$PL(d) = 10 \alpha \log_{10}(d) + \beta + 10 \gamma \log_{10}(f_C) + \chi_\sigma \qquad \text{(A1.7.3-3)}$$

● *f* = 4.7 GHz   ● *f* = 26.4 GHz
● *f* = 37.1 GHz

(a) LOS   (b) NLOS
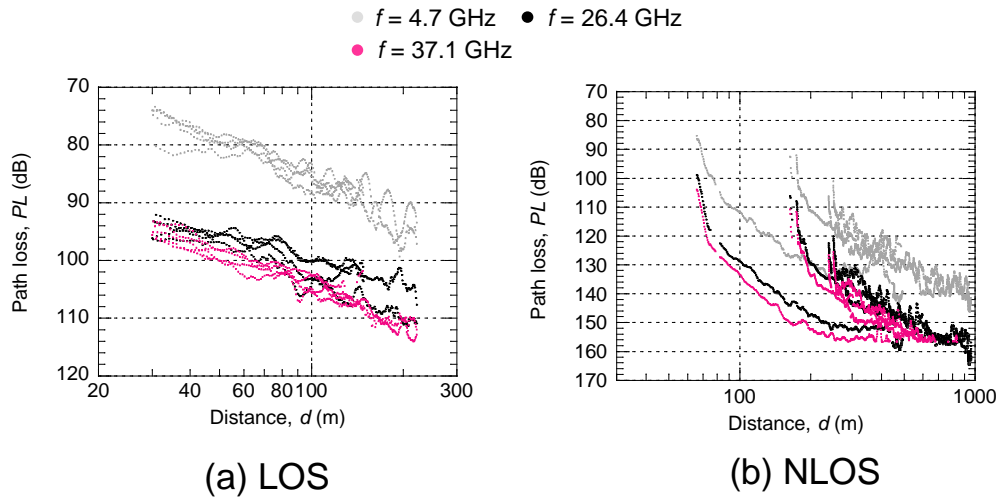
Figure A1.7.3-1: Path loss vs. distance.

Table A1.7.3-1: Regression analysis.

		Parameters			
		$n \,/\, \alpha$	β (dB)	γ	σ_{SF} (dB)
LOS	CI	2.09	N/A		3.1
NLOS	CI	3.21			6.2
	ABG	3.47	25.3	2.07	6.2

A.1.8 New York University (NYU)

A.1.8.1   Channel sounder

A set of 28 GHz and 73 GHz ultrawideband sliding correlator (or swept time delay cross correlation (STDCC)) channel sounders with superheterodyne architectures with similar baseband hardware and relatively similar intermediate frequency (IF) and radio frequency (RF) stages are used to measure the outdoor urban environment on the UT Austin campus, and downtown Manhattan in New York City [RSMZ+13, RMCS+15, MCRS15]. The baseband probing signal is a 400 megachips-per-second (Mcps) pseudorandom noise (PN) sequence generated via an 11-bit linear feedback shift register (LFSR) with digital circuitry. For the 28 GHz, 38 GHz, and 73 GHz systems, the baseband signal is modulated to an IF between 5 GHz and 6 GHz that then entered custom-designed RF front-end up-converter boxes which then modulates the IF broadband signals to RF carrier frequencies of 28 GHz, 38 GHz, and 73 GHz. At the receiver side, the incoming ultradwideband 800 MHz RF null-to-null bandwidth signal is downconverted with custom-built hardware to an IF between 5 GHz and 6 GHz and is then subsequently demodulated into its *I* and *Q* baseband components. Both the I and Q baseband signals are then mixed with a PN sequence identical to the transmitted signal, but at a slightly slower rate of 399.95 Mcps, which produces an impulse when the codes are aligned in time. The subsequent *I* and *Q* correlated voltages are then low pass filtered and digitally sampled with high-speed oscilloscope. The digital *I* and *Q* signals are then squared ($I^2 + Q^2$) to generate a raw power delay profile (PDP) of the channel for further processing. For each acquisition, 20 consecutive PDPs are averaged to improve processing gain and to reduce noise fluctuations.

Table A1.8.1-1: Channel sounder specifications for the 28, 38, and 73 GHz measurement campaigns [RSMZ+13, RQTM+12, RGBD+13, RMCS+15].

Carrier Frequency	28 GHz	73 GHz	38 GHz
Probing Signal	11th order PN sequence (length=2047)		
TX PN Code Chip Rate	400 Mcps		
TX PN Code Chip Width	2.5 ns		
RX PN Code Chip Rate	399.95 Mcps		
Slide Factor	8000		
Digitizer Sampling Rate	2 Megasamples / second		
RF Bandwidth (Null-to-Null)	800 MHz		
TX/RX IF Frequency	5.4 GHz	5.625 GHz	5.375 GHz
RX/RX LO Frequency	22.6 GHz	67.875 GHz	32.25 GHz
Center Frequency	28 GHz	73.5 GHz	37.625 GHz
TX/RX LO Power	10 dBm		-29 dBm
Max. TX Output Power	30.1 dBm	14.6 dBm	21.2 dBm
TX/RX Antenna Gain	24.5 dBi; 15 dBi	20 dBi	25 dBi/25 dBi; 13.3 dBi
TX/RX Azimuth HPBW	10.9°; 28.8°	15°	7.8°/7.8°; 49.4°
TX/RX Elevation HPBW	8.6°; 30°	15°	7.8°/7.8°; 49.4°
Max. TX EIRP	54.6 dBm	32.1 dBm	46.2 dBm
TX Antenna Height	7 m; 17 m		8 m
RX Antenna Height	1.5 m		
Max. Measureable Path Loss	178 dB	181 dB	150 – 160 dB
Multipath Time Resolution	2.5 ns		
TX Polarization	Vertical/ Horizontal	Vertical	Vertical
RX Polarization	Vertical / Horizontal	Vertical	Vertical

A.1.8.2   Channel sounding

In the 28 GHz measurements, three TX locations (heights of 7 m and 17 m) and 27 RX locations (heights of 1.5 m) were selected to conduct the measurements [RMCS+15]. Two types of horn antennas were employed: a 24.5 dBi-gain narrowbeam horn antenna with 10.9-degree and 8.6-degree half-power beamwidths (HPBWs) in the azimuth and elevation planes, respectively, and a 15 dBi-gain widebeam horn antenna with 28.8-degree and 30-degree HPBWs in the azimuth and elevation planes, respectively. The narrowbeam antenna was always utilized at the TX locations, and five of the RX locations used both the narrowbeam and widebeam antennas, including two LOS and three NLOS locations. For nine out of the ten measurement sweeps for each TX-RX location combination (except the two LOS RX locations), the RX antenna was sequentially swept over the entire azimuth plane in increments of one HPBW at elevation angles of 0 degree and ±20 degrees about the horizon, so as to measure contiguous angular snapshots of the channel impulse response over the entire 360-degree azimuth plane, while the TX antenna remained at a fixed azimuth and elevation angle. The TX antenna was swept over the azimuth plane in the last measurement sweep.

In the 73 GHz measurements [RMCS+15], five TX locations (heights of 7 m and 17 m) and 27 RX locations were used, with RX antenna heights of 2 m (mobile scenario) and 4.06 m (backhaul scenario), yielding a total of 36 TX-RX location combinations for the mobile (access) scenario and 38 combinations for the backhaul scenario. A pair of 27 dBi-gain rotatable directional horn antennas with a HPBW of 7 degrees in both azimuth and elevation planes was employed at the TX and RX. For each TX-RX location combination, TX and RX antenna azimuth sweeps were performed in steps of 8 degrees or 10 degrees at various elevation angles [MCZN+13].

38 GHz cellular measurements were conducted with one TX location chosen on one building at the UTA campus in the summer of 2011 at height of 8 m, with a maximum measurable dynamic range of 160 dB, for 10 RX
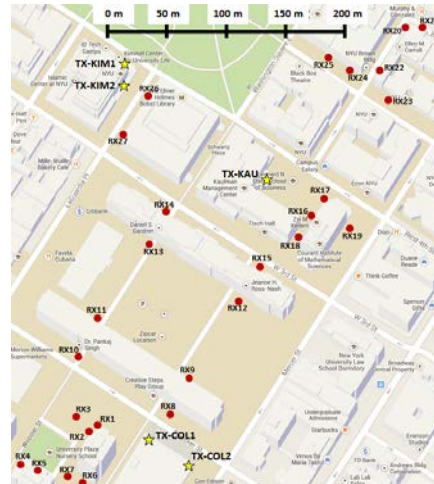
locations in the surrounding campus using narrowbeam TX antennas (7.8-degree Az. HPBW) and narrowbeam (7.8-degree Az. HPBW) or widebeam (49.4-degree Az. HPBW) RX antennas. A total of 10 TX-RX location combinations were measured for narrowbeam measurements (with T-R separation distances ranging from 29 m to 225 m) and 6 TX-RX location combinations were measured for widebeam measurements (with T-R separation distances between 29 m and 156 m) [RQTM+12, RGBD+13, RMCS+15].

Table A1.8.2-1: NYU's channel sounding site numbers and distances in New York City [MCRS15].

		Manhattan Measurements	
		28 GHz TX/RX: 10.9° HPBW	73 GHz TX/RX: 7° HPBW
# of locations measured ($d \leq 200$ m)	LOS	6	5
	NLOS	33	30
# of locations measured for all d	LOS	6	5
	NLOS	68	31
# of locations with signal ($d \leq 200$ m)	LOS	6 (31 m $\leq d \leq$ 102 m)	5 (30 m $\leq d \leq$ 54 m)
	NLOS	20 (61 m $\leq d \leq$ 187 m)	25 (48 m $\leq d \leq$ 190 m)
# of outage locations ($d \leq 200$ m)	LOS	0	0
	NLOS	13 (96 m $\leq d \leq$ 193 m)	5 (168 m $\leq d \leq$ 198 m)
# of locations with signal for all d	LOS	6 (31 m $\leq d \leq$ 102 m)	5 (30 m $\leq d \leq$ 54 m)
	NLOS	20 (61 m $\leq d \leq$ 187 m)	25 (48 m $\leq d \leq$ 190 m)
# of outage locations for all d	LOS	0	0
	NLOS	48 (96 m $\leq d \leq$ 425 m)	6 (168 m $\leq d \leq$ 216 m)
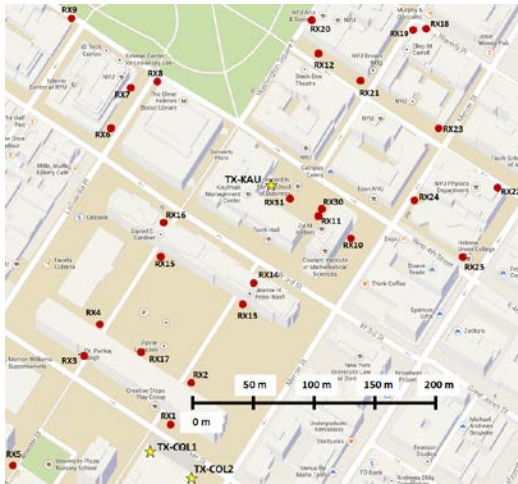
(a) Sounding sites in the 28 GHz campaign   (b) Sounding sites in the 73 GHz campaign

Figure A1.8.2-1: NYU's channel sounding sites in UMi street canyons in New York City [RSMZ+13, RMCS+15].

A.1.8.3   Findings and observations

A.1.8.3.1 Omnidirectional path loss models in the UMi scenario at 28, 38, and 73 GHz

Both the 1 m close-in (CI) free space reference distance model and the floating-intercept (FI) model were utilized to investigate omnidirectional path loss in the UMi scenario [RMCS+15]. The LOS PLEs are equal or very close to the free space PLE of 2 for all three frequencies, while the NLOS PLEs are comparable to those at microwave frequencies and have no obvious frequency dependence beyond the first meter of free space propagation in the UMi scenario [RMCS+15]. Figure A1.8.3.1-1 shows the 73 GHz omnidirectional 1 m CI and FI path loss models for

the hybrid scenario with RX antenna at heights of 2 m and 4.06 m in New York City. It is shown that the 73 GHz NLOS PLE is not vastly different from that corresponding to 1.9 GHz using omnidirectional antennas with a base station antenna height of 3.7 m and a mobile RX antenna height of 1.7 m, as displayed in Figure A1.8.3.1-1.

Table A1.8.3.1-1: Omnidirectional CI and FI path loss models at 28, 38, and 73 GHz in the UMi scenario. α is the floating intercept in the FI model, β is the slope in the FI model. Man. denotes Manhattan [RMCS+15].

					LOS		NLOS		NLOS (Floating)		
Omnidirectional Path Loss Models ($d_0 = 1$ m)											
	TX/RX scenario	TX Ht. (m)	RX Ht. (m)	NLOS Meas. Range: d (m)	PLE	σ [dB]	PLE	σ [dB]	α [dB]	β	σ [dB]
28 GHz (Man.)	Narrow/Narrow	7; 17	1.5	61≤d≤187	2.1	3.6	3.4	9.7	79.2	2.6	9.6
38 GHz (Austin)	Narrow/Narrow	23	1.5	61≤d≤150	2.0	2.4	2.8	9.1	39.1	4.0	8.9
		36		75≤d≤377	1.9	3.6	2.6	10.8	122.2	0.1	9.2
		23; 36		61≤d≤377	1.9	3.4	2.7	10.5	100.9	1.0	9.6
		8; 23; 36		29≤d≤377	1.9	4.4	2.7	10.1	96.2	1.3	9.1
	Narrow/Wide	23	1.5	d=101	1.8	2.4	2.6	-	-	-	-
		36		75≤d≤728	1.8	1.8	2.2	4.1	81.7	1.5	3.4
		23; 36		75≤d≤728	1.8	2.1	2.3	4.9	88.6	1.2	3.4
		8; 23; 36		29≤d≤728	1.8	3.2	2.3	7.4	88.2	1.3	5.7
73 GHz (Man.)	Access	7; 17	2	48≤d≤190	2.0	5.2	3.3	7.6	81.9	2.7	7.5
	Backhaul		4.06	50≤d≤190	2.0	4.2	3.5	7.9	84.0	2.8	7.8
	Hybrid		2; 4.06	48≤d≤190	2.0	4.8	3.4	7.9	80.6	2.9	7.8
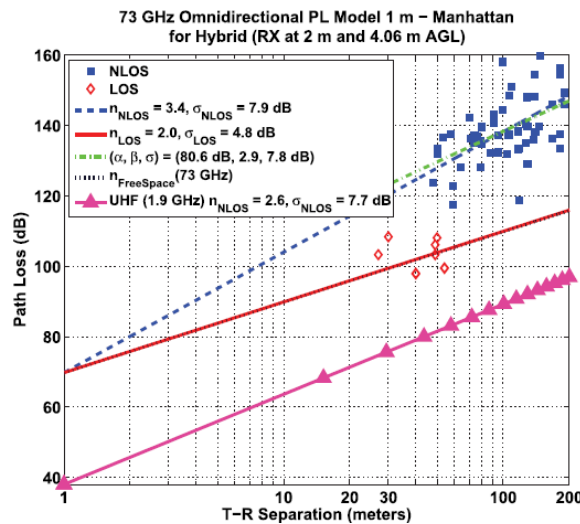
Figure A1.8.3.1-1: NYU's 73 GHz omnidirectional 1 m CI and FI path loss models for the hybrid scenario with RX antenna at heights of 2 m and 4.06 m in New York City [RMCS+15]. Blue squares represent NLOS omnidirectional path loss values and red diamonds represent LOS omnidirectional path loss values. An omnidirectional NLOS path loss model for the 1.9 GHz band measured in San Francisco is also displayed on the figure for comparison.

Additional information regarding directional and omnidirectional RMS delay spreads may be found in the following resources for 28 GHz, 38 GHz, and 73 GHz measurements: [RMCS+15, MCRS15, XRBS99].

A.1.9 Samsung / Korea Advanced Institute of Science and Technology (KAIST)

A.1.9.1 Channel sounder

The channel sounder is developed using a sliding correlator provides an accurate multipath time resolution by utilizing 250 Mega chip-per-second (Mcps) pseudo-random (PN) sequences. Figure A1.9.1-1 shows the block diagram and photograph of the developed channel sounding system. In transmitter part, PN sequence generated by software goes into two DACs which generates I and Q signal, and these analog signal is converted to the 28 GHz band with the local oscillator and mixer in RF up-converter unit. The signal is radiated at TX with up to 29

dBm transmit power. The 10° half-power beamwidth horn antennas (24.5 dBi gain) with are equipped at the RF-end of transmitter and receiver. The received RF signal at 28 GHz band is down-converted and fed into an ADC for data acquisition. Each side has its own external reference clock. It also has a common trigger signal for the synchronization. To cover all channel directions it needs multiple measurements in different angles due to the narrow beamwidth of the horn antennas. Both transmitter and receiver had each rotating module in azimuth and elevation angle for steering the horn antenna, and the pointing direction is automatically controlled on measurements.
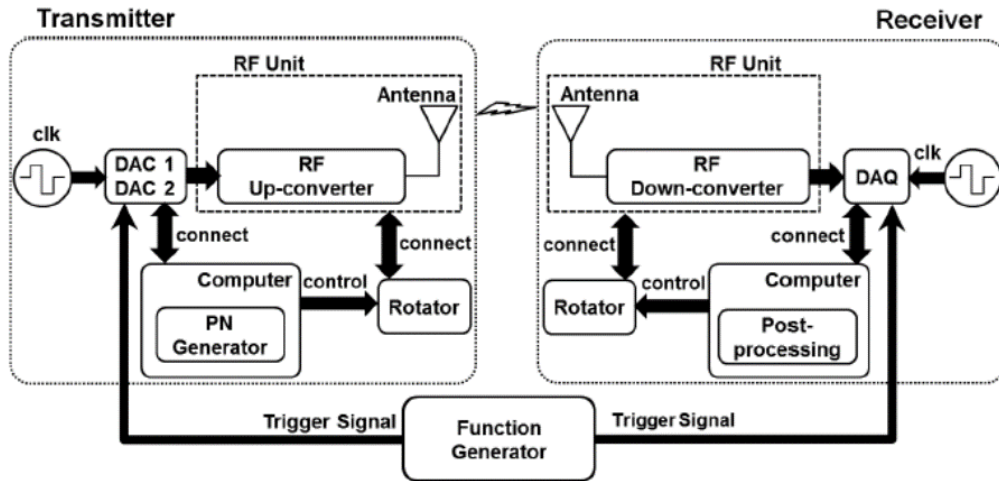
Figure A1.9.1-1: Measurement system block diagram (upper) and photograph of the system (lower).

A.1.9.2   Channel sounding

The channel sounding was performed in downtown Daejeon and the Alpensia resort in Pyeongchang, Korea. The measurement overview and the description of channel sounder are given in Table A1.9.2-1.

Table A1.9.2-1: Measurement overview.

Propagation scenario	O2O NLOS in Daejeon	O2O NLOS in Pyeongchang
Center frequency	28 GHz	
Bandwidth	500 MHz	
Polarization	Vertical linear polarization	

TX location	1 test location	2 test locations
TX velocity	Stationary	
RX location	47 test locations	15 test locations
RX velocity	Stationary	
RX height above ground level	1.5m	
TX-RX distance	43 – 209 m	55 – 207 m
Angular scanning	Rotation in azimuth 0-360° Rotation in elevation -60-60° with 10° step	
Remarks	9 test locations fell into outage	-

A.1.9.2.1 Downtown Daejeon, Korea

This channel measurements were performed in downtown Daejeon, South Korea. Environment of this scenario is densely built-up urban environment. The TX system was placed on the fifth floor of a building, 15 m height above the ground. Figure A1.9.2.1-1 shows the view at TX location and Figure A1.9.2.1-2 depicts a satellite map of the TX and RX locations. The sounding was performed for 47 NLOS RX locations in total. The TX-RX distance ranged from 43 m to 209 m.

Figure A1.9.2.1-1: Photographs of the view at TX location in downtown Daejeon.
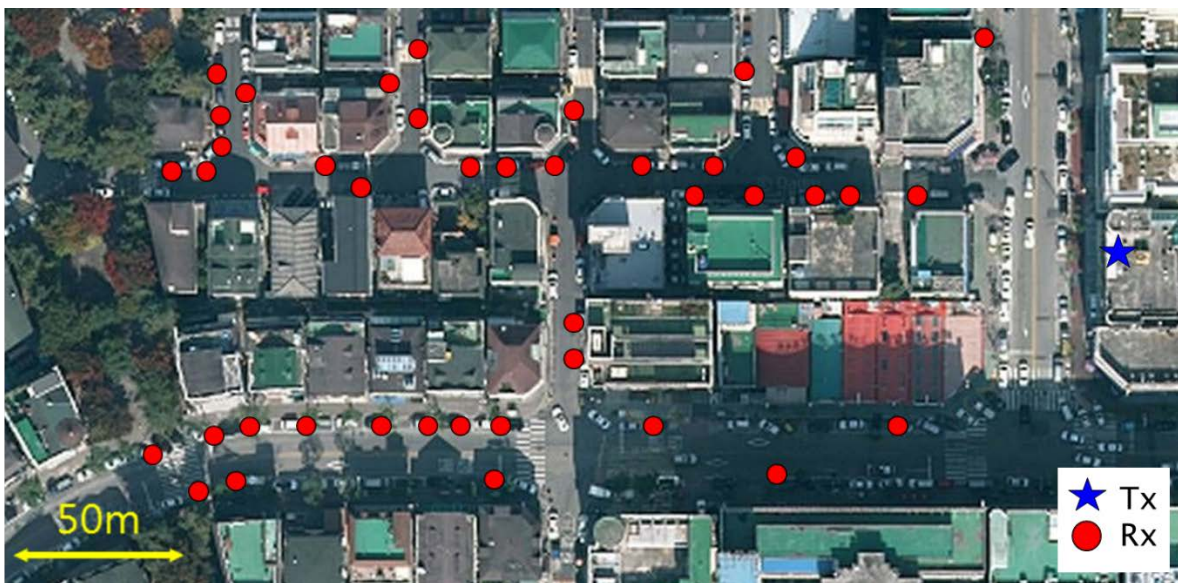

Figure A1.9.2.1-2: A satellite map of the TX and RX location in downtown Daejeon.

A.1.9.2.2 *The Alpensia resort in Pyeongchang, Korea*

The second channel measurement scenario was carried out in the Alpensia resort in Pyeongchang similar to the typical urban environment. Photographs of the measurement locations are in Figure A1.9.2.2-1. A satellite map of the measurement site marked on transmitter and receiver locations is presented in Figure A1.9.2.2-2. The TX system was located in two places, the sixth floor (17 m above the ground) of the hotel in the resort town and an external vacant lot with height of 8 m. Total 15 NLOS measurements were performed. And the TX-RX distances ranged from 55 m to 207 m.

Figure A 1.8.2.2-1: Photographs of the measurement sites of the Alpensia resort in Pyeongchang.
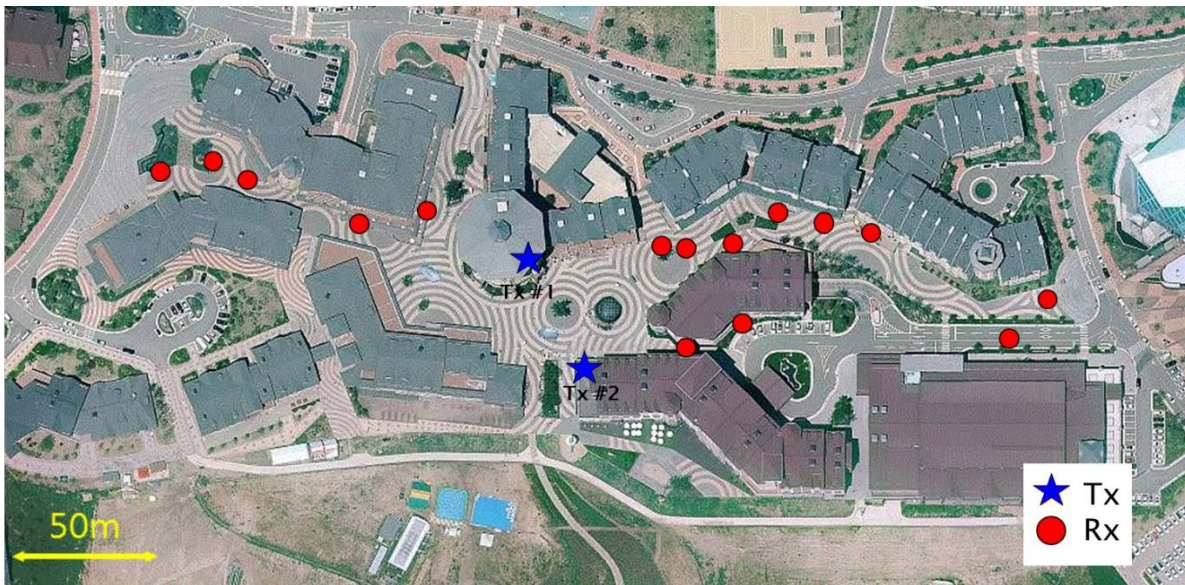

**Figure A 1.8.2.2-2: A satellite map of the TX and RX location in Pyeongchang.**

A.1.9.3 Findings and observations

A.1.9.3.1 *Path loss analysis*

From the measured data, the path loss (PL) for each location was estimated as

$$PL = P_{Tx} - P_{Rx} + G_{Tx} + G_{Rx}, \qquad \text{(A1.9.3.1-1)}$$

where P_{Tx} is the transmit power, and P_{Rx} is the received power derived by integrating the energy of paths in the omni-PDP, and G_{Tx} and G_{Rx} are the gains of the horn antennas used in the transmission and reception, respectively. For our measurement system, P_{Tx} = 29 dBm and G_{Tx} = G_{Rx} = 24.5 dBi. Two PL models are considered to fit the measured PLs; namely the close-in (CI) free space reference distance PL model and the Alpha-Beta-Gamma (ABG) PL model. Figure A1.9.3.1-1 shows the path loss plots for the NLoS channels in Daejeon and Pyeongchang, Korea. The path loss model parameters are listed in Table A1.9.3.1-1 with the valid ranges for distance.

(a) Daejeon   (b) Pyeongchang
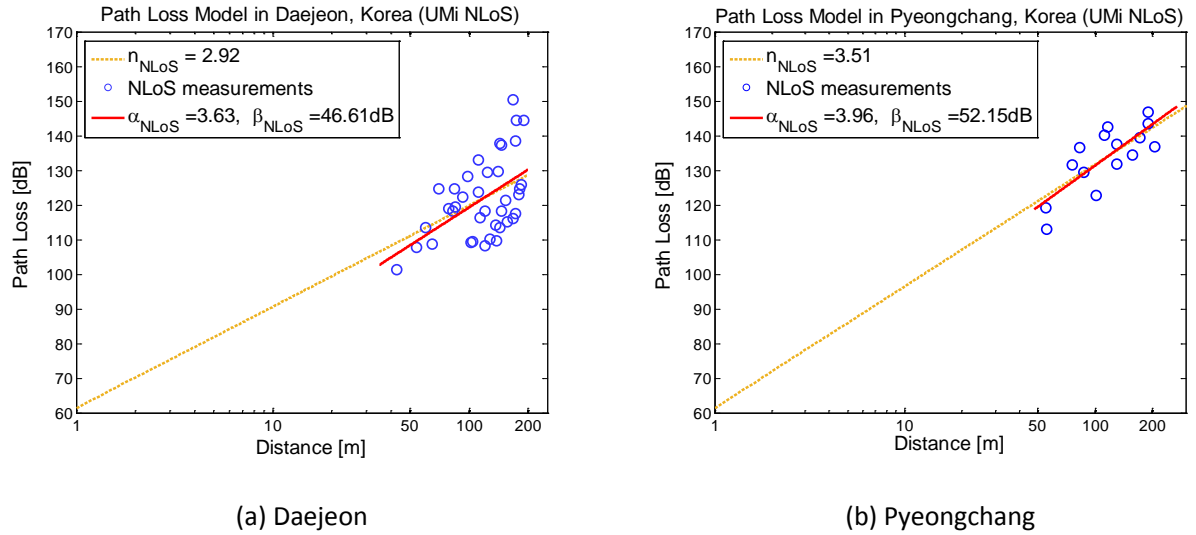
Figure A1.9.3.1-1: Path loss models for UMi street canyon scenarios in Daejeon and Pyeongchang, Korea at 28 GHz.

Table A1.9.3.1-1. The path loss parameters

| Parameters	Daejeon	Pyeongchang
d [m]	$40 < d < 210$	$50 < d < 210$
d_0 [m]	1	1
N	2.92	3.51
X_σ^{CI}	9.89	5.75
A	3.63	3.96
B	46.61	52.15
X_σ^{ABG}	9.83	5.69

A.1.9.3.2 Cluster analysis

For automatic clustering of the measured multipath components (MPCs), the K-Power-Means algorithm [Czin07] was used. This algorithm is iterative and uses a multipath component distance (MCD) as a metric for clustering. In addition to delays and angles, it also considers the power of MPCs, and thus, the clusters are defined mainly by strong MPCs. The algorithm minimizes the sum of MCDs between MPCs and their cluster centroids, which has an effect of minimizing cluster angular and delay spreads for a given number of clusters. The Kim-Park (KP) index proposed in [KiPP01] is used for determining the optimum number of clusters. Figure A.1.9.3.2-1 shows an exemplary clustering of MPCs using the KPowerMeans algorithm in which three clear clusters are observed. And from the measurements, the cumulative distribution functions (CDFs) of the number of clusters in two cases are
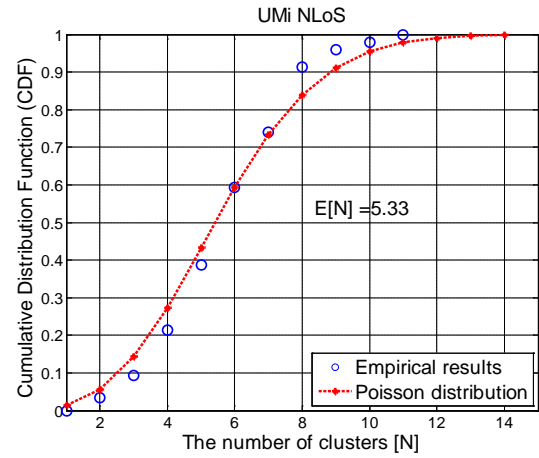
also shown in Fig. A.1.9.3.2-2 (a) and 2 (b), where the positive Poisson distribution is overlaid as the best fit. The average number of clusters were 4.58 and 5.33, respectively.
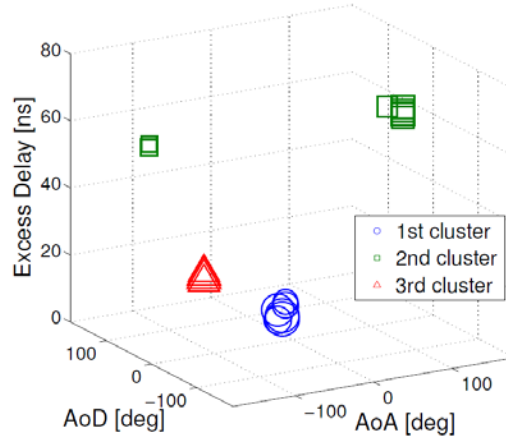
Figure A1.9.3.2-1: An exemplary clustering of MPCs using the KPowerMeans algorithm.
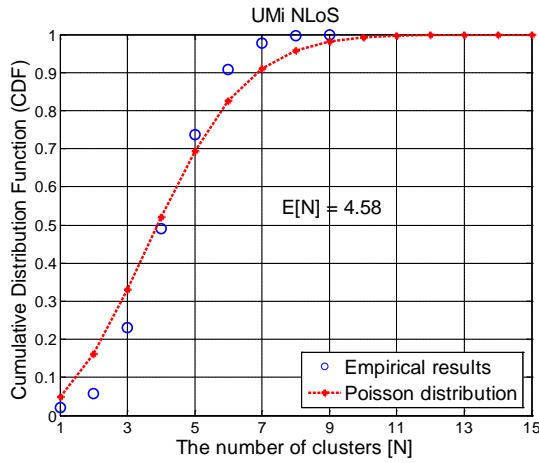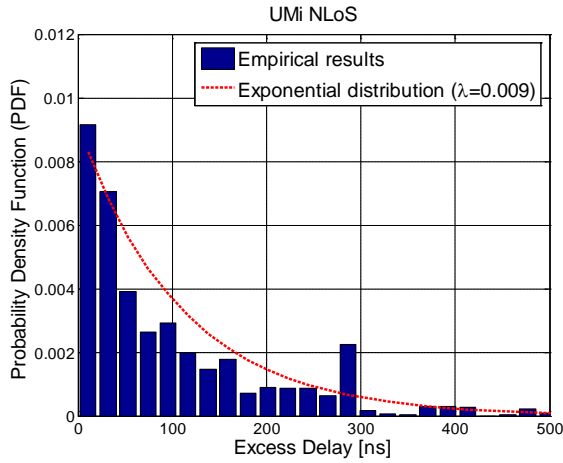

(a) Daejeon

(b) Pyeongchang

Figure A1.9.3.2-2: Cumulative distribution function of the number of clusters for UMi street canyon scenarios in Daejeon and Pyeongchang, Korea at 28 GHz.

A.1.9.3.3 Spatio-temporal analysis

1) Temporal analysis

Using the synthesized omni-directional PDPs, the temporal characteristics can be analyzed through excess delays, subpath delays, the RMS delay and subpath delay spreads. The histograms of the excess delays and subpath delays and their probability density functions (PDFs) for urban street canyon scenarios in Daejeon are illustrated in Figs. A.1.9.3.3-1(a) and (b), respectively. Note that they follow exponential distributions with the decay rate parameters of 0.009 ns and 0.027 ns, respectively. Also, the histograms and their PDFs in Pyeongchang are illustrated in Figs. A.1.9.3.3-1 (c) and (d), respectively. It can be shown that they also follow exponential distributions with the decay rate parameters of 0.0098 ns and 0.0195 ns, respectively.

(a) Excess delay in Daejeon
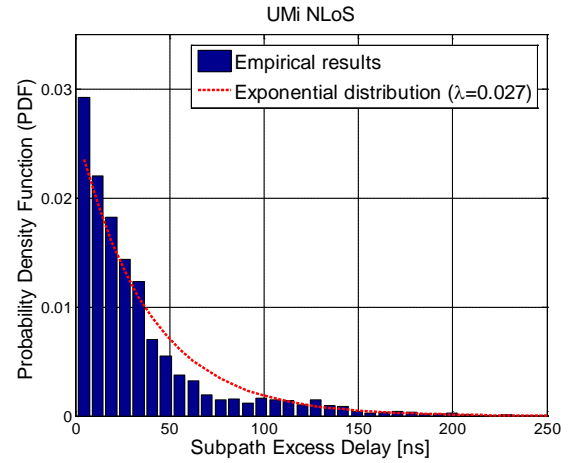
(b) Subpath excess delay in Daejeon
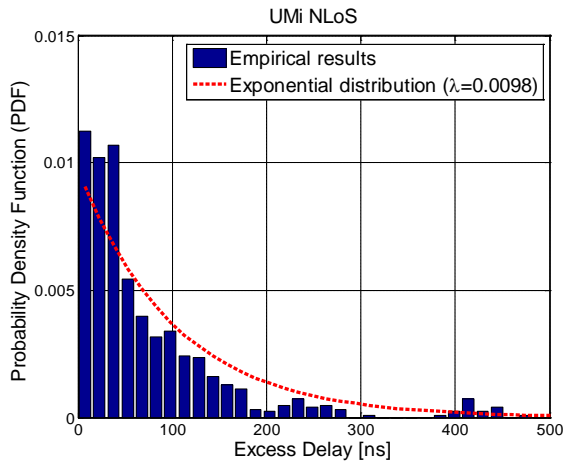
(c) Excess delay in Pyeongchang
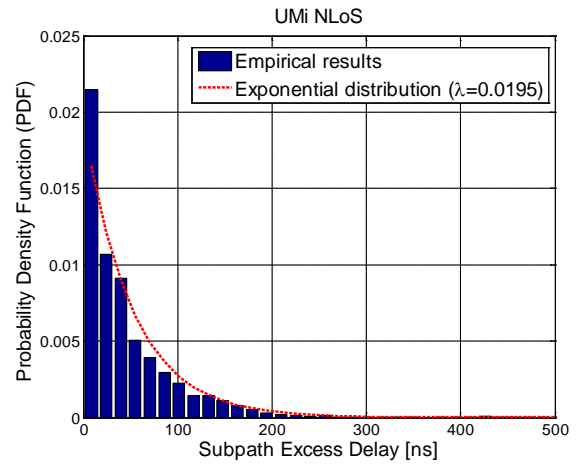
(d) Subpath excess delay in Pyeongchang

Figure A1.9.3.3-1: Probability density functions of excess delays and subpath delays for UMi street canyon scenarios in Daejeon and Pyeongchang, Korea at 28 GHz.

Figure A1.9.3.3-2 shows the CDFs of the RMS delay and subpath delay spreads along with log-normal distributions as their best fits. The average value of the RMS delay spread and the subpath delay spread from the measurements in Daejeon are 55.43 ns and 12.86 ns, respectively. For the cases of the measurements in Pyeongchang, the average value of the RMS delay spread and the subpath delay spread are 60.41 ns and 15.77 ns, respectively.
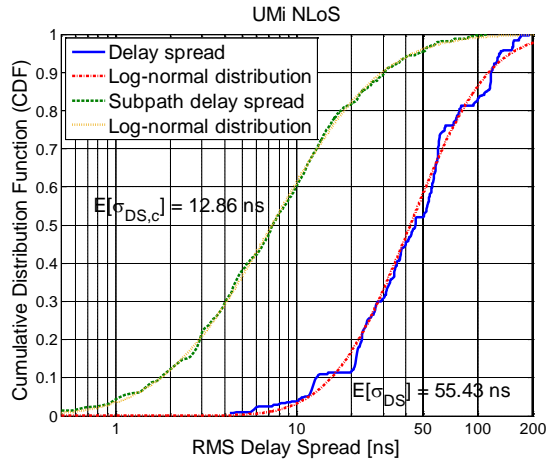
(a) Daejeon
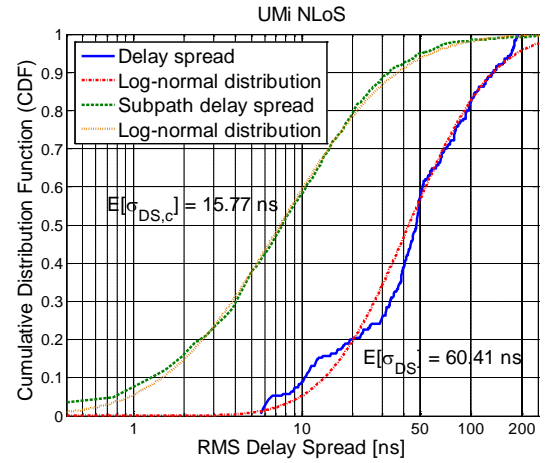
(b) Pyeongchang

Figure A1.9.3.3-2: Cumulative distribution functions of RMS delay and subpath delay spreads for UMi street canyon scenarios in Daejeon and Pyeongchang, Korea at 28 GHz.

2) Spatial analysis

The spatial characteristics for channel modeling can be analyzed through the distributions of the cluster AoD and AoA, and their corresponding circular angle spreads. In Figs. A.1.9.3.3-3 (a) and 3(b), PDFs of the measured cluster AoD and AoA in Daejeon are shown, and a Laplacian distribution is also plotted as the best fit. Note that the best-fit distribution for 28 GHz is different from the distribution for the cellular bands, which is the wrapped Gaussian distribution [Kyos07]. The PDFs of the measured cluster AoD and AoA in Pyeongchang are also shown along with Laplacian distributions as their best fits, in Figs. A.1.9.3.3-3 (c) and 3(d).

(a) Cluster AoD in Daejeon

(b) Cluster AoA in Daejeon
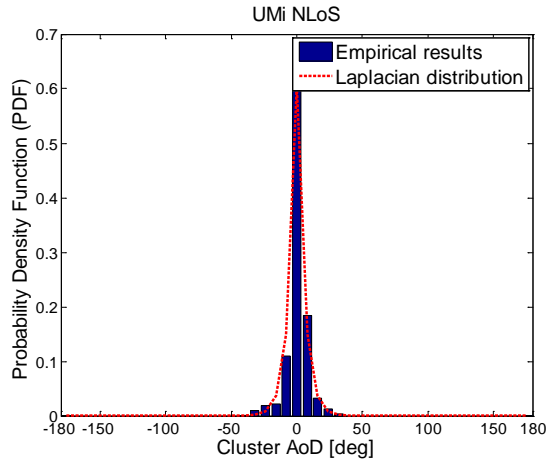
(c) Cluster AoD in Pyeongchang   (d) Cluster AoA in Pyeongchang
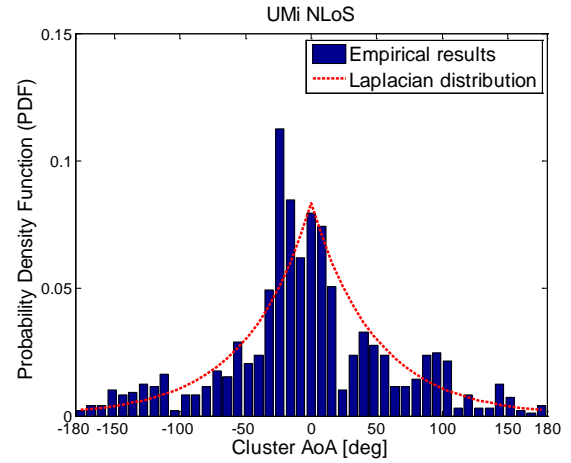
Figure A1.9.3.3-3: Probability density functions of cluster AoD and AoA for UMi street canyon scenarios in Daejeon and Pyeongchang, Korea at 28 GHz.

The AoD and the AoA spreads (ASD and ASA) from the measurements in Daejeon are illustrated with their CDFs in Fig. A.1.9.3.3-4 (a) and 4 (b). The average values of the AoD and AoA spreads are 7.68° and 31.39°, respectively. And the ASD and ASA in Pyeongchang are also shown with their CDFs in Fig. A.1.9.3.3-4 (c) and 4 (d). The average values of the ASD and ASA are 6.75° and 43.11°, respectively. In addition, the measured intra-cluster AoD/AoA spreads of the urban environments in Daejeon have the mean values of {5.82°, 15.56°}, respectively. And the mean values of the intra-cluster ASD and ASA in Pyeongchang are {4.66°, 10.75°}, respectively. Note that the intra-cluster angular spreads smaller than the beam width of the horn antennas on the Tx and Rx sides were roughly calculated and based on subpaths which appear across several adjacent angular bins; the subpaths were resolved in the delay domain thanks to the large bandwidth of the sounder. If highly precise intra-cluster angular spread values are required for any specific application, it should be considered that the limited angular resolution of the channel sounder have an impact on the intra-cluster spreads. Thus, ray-tracing analysis and/or measurements with narrower beam width for our measurement scenarios would be needed to obtain more reliable intra-cluster spread values.
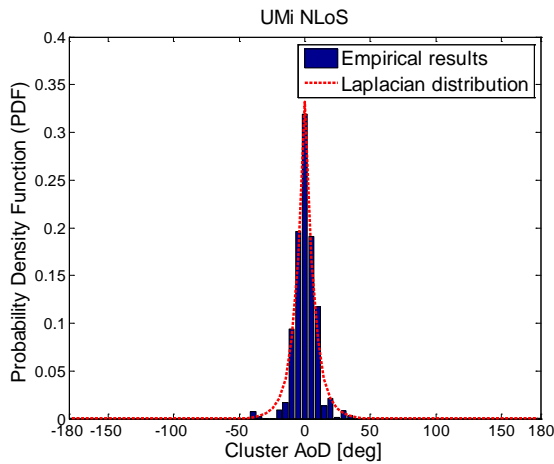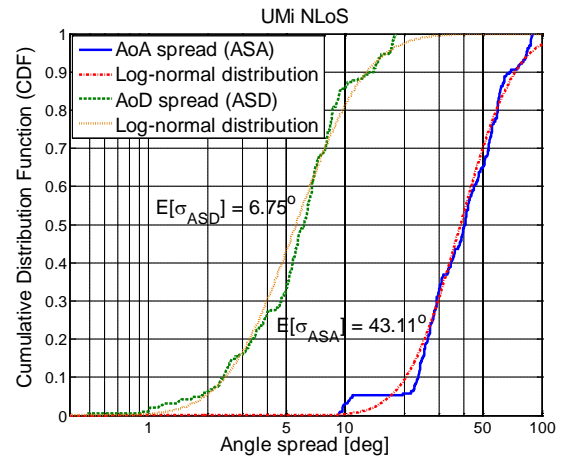

(a) Daejeon   (b) Pyeongchang
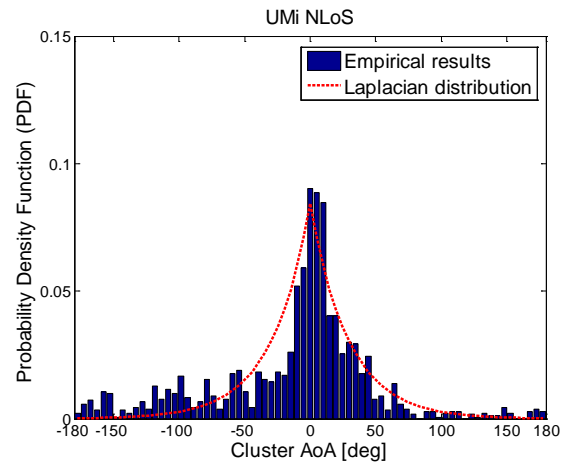
Figure A1.9.3.3-4: Cumulative distribution functions of the AoD and AoA spreads for UMi street canyon scenarios in Daejeon and Pyeongchang, Korea at 28 GHz.

A.1.9.3.4 Cross correlation properties between the large scale parameters

The large scale parameters, i.e., the inter-cluster AoD and AoA spreads, RDS and shadow fading are generally correlated with each other. The cross correlation coefficients of the two urban scenarios are listed in Table A.1.9.3.4-1. Based on our 28 GHz measurements, usually there exists a dominant reflector near the Tx site, which illuminates wide spatial areas and influences the inter-cluster AoD spread and the shadow fading, while indirectly affects the inter-cluster AoA spread and the RDS; radio wave propagation mechanisms are mainly dominated by reflections due to the weak diffraction effect at 28 GHz.

Table A1.9.3.4-1. Cross correlation coefficient of large scale parameters.

Parameters	Daejeon	Pyeongchang
DS vs SF	-0.1293	-0.0137
ASD vs SF	-0.2244	-0.1302
ASA vs SF	-0.1293	-0.0764
ASD vs DS	0.5539	0.5933
ASA vs DS	0.0685	0.4954
ASD vs ASA	0.2303	0.5772

In addition, the essential SCM parameters for the UMi NLoS street canyon environments in Daejeon and Pyeongchang are compared in Table A.1.9.3.4-2.

Table A1.9.4.3-2. Comparison of the essential channel parameters in Daejeon and Pyeongchang.

Parameters	Daejeon	Pyeongchang
α	3.63	3.96
β	46.61 dB	52.15 dB
X_σ^{ABG}	9.83 dB	5.69 dB
Number of clusters	5	
Delay distribution	Exponential distribution	
RMS delay spread	55 ns	60 ns
Subpath delay spread	13 ns	16 ns
Angle distribution	Laplacian distribution	
AoD spread (ASD)	8 deg	7 deg
AoA spread (ASA)	31 deg	43 deg
Subpath ASD	6 deg	5 deg
Subpath ASA	16 deg	11 deg

A.2 Urban microcellular scenarios – open square

A.2.1 Aalto University

A.2.1.1 Channel sounder

Please refer to Section A.1.1.1.

A.2.1.2 Channel sounding

Aalto's channel sounding for the open square scenario was performed outside the Kamppi shopping center in Helsinki, Finland. The square is about 80 x 80 m2 in size and is surrounded by six-story buildings with average height of 40 m. The square includes some lampposts, a sculpture in the middle and some shops, trees and vegetation at the side. The sounding was performed during the day and hence there was a continuous traffic of people passing through the square. The transmit and receive antennas were placed in the middle of the square at a height of 2 m, and their separation distance was between 4.5 and 19.2 m. The 60 GHz sounding was

performed with 13 co-polarized and two cross-polarized links, among which three links were with obstruction of LOS due to lamp posts and the sculpture.

(a) Photo of the sounding site.
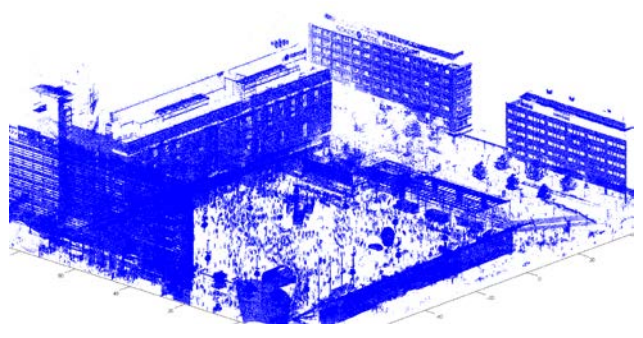
(b) Point cloud environmental description of the sounding site.

Figure A2.1.2-1: Aalto's channel sounding in an open square.

A.2.1.3   Channel simulations

Please refer to A1.1.3.

A.2.1.4   Findings and observations

A.2.1.4.1 LOS probability in open square is similar to other UMi scenarios

To estimate the LOS probability in the open square, a point cloud was captured to describe the environment and a large number of mobile and base stations were defined in the simulation tool, as depicted in Figure A.2.1.4.1 (a). For a single link, shadowing was detected by looking for points inside the first Fresnel zone [JNHN+16]. The resulting LOS probability as a function of link distance is presented in Figure A.2.1.4.1-1 (b), which shows a linear decrease of the probability until the curve saturates at 0.2 due to the open areas between the buildings, which allows also long links with LOS. Furthermore, the result is similar to other UMi scenarios [SaRM15].
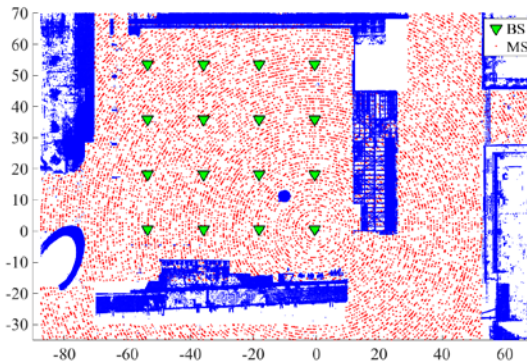
(a) BS and MS deployment in open square.
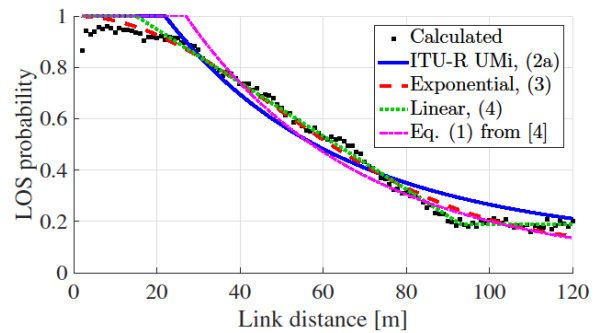
(b) LOS probability as a function of link distance.

Figure A.2.1.4.1-1: LOS probability evaluation in open square.

A.2.1.4.2 Large-scale parameters and correlation distances

There were 648 channels including LOS and OLOS links generated using point cloud based ray-tracing tool to analyze the path loss and other large-scale channel parameters in the open square. The BS antenna height was set to 6 m and the MS antenna height was set to 1 m in the simulations. In all calculations, a 30-dB threshold was used to limit the number of MPCs obtained from the ray tracer. The results show that the PLE of the close-in free

space reference distance model is 2.07 in LOS and 2.83 in LOS. Parameters in floating-intercept path loss model are also shown in Table A2.1.4.2-1.

Table A2.1.4.2-1: Parameters in floating and close-in path loss models.

LOS	Floating model	A = 20.05, B = 67.71, σ = 0.26
	Close-in model	n = 2.07, σ = 0.26, σ = 0.26
OLOS	Floating model	A = 21.50, B = 74.91, σ = 3.1
	Close-in model	n = 2.83, σ = 3.1
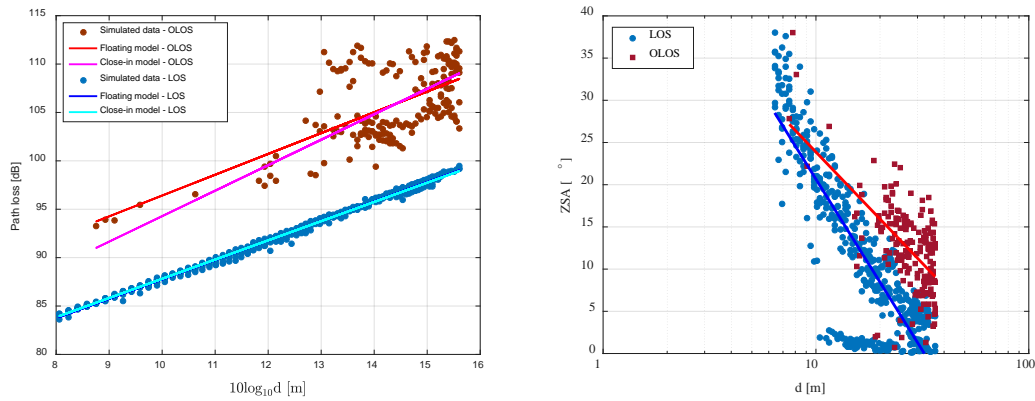
Figure A.2.1.4.2-1: Simulated path loss data and path loss models (left), and ZSA versus link distance (right) in UMi – open square.

Beside path loss, the analysis also reveals a clear dependence of ZSA on the distance in both LOS and OLOS links. Parameters for generic models and the correlation distance of all large-scale parameters are shown in Table A2.1.4.2-2 and Table A2.1.4.2-3, respectively.

Table A2.1.4.2-2: Channel model parameters for UMi – open square.

Parameters		60 GHz	
		LOS	NLOS
Delay spread (DS)	μ_{DS}	-8.35	-7.61
$\log_{10}([s])$	σ_{DS}	0.32	0.19
AoD spread (ASD)	μ_{ASD}	1.34	1.56
$\log_{10}([°])$	σ_{ASD}	0.56	0.22
AoA spread (ASA)	μ_{ASA}	0.56	1.45
$\log_{10}([°])$	σ_{ASA}	0.5	0.27
ZoD spread (ZSD)	μ_{ZSD}	0.62	0.83
$\log_{10}([°])$	σ_{ZSD}	0.25	0.26
ZoA spread (ZSA)	σ_{ZSA}	0.85	1.05
$\log_{10}([°])$	σ_{ZSA}	0.55	0.23
Shadow fading (SF) [dB]	σ_{SF}	0.26	3.10
K-factor (K)	μ_{K}	7.95	N/A
[dB]	σ_{K}	2.03	N/A

Table A2.1.4.2-3: Correlation distance (in meters) of large-scale parameters for UMi – open square.

Parameters	60 GHz	
	LOS	NLOS
Delay spread (DS)	3.0	4.0
AoD spread (ASD)	6.5	3.0
AoA spread (ASA)	1.5	6.5
ZoD spread (ZSD)	7.5	1.5
ZoA spread (ZSA)	7.0	1.0
Shadow fading (SF)	5.5	10
K-factor (K)	5.0	N/A

A.3 Indoor hotspot scenarios – office

A.3.1 China Mobile (CMCC) & Beijing University of Posts and Telecommunications (BUPT)

A.3.1.1 Multi-frequency pathloss measurements

A.3.1.1.1 Channel sounder

The measurement platform in the measurements is setup based on instruments of Rohde & Schwarz as Fig. A3.1.1-1. R&S SMW200A vector signal generator is used as transmitter at the Tx side, whose frequency ranges from 100 KHz to 40 GHz. The transmitted power before Tx antenna can be up to +30 dBm, which guarantees long enough measurement distance for indoor office scenario. At the Rx side, R&S FSW signal and spectrum analyzer is utilized and its maximum analysis bandwidth can be 320 MHz. In the measurement campaign, the center frequency of transmitter is set to multiple frequencies (3.5/6/14/20/26/28/GHz) with 250 MHz bandwidth and the PN sequence whose length is 2^16 are transmitted at a rate of 125 Mcps. Thus, this platform allows a multipath time resolution of 4 ns (double sampling) and the total time of a PN sequence is 524 us (about 0.5 ms). Double-ridged waveguide horn antennas and dipole antennas are used separately. The basic parameters of these two kinds of antennas are listed in Table A3.1.1-1. Where E and A indicate the angle of elevation and azimuth, respectively.
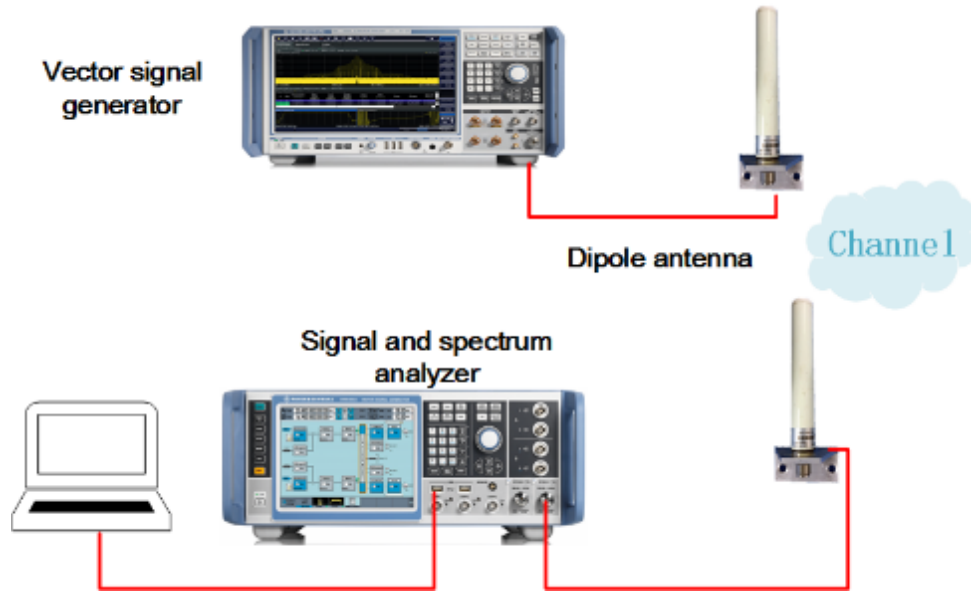
Figure A3.1.1.1-1: Channel sounder architecture.

Table. A3.1.1.1-1: Antenna parameters.

Item	Horn antenna	Omni-directional antenna
Frequency range [GHz]	0.8 to 18	3.5-18,18-40
Polarization	Vertical	Vertical
Gain [dBi]	14.1	2-5
3dB beam width(E)	-18°~ 18°	-30°~ 30°
3dB beam width(A)	-16°~ 16°	-180°~ 180°

A.3.1.1.2 Channel sounding

The channel sounding of the indoor office scenario was performed in China Mobile's office in Beijing. The layout is shown in Fig. A3.1.1.2-1. The open office includes concrete pillars, cubicles and meeting rooms, glass wall and corridor. The sounding was performed at weekends without human moving. The antennas height at transmitter and receiver are 1.6m, and located at the star point and the round spots.
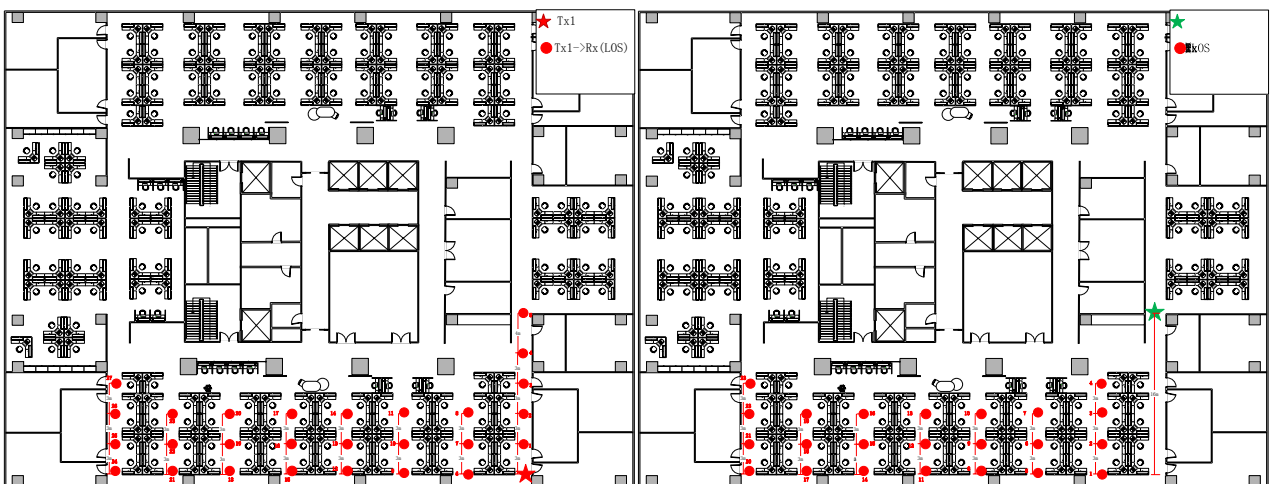
Figure A3.1.1.2-1: the layout of the indoor office scenario.

A.3.1.1.3 Findings and observations

Fig. A3.1.1.3-1 shows Path Loss model of 3.5, 6, 14, 23, 26, 28 GHz LOS and NLOS channels measured at the same locations by omni-direction antenna. Fig. A3.1.1.3-2 shows the fitting results if considering multiple center frequencies.

| (a) | (b) |
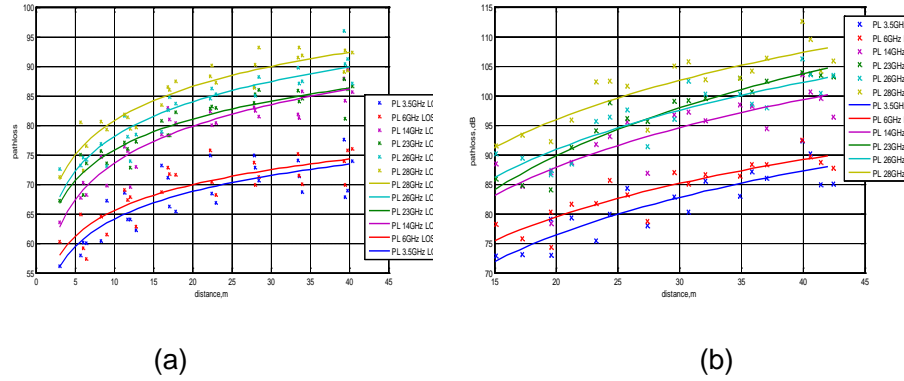
Figure A3.1.1.3-1: Path Loss model of LOS (left) and NLOS (right) case.

Table A3.1.1.3-1: Parameters in the ABG path loss model on specific frequencies in indoor office. scenario.

Scenario	Environment	Distance [m]	Model	Frequency [GHz]	PLE/α	β [dB]	SF[dB]
Indoor office	LoS	1-40	ABG	3.5	1.54	48.67	5.4665
				6	1.45	51.09	5.0497
				14	2.07	52.9	6.4726
				23	1.74	58.47	5.4219
				26	1.95	58.59	6.2883
				28	1.92	61.58	6.0239
	NLoS	15-45	ABG	3.5	3.6	29.52	5.4788
				6	3.21	37.69	4.3506
				14	3.8	38.32	6.1355
				23	4.6	29.86	6.3095
				26	3.78	41.76	5.7847
				28	3.77	46.84	5.7844

| (a) | (b) |
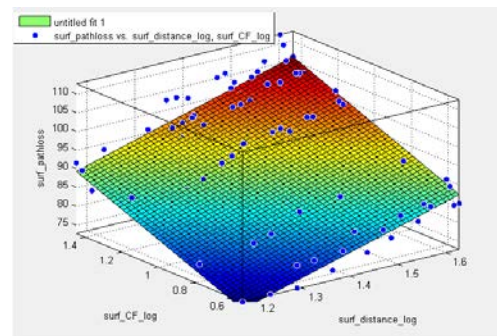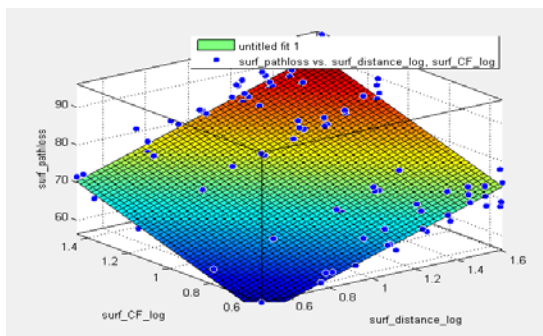
Figure A3.1.1.3-2. Multiple frequency path loss fitting LOS (left) and NLOS (right) case.

Table A3.1.1.3-1: Parameters in the ABG path loss model in indoor office scenario.

Scenario	Environment	Distance [m]	Model	Frequency [GHz]	PLE/α	β [dB]	γ
Indoor office	LoS	1-40	ABG	3.5-28	1.78	34.1	1.89
	NLoS	15-45	ABG	3.5-28	3.67	16.68	2.03

Fig. A3.1.1.3-2 shows rms delay spread at different distance in both LoS and NLoS case. The trend of rms delay according to the distance is increased and the dynamic range increases accordingly. The LOS case has a slightly higher slope of upper bound, which means the fluctuation of rms delay spread may increase faster than NLOS case. Fig. A3.1.1.3-3 shows the trends of mean values of rms delay spread will decrease while the center frequency increase.
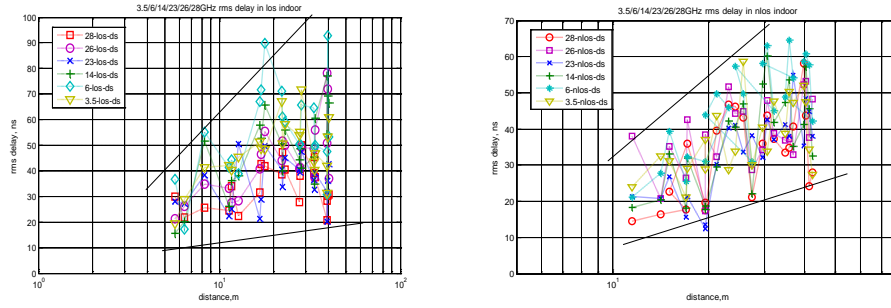
Figure A3.1.1.3-2: rms delay spread at each distance in both LoS(left) and NLoS(right) case.
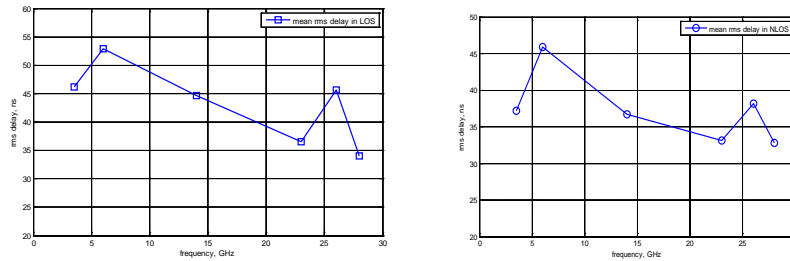
Figure A3.1.1.3-3: mean value of rms delay spread in both LoS(left) and NLoS(right) case.

A.3.1.2   Directional channel sounding

A.3.1.2.1 Channel sounder

The measurement platform in our measurements is based on Keysight's instruments. The signal generator could cover the center frequencies from 100 kHz to 44 GHz The RF modulation bandwidths is up to 1GHz. During the measurement campaign, the center frequency was set to 28 GHz with 1 GHz bandwidth and the length of waveforms is 1024. Thus, the time resolution is 1 ns and the total time of a PN sequence is 1 us. Omni-directional antenna is used at transmitter and horn antenna which could be rotated are used at receiver.

Figure A3.1.2.1-1 Channel sounder receiver and transmitter.

A.3.1.2.2 Channel sounding

The channel sounding was performed in the CMCC's office in Beijing. The transmitters location is the same as illustrated in Figure A3.2.1.2-1. At each location, horn antenna rotated in horizontal at steps of 5 degree. And the received power from each direction could be used for angle analysis. 20GHz, 23GHz and 28GHz are set as the center frequencies of the measurements. The locations of each frequency are kept the same.

A.3.1.2.3 Findings and observation

Multiple paths or clusters could be observed from initial angle measurements in Figure A3.1.2.3-1. Multiple reflection transmissions could be observed from the measurement results.
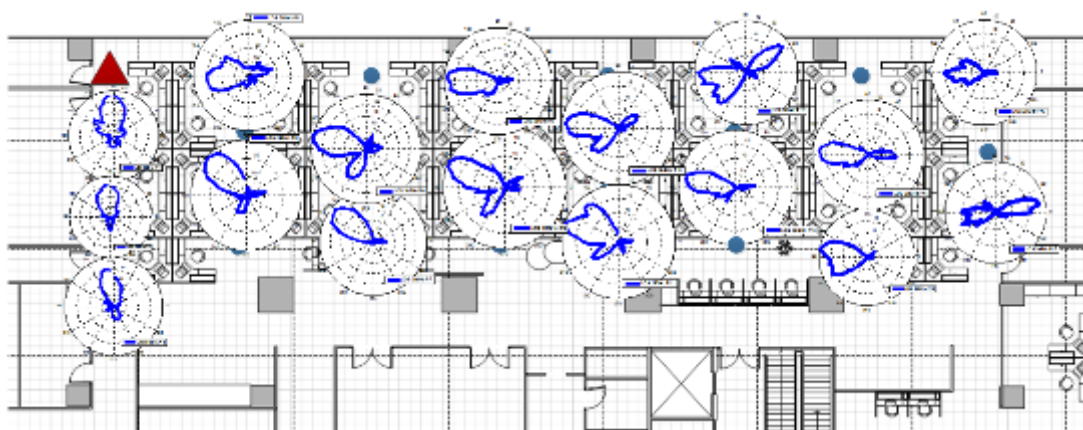
Figure A3.1.2.3-1. Angle spread of each location at 28GHz.

Angle spreads after the process of SAGE, which help to de-couple the antenna response, are list below.

Table A3.1.2.3-1: parameter of 20, 23 and 28 GHz channels in an indoor office scenario.

Freq.	20GHz	23GHz	28GHz

LOS/NLOS	LOS	NLOS	LOS	NLOS	LOS	NLOS
Mean(^{o})	16.76	22.63	14.74	36.21	16.70	24.80
std (^{o})	4.15	9.52	4.87	14.05	4.26	8.34
Mean,log10(^{o})	1.21	1.32	1.15	1.53	1.21	1.37
Std,log10(^{o})	0.11	0.16	0.13	0.16	0.11	0.13

A.3.2 Ericsson

A.3.2.1   15 GHz measurements

A.3.2.1.1 Channel sounder

The channel sounder described in section A.1.3.1 have been used also for indoor measurements.

A.3.2.1.2 Measurements

The measurements were performed in an indoor exhibition area of size approximately 30 by 55 m containing both open areas and some corridors and smaller rooms, see Figure A3.2.1.2-1. In these measurements the transmission point TP1 was used where the green arrow indicated the pointing direction of the sector antenna which was installed at a height of 3.7 m. The terminal was moved along the route marked in blue using an electric scooter. Both LOS and NLOS conditions are experienced along this route. The terminal antenna height was 1.6 m.
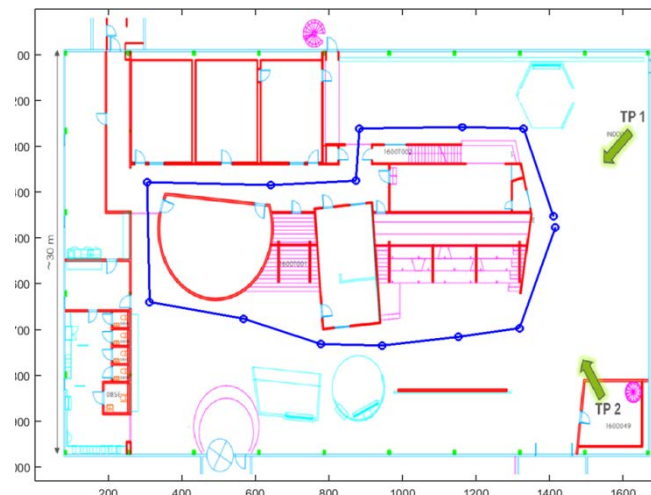
Figure A3.2.2-1

4x4 MIMO channel estimates with 100 MHz bandwidth and 1 MHz resolution was continuously recorded along the measurement route. These were transformed from the frequency to the delay domain and power averaged over all combinations of Tx and Rx antennas to form power delay profile estimates. In total about 50000 PDPs were logged. The rms delay spread was estimated using a 30 dB threshold in the PDP and only measurements with at least 20 dB SNR were included in the subsequent analysis.

A.3.2.1.3 Findings and observations

The rms delay spread cdfs in LOS and NLOS are presented in Figure Y, and the corresponding parameters are summarized in Table A3.2.1.3-1. The range of values compare quite favourably with the Indoor Hotspot model of the ITU-R M.2135 model.

15 GHz indoor measurements
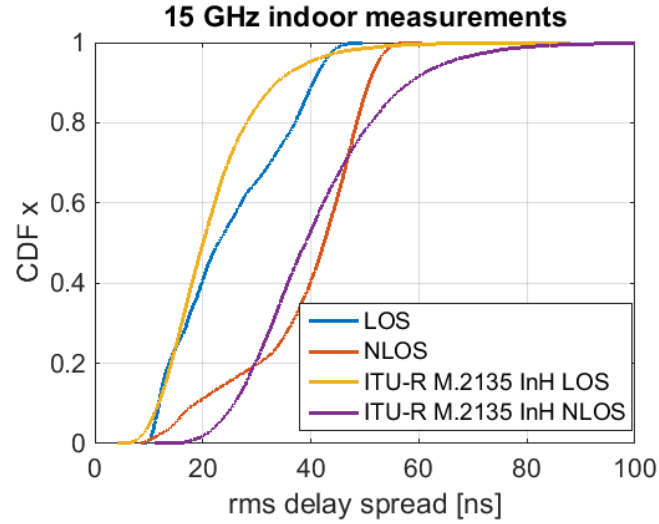
Figure A3.2.1.3-1: RMS delay spread CDFs from the 15 GHz indoor measurements. The CDFs for the ITU-R M.2135 Indoor hotspot model are provided for comparison.

Table A3.2.1.3-1: Delay spread parameters from the 15 GHz indoor measurements.

|	LOS	NLOS
Median delay spread [ns]	22.9	42.4
μ_{DS} **[log10(s)]**	-7.65	-7.43
ε_{DS} **[log10(s)]**	0.20	0.17

A.3.2.2   Multi-frequency measurements

A.3.2.2.1 Channel sounder

The channel sounder described in section A.1.3.2.1 have been used also for indoor measurements.

A.3.2.2.2 Channel sounding

The measurements are described in [R1-161688].

A.3.2.2.3 Findings and observations

The findings and observations are described in [R1-161688].

A.3.3 Huawei Technologies

A.3.3.1   Channel sounder

A dual-band ultra wideband channel sounder is designed to measure the 28G and E-band channel model. The sounder systems base on a vector network analyzer (VNA) from Rohde & Schwarz, which provides an intermediate frequency (IF) signal and sampling receive IF signal from down converter.

In our configuration, the frequency increases linearly in the measurement bandwidth with an increment of 10MHz. A local oscillator (LO) frequency is generated by an integrated frequency synthesizer of Agilent. The LO frequency is then sextupled to around 73GHz by a frequency converter for E-band. Meanwhile, the LO frequency is doubled for 28G. After that, the measurement sequence of IF signals generated by the VNA is mixed with the LO signal one by one to generate a RF signal ranging from 72GHz to 74GHz for E-band and 27GHz to 29GHz for 28G, which is then received by the Rx. When the measurements for the whole bandwidth at some posture finish, the azimuth and elevation angles or the location of Rx is changed. And the process mentioned repeats to acquire the data for other positions. Vertically polarized horn antennas with 25dBi gain and 10° half power beam width are used for E-band and 28GHz in this measurement. The dual-band UWB sounder systems are calibrated with a

back-to-back measurement which connects the transmitter and receiver through 50 dB attenuator. A channel sounder system for measurement is demonstrated as figure A.3.3.1-1.

Figure A3.3.1-1: Huawei's channel sounder.

A.3.3.2   Channel sounding

Huawei's channel measurement for Open office scenario was implemented at U5-1-A building at Huawei institution in Chengdu. The campaign contains more than 50 Tx-Rx positions in office scenario Overall. The height of Tx antenna is about 2.8m while the Rx is setup to about 1.5m for the indoor case. The cable driven by rubidium clock helps to synchronize the Tx and Rx. The office is about 15 x 45 m^2 and composed of desk, chair and clapboard. Computer, screen and plants are also in the office. The locations of Tx and Rx are shown in Fig. A3.3.2-1 for LOS and NLOS scenarios respectively. Location of Tx was configured at end of the office area to acquire a maximum length about 35m. The Tx for LOS scenario was chosen as marked with a green triangle and the positions of Rx (marked with green five-pointed stars) were located at the straight line. In NLOS scenario, the Tx site (marked with a red triangle) was placed at one corner of the office area to ensure that the LOS path was obstructed by the wall and the Rx sites (marked with red squares) were chosen randomly at the NLOS area.

Table A3.3.2-1: Channel Sounder System parameters.

Configuration	Open Office	
	LOS	NLOS
Tx Height	2.8 m	2.8 m
Rx Height	1.5m	1.5m
TX Ant Gain	10dB	10dB
Rx Ant Gain	25dB	25dB
Tx Antenna	Horn Ant of 55°	Horn Ant of 55°
Rx Antenna	Horn Ant of 10°	Horn Ant of 10°
Polarization	Vertically	Vertically
Central Frequency	28G/73 GHz	28G/73 GHz
Sweep point	2001	2001
Bandwidth	2 GHz	2 GHz
Tx Locations	1	1
Rx Locations	20	30
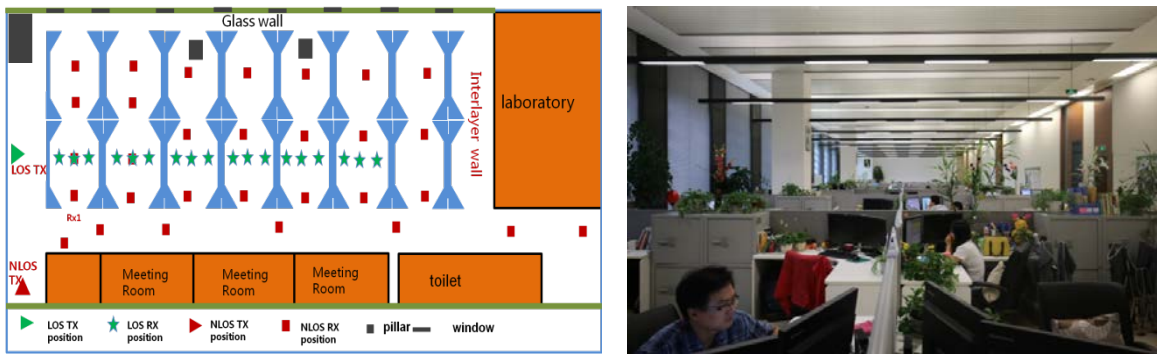
Figure A3.3.2-1: Huawei channel sounding in Open Office.

A.3.3.3   Channel simulations

The channel simulation is based on the Ray-Tracing theory, which implements the electromagnetic wave radiation by the ray-based approach. It models the physical characteristics of the geometry environment, performs the electromagnetic calculations, and evaluates the signal propagation characteristics, such as, power, time of arrival, DOAs/AOAs and so on; the calculations are made by shooting rays from the transmitters, and propagating them through the defined environment input, like, walls, grounds, object faces, diffractions around objects, and transmission through features.

Large and small scale parameters would be calculated by the data collected from the channel simulations, which should be calibrated by the measurement results in the reality.

A.3.3.4   Findings and observations

A.3.3.4.1 Antenna de-coupling

The final channel model should be independent of any specific antenna type, Reconstruction of omni-directional channel based on decoupling of directional antenna measurements; Decoupling of directional beam-based spatial sampling channel model method generates better channel model than Summing-Power-based model and synthesized-PDP-based model. The decoupling method can eliminate the antenna pattern effects from directional antenna measurements, and the pattern-independent Omni channel model can be reconstructed. From measurement show that without antenna decoupling, both large- scale and small-scale channel model will be antenna dependent. Pathloss channel modelling based on total received power and angular spread should be obtained after decoupling.

Raw data   after reconstruction
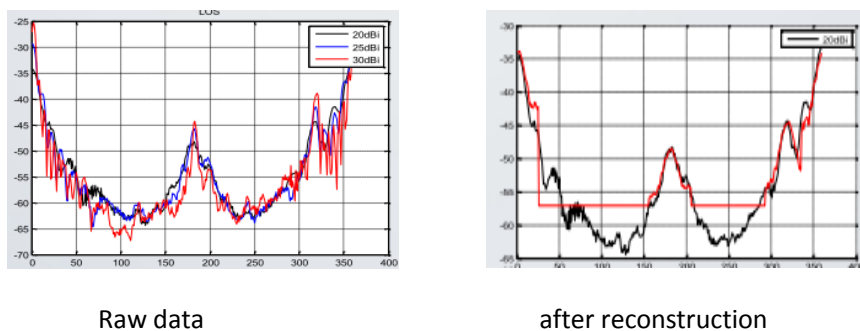
Figure A.3.3.4.1-1

A.3.3.4.2 Multi zone pathloss modeling

It is not quite accuracy to predict the propagation loss with all sample in a single linear fitting approach. With limited complexity increasing, such as, sector/zone grouping, the model predict accuracy can be increased significantly. 72GHz and 28GHz large-scale pathloss were measured and analyzed for indoor office scenario. Multi Zone model was investigated for indoor office. At least two zones can be observed for the measured distance range. The std. deviation and the prediction error can be adopted as model evaluation criteria.
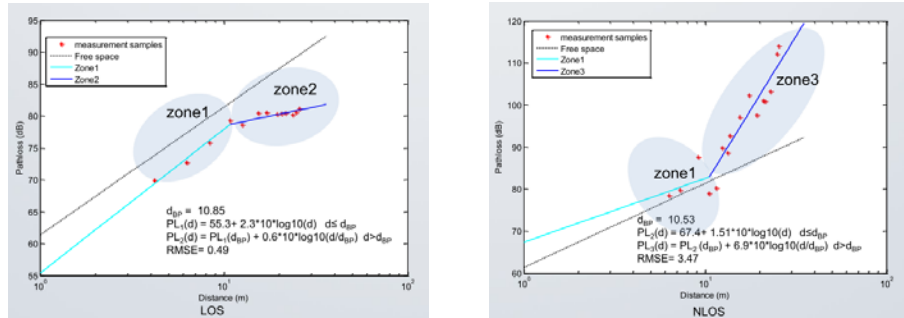
Figure A.3.3.4.2-1

A.3.3.4.3 Penetration and O2I

The measurement of O2I and penetration in InH scenario show many interesting and important result. From the measurement show absorbing material around door is important to eliminate the impact of environment .The penetration is closely related to the material and the penetration loss of full spectrum present periodic fluctuation, the fluctuation of homogeneous materials is more regular than more complex material, such as wooden door.

Two layer glass   wooden door
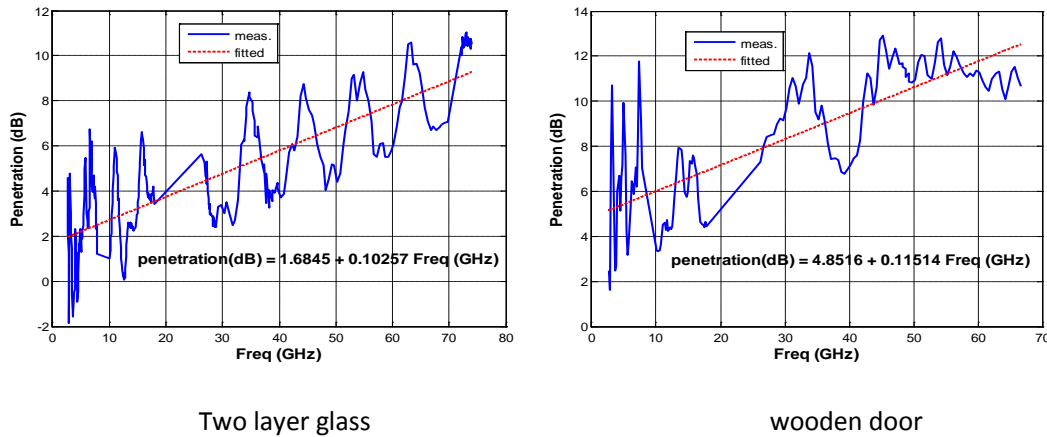
Figure A.3.3.4.3-1

A.3.3.4.4 Impact of measurement bandwidth on large-scale parameters

From Figure A.3.3.4.4(a) show delay spread shrinks with increased bandwidth. Minor difference between 28GHz and 73GHz at each bandwidth. The delay spread trends to a constant beyond 400MHz. Figure A.3.3.4.4-1(b) show AoA spread keeps almost stable with increased bandwidth. 2. Minor difference between 28GHz and 73GHz at each bandwidth. From figure A.3.3.4.4-1(c) show ZoA spread keeps almost stable with increased bandwidth. Minor difference between 28GHz and 73GHz at each bandwidth.

(a)   (b)   (c)
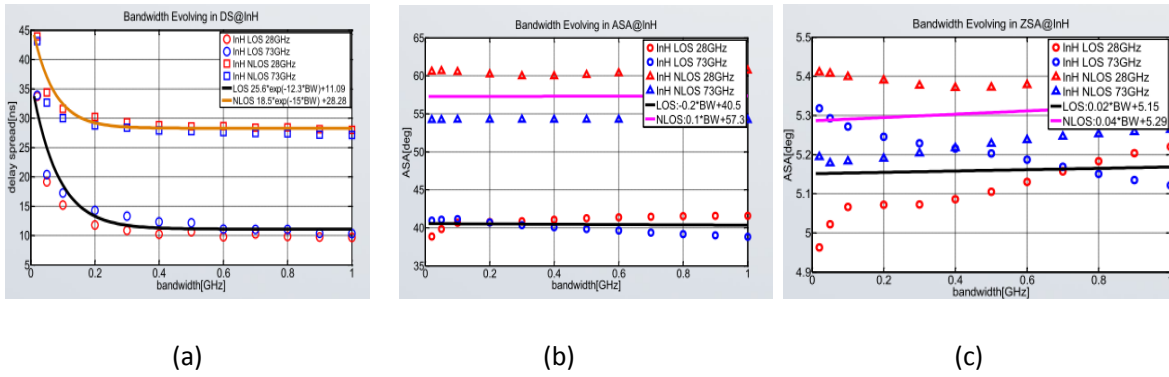
Figure A.3.3.4.4-1

A.3.3.4.5 VA-SCM

The reference channel model in HFB need to support variant angles when user terminal is moving. The reference channel model can be used together with beam-forming and beam-tracking algorithms in simulations of mobile communications in HFB, including system-level simulation and link-level simulation; In case of 2D channel model, the time-varying angles in the reference model include angle of arrival (AoA) and angle of departure (AoD). In case of 3D channel model, the time-varying angles include AoA, AoD, zenith of arrival (ZoA), and zenith of departure (ZoD). The approach in this proposal is to linearly approximate the time-varying angles suppose receiver is moving in a short range where spatial consistency is guaranteed. Variant angles are included based on 3GPP SCM model, but other channel models are also possible to include variant angles with the linear approximation method.

A.3.4 NTT DOCOMO, INC.

A.3.4.1   Measurement of path loss

A.3.4.1.1 Measurement system

Table A3.4.1.1-1 shows specifications of measurement equipment. Transmitter sends continuous wave (CW) and received power is recorded at receiver.

Table A3.4.1.1-1: Specifications of measurement equipment and parameters.

| Parameters		Values
Tx (BS)	Frequency	19.85 GHz
	Power	6.1 dBm
	Antenna	Sleeve antenna
	Antenna height	2.6 m
Rx (MS)	Antenna	Sleeve antenna
	Antenna height	1.5 m

A.3.4.1.2 Measurement campaign

Path loss measurements are carried out in an office of NTT DOCOMO R&D center in Yokosuka, Japan. Figure A3.4.1.2-1 shows measurement site and measurement route. Table A3.4.1.1-1 gives the measurement parameters. Measurement was performed in only LOS environment. In the measurements, continuous wave (CW) is transmitted from a BS antenna, and the received power level is recorded at the MS while the MS is moving. The BS antenna height is set to 2.6 m. The MS antenna is established on a hand truck with the height of 1.5 m. The antennas used for the BS and MS are sleeve antennas. The measurement frequency is 19.85 GHz. The

distance between the BS and MS is from 3 to 25 m. Path loss is obtained every 0.1 m by taking median value of received power levels within 1 m (before and after 0.5 m).

floor-to-ceiling height: 2.7 m
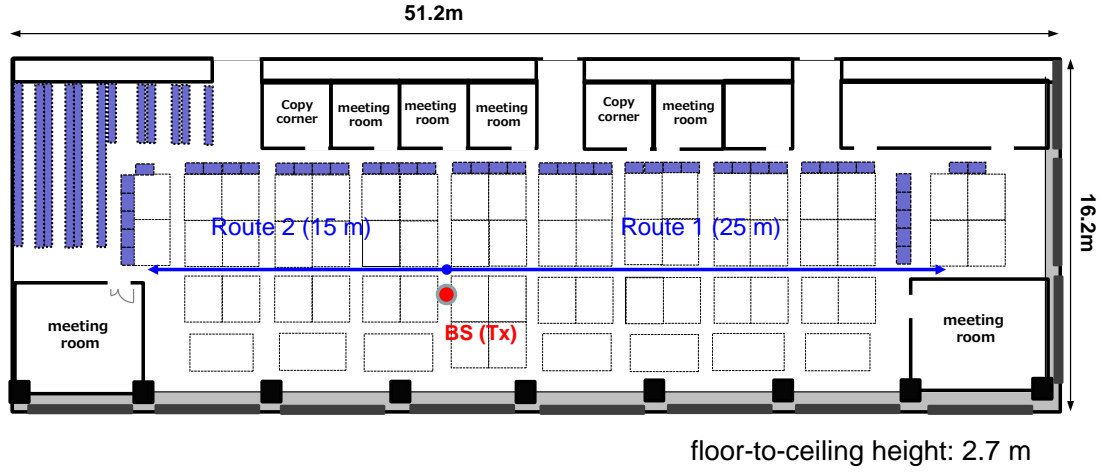
Figure A3.4.1.2-1: Measurement site and route.

A.3.4.1.3 Findings and observations

Figure A3.4.1.3-1 shows path loss over distance from BS to MS. Moreover, regression analysis is applied to the measurement data by using CI and regression results, which are summarized in Table A3.4.1.3-1.

CI model is expressed as

$$PL(d) = 10 n \log_{10}(d) + \text{FSPL}(f_C, 1) + \chi_\sigma \qquad \text{(A3.4.1.3-1)}$$

$$\text{FSPL}(f_C, d) = 32.44 + 20 \log(f_C) + 20 \log(d) \qquad \text{(A3.4.1.3-2)}$$

where *PL* is path loss in dB, *d* is distance from BS to MS in meters, f_c is frequency in GHz, and χ_σ is shadow fading factor in dB, which is log-normal distribution with standard variation of σ_{SF}.
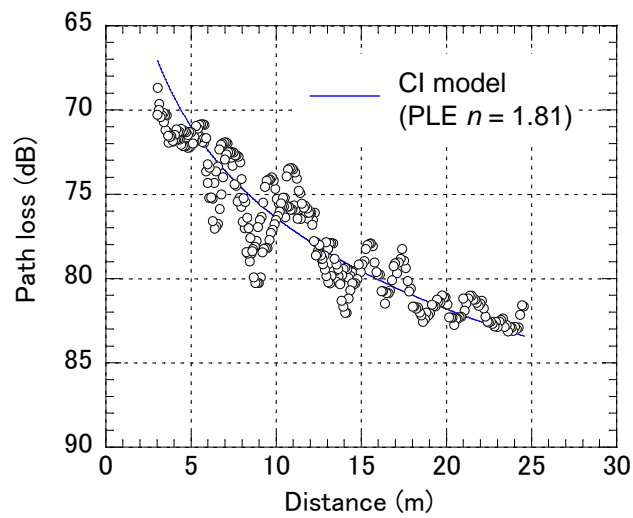
Figure A3.4.1.3-1: Path loss vs. distance.

Table A3.4.1.3-1: Regression analysis.

		Parameters	
		n	σ_{SF} (dB)
LOS	CI	1.81	1.7

A.3.4.2   Measurement of channel model parameters

A.3.4.2.1 Channel sounder

Figure A3.4.2.1-1 shows the configuration and Table A3.4.2.1-1 gives the specifications for the channel sounder for the 20 GHz band. On the transmitter (Tx) side, Orthogonal Frequency-Division Multiplexing (OFDM) signals with a 50 MHz bandwidth at the 20 GHz band are generated and transmitted from a 2.4 dBi sleeve antenna. The transmission power is 30 dBm. On the receiver (Rx) side, a 19.1 dBi horn antenna with a 20 degree half-power beamwidth is used. After down-converting the received RF signals to an intermediate frequency (IF) band, the complex amplitudes of the subcarriers (transfer functions) are stored in a PC. The Power Delay Profiles (PDPs) are obtained by converting stored data into channel impulse responses.
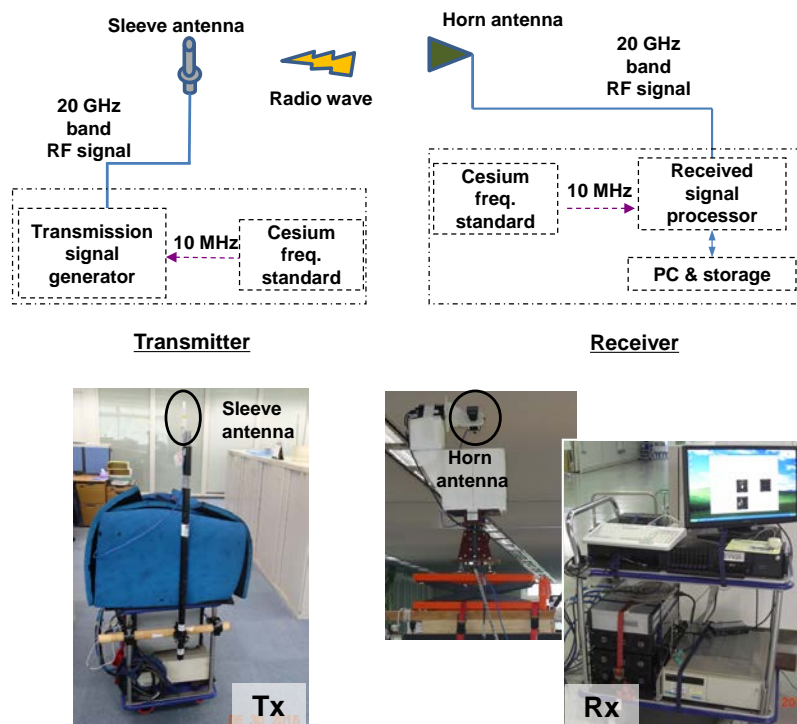
Figure A3.4.2.1-1: The channel sounder architecture.

Table A3.4.2.1-1: The channel sounder specifications.

Center frequency	19.85 GHz
Bandwidth	50 MHz
Transmission signal	OFDM
Number of subcarriers	449
Transmission power	30 dBm
Tx antenna	Sleeve (2.4 dBi)
Rx antenna	Horn (19.1dBi: 20 deg. HPBW)

A.3.4.2.2 Channel sounding

The channel sounding for indoor hotspot scenarios was performed in an office of NTT DOCOMO R&D center in Yokosuka, Japan. The office size is 51.2 m × 16.2 m × 2.7 m. There are wooden or metal desks and drawers, chairs, and lockers arranged in the office. There are also some meeting rooms and office equipment rooms that are surrounded by glass with metal frames and metal doors. The windows are glass with aluminum frames. Nearby the windows, there are some concrete pillars.

In measurements, the transmitter of the channel sounder was considered to be the mobile station and was located at points A1-A6, B1-B6, C1, C4, C5, D1, and D4 as shown in Figure A3.4.2.2-1. The height of the sleeve antenna (Tx) was 1.5 m. The receiver of the channel sounder was considered to be the indoor base-station (BS) and was located at point P0 with the antenna height of 2.3 m. At each Tx location, we rotated the horn antenna in both azimuth and elevation and measured five PDPs at each angle combination on the Rx side. At A3, the azimuth angle of the horn antenna was changed from -180 degrees to +180 degrees with 1 degree step, and the elevation angle was changed from -80 degrees to +50 degrees with 1 degree step. For other Tx locations, the range and resolution of the azimuth angle was not changed, but the elevation angle was changed from -50 degrees to +50 degrees with a 10 degree step. Here, the azimuth and elevation angles of the horn antenna were defined as shown in Figure A3.4.2.2-2. There were no people moving in the office during the measurements. The antennas were kept within line-of-sight (LOS). The data acquisition was performed automatically.
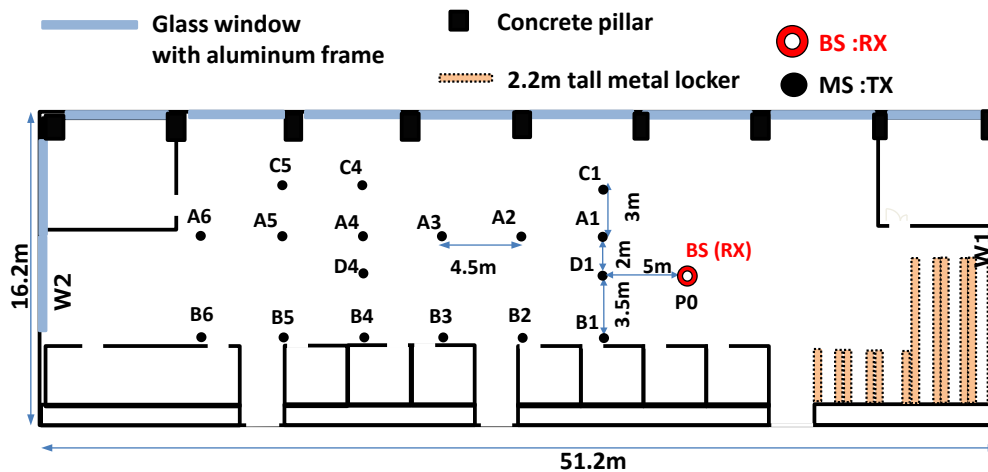

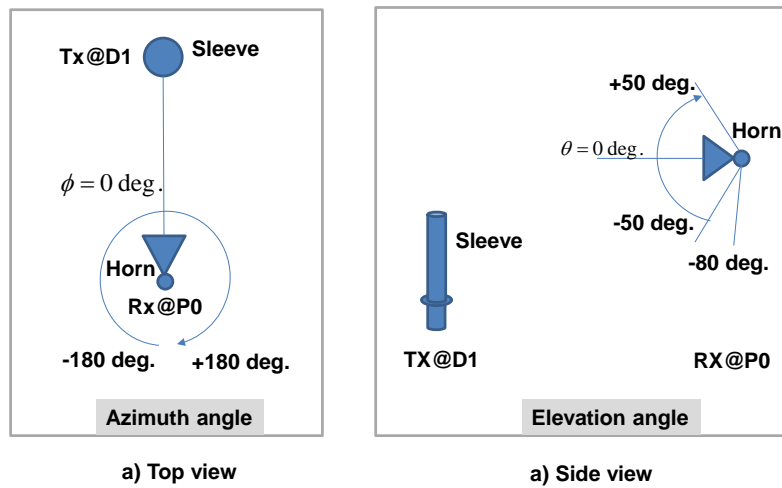**Figure A3.4.2.2-1: Channel sounding in Office.**
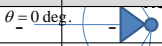
a) Top view   a) Side view
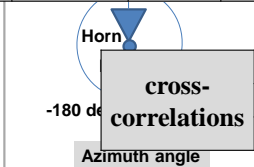
Figure A3.4.2.2-2: Definition of azimuth /elevation angle at BS.

A.3.4.2.3 Findings and observations

Table A3.4.2.3-1 shows the measurement results for indoor hotspot scenarios or office. Here, the K-Power-Mean method was used to cluster multipaths. The delay times, azimuth angles, elevation angles of cluster centroids were used to obtain DS, ASD, ZSD at each position.

Table A3.4.2.3-1: Measurement results for indoor hotspot scenarios-office.
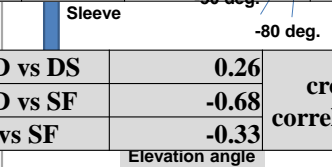
TX positions	Tx-Rx distances	DS[ns]	ASD [deg.]	ZSD [deg.]	# of Paths	# of Clusters	#of Rays per Cluster	Cluster DS [ns]	Cluster ASD [deg.]	Cluster ZSD [deg.]
D1	5	57.3	58.7	1.2	61	8	7.6	42.5	16.2	6.1
A1	5.39	59.4	64.2	5.3	70	8	8.8	41.1	14.2	5.7
B1	6.1	42.5	75.2	7.6	72	5	14.4	51.0	25.1	10.1
C1	7.07	36.9	64.7	0.0	65	7	9.3	43.0	35.7	0.0
A2	9.71	46.4	52.9	1.3	52	9	5.8	29.8	15.3	5.4
B2	10.12	49.0	95.8	1.9	80	7	11.4	56.1	19.1	7.2
A3	14.14	57.5	46.2	4.3	54	8	6.8	36.7	23.6	2.6
B3	14.43	46.7	67.4	1.6	67	6	11.2	41.2	28.7	1.8
D4	18.5	36.1	62.9	0.4	82	5	16.4	60.6	26.5	2.1
A4	18.61	58.0	58.9	1.2	77	6	12.8	62.0	17.7	3.3
B4	18.83	27.3	59.0	0.3	70	5	14.0	60.2	30.1	3.8
C4	19.16	45.0	61.8	1.0	82	7	11.7	47.6	14.5	2.3
A5	23.09	39.8	41.4	0.1	72	6	12.0	48.7	22.6	2.2
B5	23.26	55.5	89.0	0.4	86	7	12.3	33.6	17.5	2.7
C5	23.54	40.2	53.2	0.3	80	7	11.4	43.9	16.7	1.6
A6	27.57	61.6	69.2	0.5	87	9	9.7	46.7	19.0	2.4
B6	27.72	61.2	82.9	1.3	92	9	10.2	53.6	16.0	2.8
	Mea.	48.3	64.9	1.7	73.5	7.0	10.9	47.0	21.1	3.6
	Std.	10.0	13.9	2.0	11.0	1.3	2.7	9.2	6.1	2.4
log10	μ	-7.33	1.8	0	-	-	-	-	-	-
	σ	0.1	0.09	0.48	-	-	-	-	-	-

cross-correlations	ASD vs DS	0.26	cross-correlations	ZSD vs SF	0.02
	ASD vs SF	-0.68		ZSD vs DS	0.24
	DS vs SF	-0.33		ZSD vs ASD	0.1

A.3.5 New York University (NYU)

A.3.5.1   Channel sounder

A set of 28 GHz and 73 GHz ultrawideband sliding correlator (or swept time delay cross correlation (STDCC)) channel sounders with superheterodyne architectures with identical baseband hardware and relatively similar intermediate frequency (IF) and radio frequency (RF) stages are used to measure the indoor office environment by the NYU WIRELESS research center [DSMC+14, DESR15, NMCS+13]. The baseband probing signal is a 400 megachips-per-second (Mcps) pseudorandom binary sequence (PRBS) generated via an 11-bit linear feedback shift register (LFSR) with digital circuitry. For both the 28 GHz and 73 GHz systems, the baseband signal is modulated to an IF between 5 GHz and 6 GHz that then entered custom-designed RF front-end up-converter boxes which then modulates the IF broadband signals to RF carrier frequencies of 28 GHz and 73 GHz. At the receiver side, the incoming ultradwideband 800 MHz RF null-to-null bandwidth signal is downconverted with custom-built hardware to an IF between 5 GHz and 6 GHz and is then subsequently demodulated into its I and Q baseband components. Both the I and Q baseband signals are then mixed with a PRBS sequence identical to the transmitted signal, but at a slightly slower rate of 399.95 Mcps, which produces an impulse when the codes are aligned in time. The subsequent I and Q correlated voltages are then low pass filtered and digitally sampled with high-speed oscilloscope. The digital I and Q signals are then squared (I^2+Q^2) to generate a raw power delay profile (PDP) of the channel for further processing. For each acquisition, 20 consecutive PDPs are averaged to improve processing gain and to reduce noise fluctuations.

In order to overcome high path loss at millimeter-wave frequencies, high-gain directional horn antennas are employed at the transmitter (TX) and receiver (RX) to increase link-margin, and this also allows for capturing high resolution angles of departure (AOD) and angles of arrival (AOA). The horn antennas are attached to the up and downconverter hardware which are subsequently mounted on highly-precise FLIR motion control gimbals for precise positing in the azimuth and elevation planes. The 28 GHz measurements use 15 dBi gain horn antennas at the TX and RX while the 73 GHz measurements use 20 dBi gain horn antennas at the TX and RX, with maximum TX output power of 23.9 dBm and 12.1 dBm at 28 GHz and 73 GHz respectively. Table A3.5.1-1 provides additional specifications and details pertaining to the 28 GHz and 73 GHz channel sounders for indoor office measurements.

Table A3.5.1-1: NYU Channel Sounder for Indoor Office Measurements [MCRS+15].

Carrier Frequency	28 GHz	73 GHz
Probing Signal	11th order PRBS (length=2047)	
TX PN Code Chip Rate	400 Mcps	
TX PN Code Chip Width	2.5 ns	
RX PN Code Chip Rate	399.95 Mcps	
Slide Factor	8000	
Digitizer Sampling Rate	2 Megasamples / second	
RF Bandwidth (Null-to-Null)	800 MHz	
TX/RX IF Frequency	5.4 GHz	5.625 GHz
RX/RX LO Frequency	22.6 GHz	67.875 GHz
Center Frequency	28 GHz	73.5 GHz
TX/RX LO Power	10 dBm	
Max. TX Output Power	23.9 dBm	12.1 dBm
TX/RX Antenna Gain	15 dBi	20 dBi
TX/RX Azimuth HPBW	28.8°	15°
TX/RX Elevation HPBW	30°	15°
Max. TX EIRP	38.9 dBm	32.1 dBm
TX Antenna Height	2.5 m	
RX Antenna Height	1.5 m	
Max. Measureable Path Loss	152 dB	162 dB
Multipath Time Resolution	2.5 ns	
TX Polarization	Vertical	
RX Polarization	Vertical / Horizontal	

A.3.5.2 Channel sounding

The channel sounding measurements for indoor office were conducted in the NYU WIRELESS research center on the 9th floor of 2 MetroTech Center in downtown Brooklyn, New York, which is a 10-story building constructed in the early 1990's with tinted windows and steel reinforcement between each floor. Five TX locations and 33 RX locations were selected, resulting in measurements from 48 TX-RX location combinations that had 3D T-R separation distances ranging from 3.9 m to 45.9 m, with RX locations chosen in LOS and NLOS environments (the floor dimensions were 35 m × 65.5 m). The 10 LOS measurement locations had 3D distances ranging from 4.6 m to 21.3 m, and the 38 NLOS measurement locations had 3D distances that ranged from 3.9 m to 45.9 m. Figure A3.5.2-1 shows a map of the five TX locations, the 33 RX locations (some were used for multiple transmitters), and basic descriptions of the surrounding obstructions. The TX locations were selected to study specific indoor environments such as open- and closed-plan settings, indoor hotspots, hallways, corridors, and office spaces. Measurements at 28 GHz and 73 GHz were conducted at identical locations and for each TX-RX location combination (See Table A3.5.2-1) 16 unique antenna azimuth sweeps were performed. An antenna sweep consisted of fixed TX and RX antenna in the elevation plane, with either a fixed TX or RX antenna in azimuth, while the other was rotated in the azimuth plane at discrete HPBW increments which for each position a PDP was recorded. Overall, 8 sweeps were conducted for vertical-to-vertical (V-V) polarized antennas (2 TX and 6 RX sweeps) and 8 sweeps were conducted for vertical-to-horizontal (V-H) polarized antennas (2 TX and 6 RX sweeps). TX antenna heights were always set to 2.5 m above the floor and RX antennas heights were set to 1.5 m above the floor.
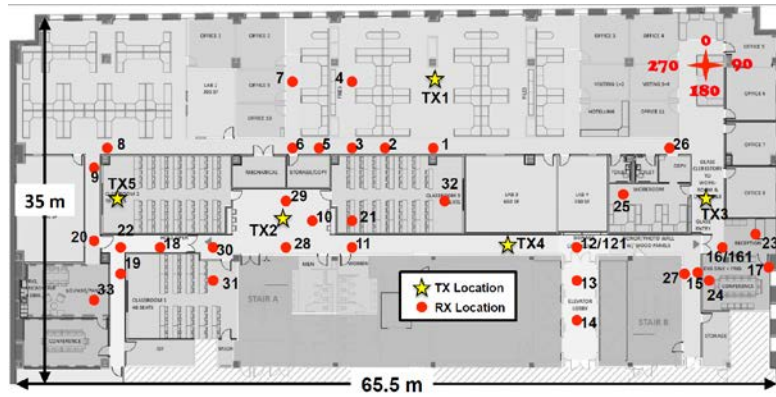
Figure A3.5.2-1: Map of 2 MetroTech 9th floor at NYU. The RX 121 and RX 161 locations are identical to the RX12 and RX16 locations; however, the glass door near RX16 was propped open for the RX121 and RX161 measurements [DSMC+14, MCDR16].

Table A3.5.2-1: TX and RX measurement locations for 28 GHz and 73 GHz indicating locations with outages [RSMZ+13].

TX ID	RX IDs	T-R Dist. (m)
1	1-9	6.4 ≤ d ≤ 32.9
2	10, 11-22, 161	4.1 ≤ d ≤ 45.9
3	15, 17, 23-27	5.3 ≤ d ≤ 8.7
4	11-16, 18, 28, 121, 161	7.1 ≤ d ≤ 33.0
5	8, 19, 28-33	3.9 ≤ d ≤ 31.2

A.3.5.3 Findings and observations

A.3.5.3.1 Frequency dependency of path loss in indoor office environment

For multi-frequency path loss models in the indoor office environment, path loss attenuation tends to increase as frequency increases in NLOS environments as indicated by the *b* parameter (frequency-dependence term) in the CIF model and the *γ* parameter in the ABG model for omnidirectional path loss as displayed in Table A3.5.3.1-1 [DSMC+14]. The CI and CIF models for both indoor and outdoor measured data have more stability over various frequencies and use cases when compared to the ABG model as demonstrated in [Sun16]

Table A3.5.3.1-1: 28 GHz and 73 GHz multi-frequency combined polarization CI, CIF, and ABG omnidirectional path loss models for NLOS environments [DSMC+14].

28 GHz and 73 GHz NLOS Multi-Frequency Combined Polarization Omnidirectional CIF and ABG Path Loss models with $d_{0=1m}$			
n	*b*	f_0	*σ* [dB]
3.4	0.22	49 GHz	11.9
α	*β*	*γ*	*σ* [dB]
2.9	4.5	4.1	11.6

A.3.5.3.2 Omnidirectional co- and cross-polarization path loss in LOS and NLOS environments at 28 GHz and 73 GHz

Both 28 GHz and 73 GHz CI path loss models yielded path loss exponents lower than Friis' free space path loss in the LOS indoor environment (n = 1.1 at 28 GHz, n = 1.3 at 73 GHz). This observation is attributed to a waveguiding effect down hallways and in closed corners in addition to constructive interference in the indoor office propagation environment.

Omnidirectional path loss models from co- and cross-polarized antenna measurements revealed larger cross-polarization discrimination factors at 73 GHz than at 28 GHz in both LOS and NLOS environments, likely increased diffuse scattering of weaker paths at 73 GHz that were not detected in the cross-polarization measurements compared to 28 GHz which has a larger wavelength than 28 GHz. The CIX model [DSMC+14] indicated 14.0 dB and 22.8 dB cross polarization discrimination factors (XPDs) in LOS environments at 28 GHz and 73 GHz, respectively, and 10.4 dB and 15.4 dB XPDs in NLOS at 28 GHz and 73 GHz, respectively, as shown in Figures A3.5.3.2-1 a) and b). The large cross-polarization isolation in LOS environments is encouraging for future dual-polarization millimeter-wave communications systems in indoor environments.
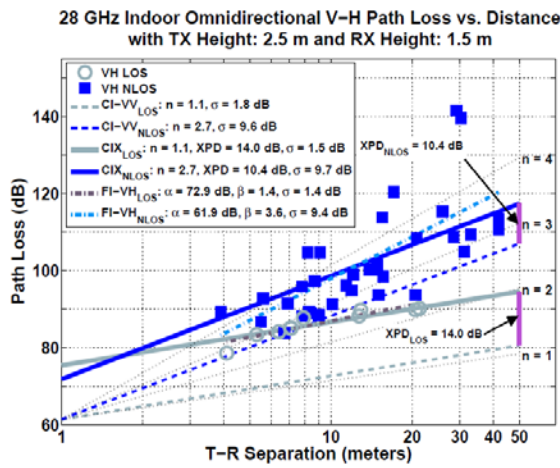
(a) 28 GHz V-H indoor omnidirectional path loss
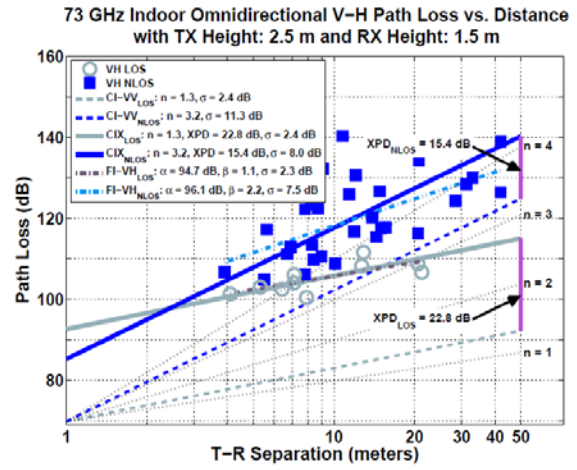
(b) 73 GHz V-H indoor omnidirectional path loss

FIGURE A3.5.3.2-1: 28 AND 73 GHZ INDOOR OMNIDIRECTIONAL PATH LOSS FOR V-H ANTENNAS [DSMC+14].

Additional indoor measurements were conducted to study spatial and temporal characteristics at 60 GHz in a typical office environment [XUKR02]. Durgin *et al.* also studied radio path loss and penetration in and around homes at 5.85 GHz in a suburban environment for outdoor transmitters at a height of 5.5 m and at distances ranging from 30 m to 210m from the homes [DURX02, DUXR97]. Furthermore, Anderson *et al.* measured propagation path loss and delay spreads in an indoor office environment to study partition loss for wideband propagation for distances ranging from 3.5 m to 27.4 m [ANRA04, Ande02, ARBV+02].

A.4   Indoor hotspot scenarios – shopping mall

A.4.1 Aalto University

A.4.1.1   Channel sounder
Please refer to A.1.1.1.

A.4.1.2   Channel sounding
Aalto's channel sounding in a shopping mall scenario was conducted in Sello, Espoo, Finland. The sounding covers first, third and fourth floors for the same-floor and inter-floor channel measurements. Photos of the sounding site are shown in Fig. A4.1.2-1; an open area with glass ceiling is surrounded by corridors and shops, and has four floors. The ceiling of the open area is about 20 m high above the ground floor. Table A4.1.2-1 summarizes the number of links measured in the campaign; about half of the antenna locations are common among the channel sounding at three different frequencies, making it possible to compare channels at different frequencies. The separation distance between the transmit and receive antennas vary from 1.5 to 60 m. A blocked-LOS scenario due to pillars represents the OLOS channel, while the NLOS is defined by a total obstruction of the LOS due to antennas located in different corridors or shops. The transmit and receive

antennas are 2 m above the floor in 2014 campaigns, while they are both at 3 m in the 2015 campaigns. All measurements were performed during a day, hence there are people moving around in the channel sounding.

(a) Photo of the sounding site.

(b) Point cloud environmental description of the sounding site; the yellow and red dots represents antenna locations where channel simulations were performed.
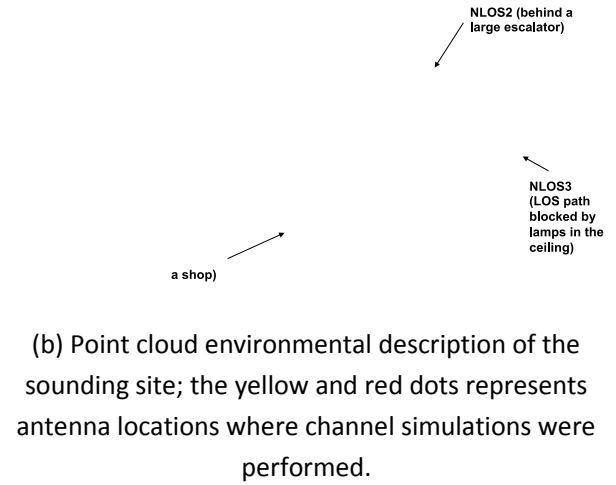
Figure A4.1.2-1: Aalto's channel sounding and simulations in a shopping mall.

Table A4.1.2-1: The number of links measured at each frequency band in Aalto's shopping mall measurements.

| 60GHz	30GHz	15GHz
2014 campaign 0: 33 LOS (1st floor) 7 LOS + 14 OLOS (3rd floor) 2015 campaign (February): 5 LOS + 2 OLOS (3rd + 4th floors)	2015 campaign (June): 7 LOS + 3 NLOS (3rd + 4th floors)	2015 campaign (July): 7 LOS + 3 NLOS (3rd + 4th floors)

A.4.1.3   Channel simulations

The point cloud-based channel simulation tool, calibrated by the measurements as detailed in A.1.1.3, is used for the simulating channels of the shopping mall scenario. The point cloud environmental database of the shopping mall is shown in Fig. A4.1.2-1(b). The Tx and Rx antenna heights were 4.0 and 1.5 m above the floor, respectively.

A.4.1.4   Findings and observations

A.4.1.4.1 Among large-scale parameters, zenith angle-of-arrival and departure as well as K-factor showed the clearest dependence on a link distance

Figure A4.1.4.1-1 shows exemplary plots of large-scale parameters on the link distance. The plot of azimuth spread of arrival at 15 GHz shows increasing trend as the distance is longer, but the same plots at 28 and 60 GHz did not show as clear increasing trend at 15 GHz. The azimuth spreads at the transmit and receive side were therefore regarded rather independent of link distance in our shopping mall scenario. While the zenith spreads at the transmit and receive sides, as well as the K-factor showed clearly decreasing trend as the link distance is longer, at all the measured frequencies of 15, 28 and 60 GHz. It is motivating to model them as a function of the distance. The delay spread showed a peculiar behaviour, where it first increased as the distance is longer and then decreased after a link distance of 50 m. The behaviour is due to the structure of the shopping mall, where a receiving antenna is facing a large open hall until 50 m link separation distance, and after that it is in a corridor. The channels in a hall have more long-delayed multipaths than in the corridor.

(a) Azimuth spread of arrival, 15GHz

(b) Zenith spread of departure, 28GHz

(c) K-factor, 60GHz
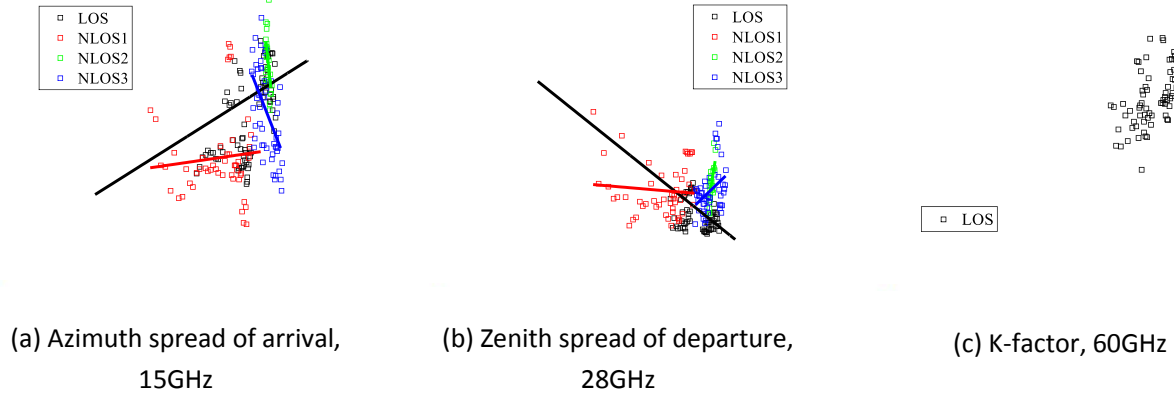
Figure A4.1.4.1-1: Distance dependence of the large-scale parameters.

A.4.1.4.2 LOS probability in shopping mall is slightly frequency dependent

The LOS probability described in A.2.1.4.1 was studied similarly in the shopping mall, as presented by Figure A.4.1.4.2-1. The results showed that the LOS probability at 63 GHz is around 10 percentage points higher than at 2.4 GHz [JNHN+16]. Compared to results found in the literature, it was observed that the other results overestimate the LOS probability due to the absence of shadowing objects such as walls and pillars that were found in the shopping mall under study.

(a) BS and MS deployment in shopping mall.

(b) LOS probability as a function of link distance.
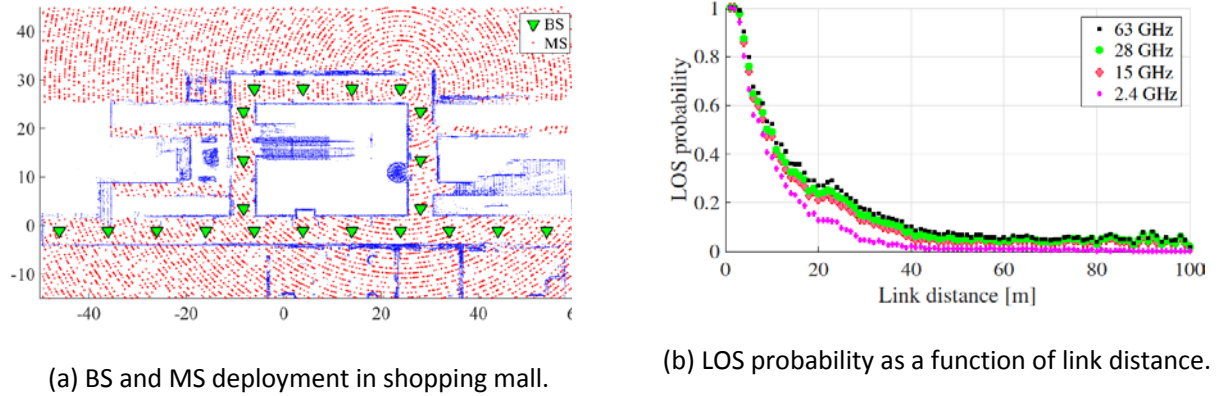
Figure A.4.1.2-1: LOS probability evaluation in shopping mall.

A.4.2 China Mobile (CMCC) & Beijing University of Posts and Telecommunications (BUPT)

A.4.2.1 Channel sounder

The channel sounder is composed of a microwave signal transmitter and a microwave signal receiver as shown in Fig. A4.2.1-1. The sounder is capable of measuring 28 GHz bands with a bandwidth of 800MHz. A PN sequence with the code length of 511 is firstly generated at the chip rate of 400 Mchips/s. Then, the signal goes through the up-converter which modulates center frequency to 28 GHz. The transmitting power fed to the antenna port can reach to 30 dBm after the power amplifier. On the receiving side of the channel sounder, the signal sampling rate is 1.2 GHz which is 3 times of the original PN sequence. Thus, the multi-path resolution is 0.833 ns whilst the whole duration for a PN sequence is 1.28 us. A back-to-back calibration measurement that connects the transmitter and receiver sides through 10 dB attenuator is always performed before the channel sounding to obtain channel transfer functions of the sounder. Two types of the antennas are used, which are horn antenna and biconical antenna as illustrated in Fig. A4.2.1-2. The antenna gain of the horn antenna is 25 dBi with HPBW of 10° both in the horizontal and vertical directions. The biconical antenna with 12.5 dBi antenna gain is omni-directional in the horizontal plane with 5° in the vertical plane
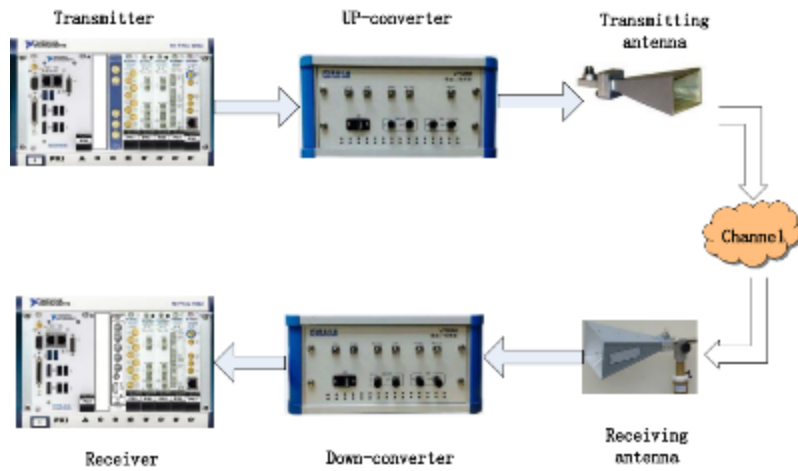
Figure A4.2.1-1: BUPT's channel sounder architecture.

(a) Horn antenna   (b) Biconical antenna
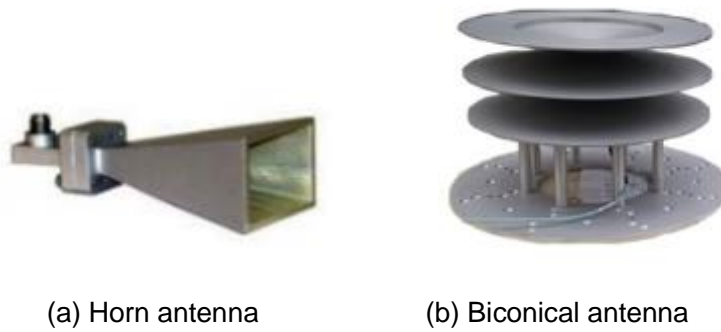
Figure A4.2.1-1: Antennas for 28 GHz.

A.4.2.2   Channel sounding

Channel sounding for the shopping mall scenario was performed in a teaching building of BUPT, the layout of which is quite similar to that of shopping mall as shown in Fig A4.2.2-1. The square includes some concrete pillars, up and down escalators, vertical lifts and stairs, glass wall and corridor. The antennas of TX and RX are set up at the same height of 1.6 m, The red star in the figure is the location of the TX and the spots are the RX locations. Two areas of NLoS and on area of LoS are measured.
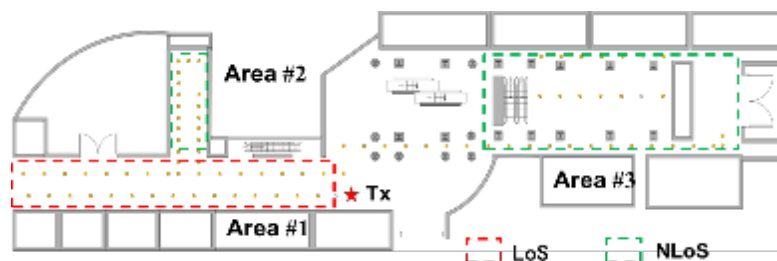
Figure A4.2.2-1: BUPT's channel sounding in a shopping mall.

A.4.2.3   Findings and observations

A.4.2.3.1 Path loss measured by horn antenna is larger than that measured by biconical antenna in LoS for 28 GHz

Figure A4.2.3.1-1 shows the path results of 28 GHz in both LoS and NLoS. It can be observed that PL of horn-to-horn is a little larger than that of bi-to-bi. Both the PL exponents of two antenna configurations are smaller than the free space. For NLoS case, the PL exponent of bi-to-bi is 2.5.
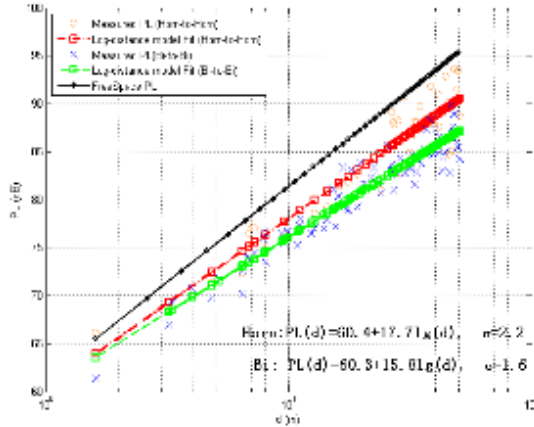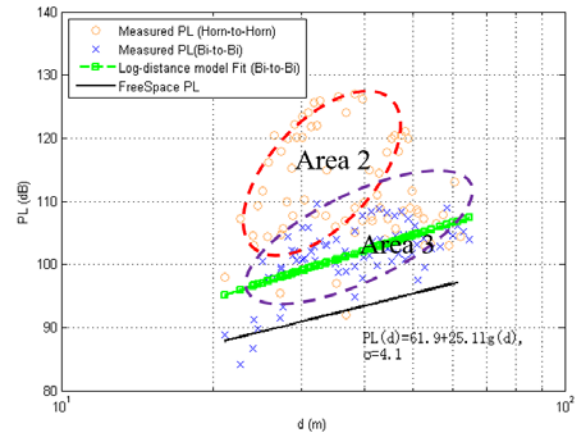
(a) LoS case   (b) NLoS case

Figure A4.2.3-1: Path loss results in LoS/ NLoS case.

A.4.2.3.2 Delay spread follows the log-normal distribution both in LoS and NLoS. DS is smaller using the horn antenna compared with the omni-directional antenna.

Figure A4.2.3.2-2 shows probability density of delay spread of two antenna configurations in both LoS and NLoS case, in which the log normal distribution fits all the delay spread results well. For LoS, the mean value of DS in horn-to-horn case is 3 ns which is smaller than that of 11 ns in bi-to-bi case. For NLoS, the same trend is also observed. The DS mean value in horn-to-horn and bi-to-bi cases are 37 ns and 42 ns, respectively.
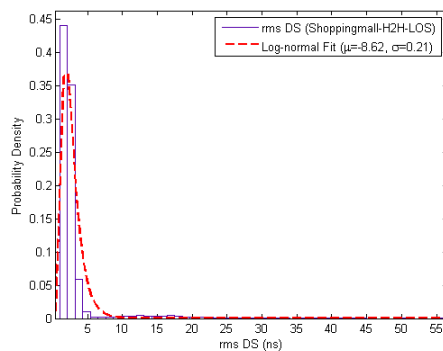
(a) LoS, horn-to-horn   (b) LoS, bi-to-bi
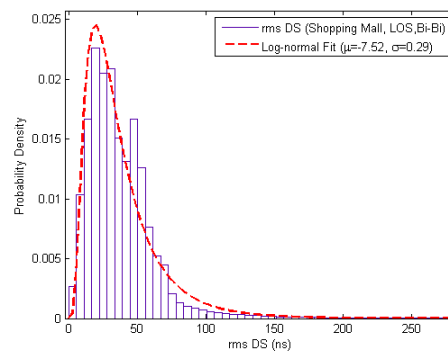
(c)NLoS, horn-to-horn   (d)NLoS, bi-to-bi
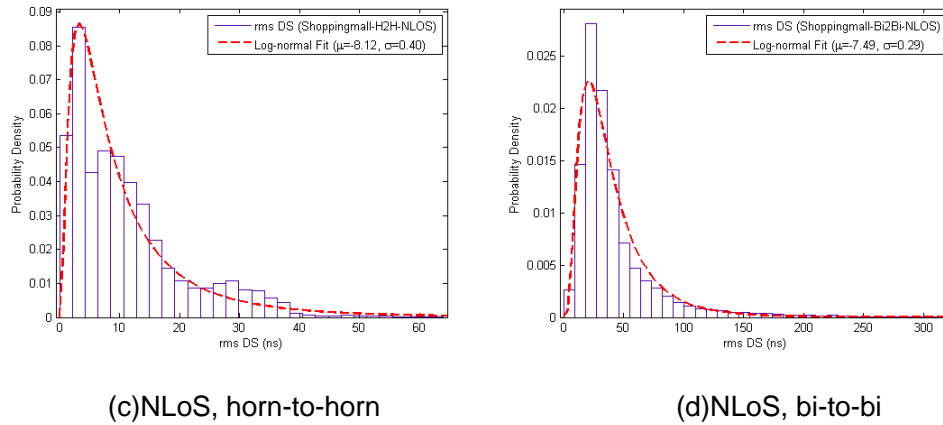
Figure A4.2.3-2: Probability density of delay spread of different antenna in both LOS and NLOS cases

A.4.3 Ericsson

A.4.3.1   Channel sounder

In this scenario a 60 GHz radio was used in parallel with the 28 GHz radio presented in A.5.1.1. The measurement was conducted in the exact same way, though with slightly different link margins and antenna gains for the two frequencies are detailed below.

A.4.3.2   Channel sounding

Ericsson's indoor propagation measurement was conducted in an open entrance area in Gothenburg, Sweden, resembling a shopping mall scenario. The Tx was placed on a fourth floor balcony and the Rx positions were on the ground floor in the open area and into the hidden corridors leading from the open area. A photo of the site taken from the Tx position is shown in Figure A4.3.2-1(a); an open area that ends on both sides with glass walls. The canyon walls are a mixture of concrete, glass and wood. Some very sparse trees are placed on the ground level. The floor plan is shown in Figure A4.3.2-1(b) and (c) with the Rx locations for the 28 and 60 GHz measurements respectively.

The distance between the Rx and Tx was 12 to 70 meters. The Tx antenna was placed at about 12 meter height while the Rx antenna was placed at 1.6 m height at all measurement points. All measurements were done after business hours but there where people occasionally blocking Rx-Tx paths. The two frequencies were not measured during the same day but the furniture placement and general environment were very similar between the two campaigns.

(a) Photo taken from the Tx location.

(b) Cut out of street level floor plan with 28 GHz Rx locations marked with stars and excess loss for the NLOS (red) positions. The Tx location projected with a blue cross.

(c) Cut out of street level floor plan with 60 GHz Rx locations marked with stars and excess loss for the NLOS (red) positions. The Tx location projected with a blue cross.

Figure A4.3.2-1: Ericsson 'shopping mall scenario' i.e. open indoor hot spot area.

A.4.3.3 Findings and observations

In these measurements, the radio channel behaved very similarly at 60 and 28 GHz in terms of path loss and angular spread. There are good coverage for both frequencies in the open area with LOS and shallow NLOS but the path loss drastically increase when moving into hidden corridors/areas.

Table A4.3.3-1: Measurement set-up info.

	28 GHz	**60 GHz**
Date	2015 Oct	2015 Nov
No of Rx positions	5 LOS	3 LOS
	6 NLOS	7 NLOS
Height of Tx position	12 meter	12 meter
Height of Rx position	1.5 meter	1.5 meter
Antenna gain Tx	10 dBi	10 dBi
Antenna gain Rx	34 dBi	32 dBi
Tx power	12 dBm	8 dBm
Link margin	152 dB	146 dB
Polarization	Vertical	Vertical

Excess loss 27 dBm
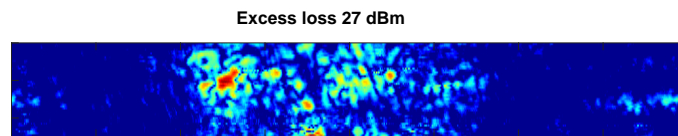
(a) A deep NLOS position for 28 GHz

Excess loss 30 dBm
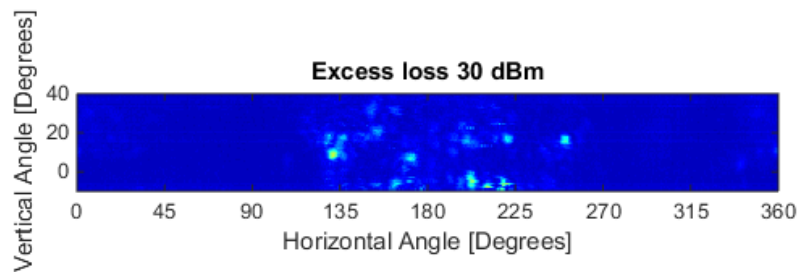
(b) Same location for 60 GHz, due to link budget limitation the different paths are less visible.

Figure A4.3.3-2

A.4.4 Samsung / Korea Advanced Institute of Science and Technology (KAIST)

A.4.4.1 Channel sounder

Please refer to Section A.1.9.1.

A.4.4.2 Channel sounding

The channel sounding was performed in a five-story building on KAIST campus similar to a small shopping mall. The measurement overview and the description of channel sounder are given in Table A4.4.2-1.

Table A4.4.2-1: Measurement overview.

Propagation scenario	InH shopping mall LOS	InH shopping mall NLOS

Center frequency	28 GHz	
Bandwidth	500 MHz	
Polarization	Vertical linear polarization	
TX location	3 test location	3 test locations
TX velocity	Stationary	
RX location	9 test locations	26 test locations
RX velocity	Stationary	
RX height above ground level	1.5m	
TX-RX distance	10 – 35 m	14 – 55 m
Angular scanning	Rotation in azimuth 0-360° Rotation in elevation -60-60° with 10° step	

A.4.4.2.1 A five-story building on KAIST campus in Daejeon, Korea

This channel measurement scenario is performed in a building on KAIST campus. Photographs of the building environment is shown in Figure A4.4.2.1-1. The floor maps of the building and measurement locations of TX and RX are presented in Figure A4.4.2.1-2. The atrium with glass ceiling is located in the centre of the building. The space for elevators and stairs are located next to the atrium. The transmitter was installed at either the first floor (TX position 1, 2) or the third floor (TX position 3), and thirty five different measurements were performed at each receiver locations with the dedicated transmitter location, either on the same floor experiments or on the different floor experiments The measurement scenario is defined via the index of the Rx antenna location, including both LoS and NLoS channels. The Tx-Rx distance ranged from 10 m up to 55 m.
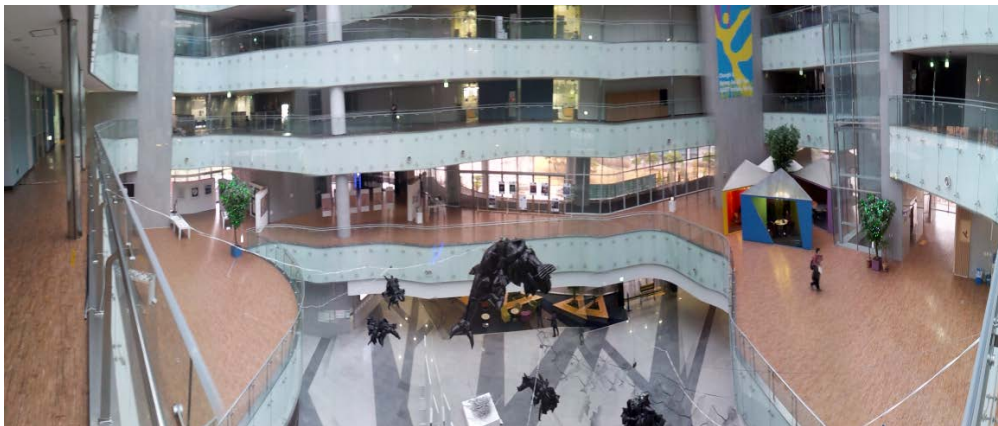
Figure A4.4.2.1-1: Photographs of a building environment similar to a small shopping mall.
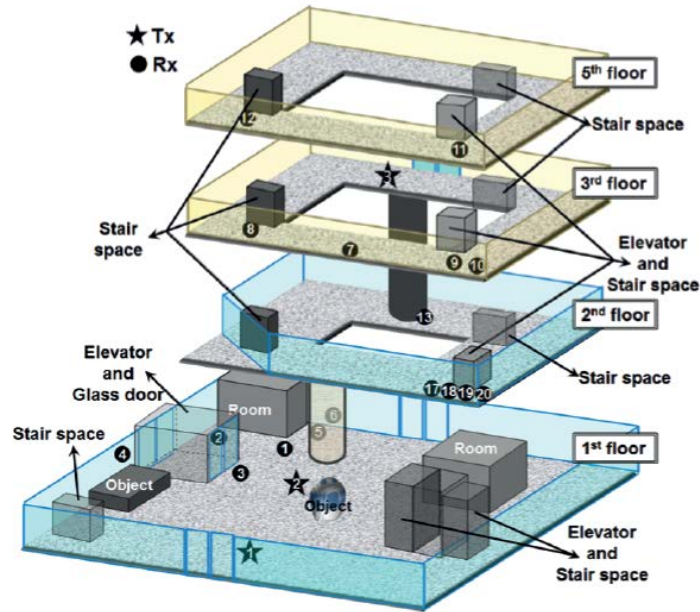
Figure A4.4.2.1-2: A floor map with the TX and RX location in a building on KAIST campus.

A.4.4.3   Findings and observations

A.4.4.3.1 Path loss analysis

From the measured data, the path loss (PL) for each location was estimated using the two PL models which are introduced in Sec. A.1.9.3.1, the CI free space reference distance PL model and the ABG PL model. Figure A4.4.3.1-1 shows the path loss plots for both the LoS and NLoS channels in the building. The path loss model parameters are listed in Table A4.4.3.1-1 with the valid ranges for distance.
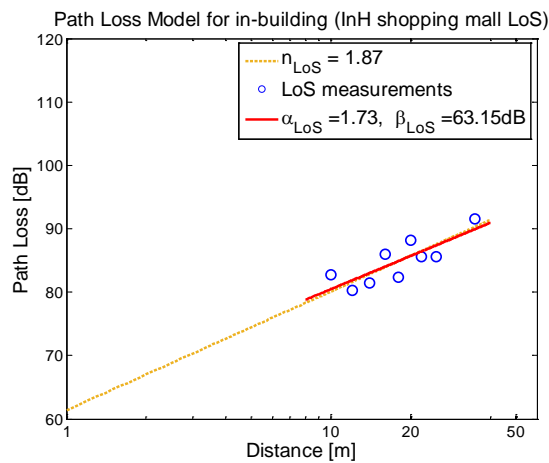
(a) LoS measurements
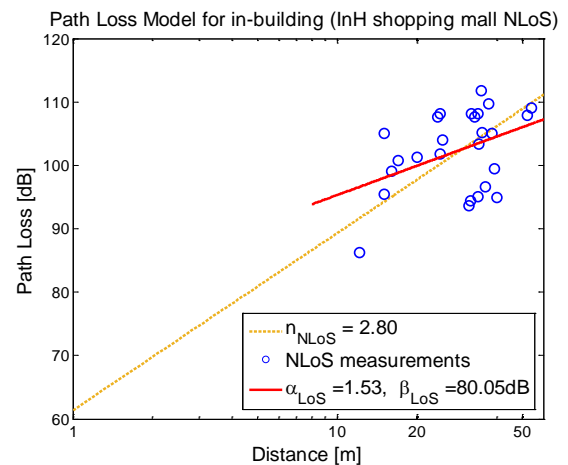
(b) NLoS measurements

Figure A4.4.3.1-1: Path loss models for InH shopping mall scenarios in KAIST campus at 28 GHz.

Table A4.4.3.1-1. The path loss parameters.

Parameters	InH shopping mall LoS	InH shopping mall NLoS
d [m]	$10 < d < 40$	$10 < d < 60$
d_0 [m]	1	1
n	1.87	2.80
X_σ^{CI}	2.07	6.18
α	1.73	1.53
β	63.15	80.05
X_σ^{ABG}	2.06	5.79

A.4.4.3.2 Cluster analysis

From the measurements, the cumulative distribution function (CDF) of the number of clusters in NLoS scenario is shown in Fig. A.4.4.3.2-1, where the positive Poisson distribution is overlaid as the best fit. The average number of clusters were 3.52.
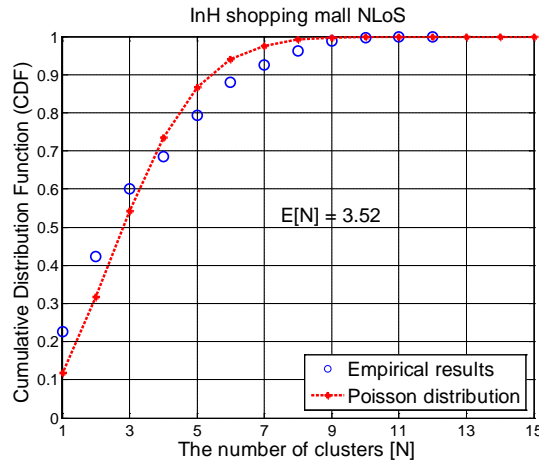
Figure A4.4.3.2-1: Cumulative distribution function of the number of clusters for InH shopping mall NLoS scenarios in a building in KAIST campus at 28 GHz.

A.4.4.3.3 Spatio-temporal analysis

1) Temporal analysis

Using the synthesized omni-directional PDPs, the temporal characteristics can be analyzed through excess delays, subpath delays, the RMS delay and subpath delay spreads. The histograms of the excess delays and subpath delays and their probability density functions (PDFs) for InH shopping mall NLoS scenarios are illustrated in Figs. A.4.4.3.3-1(a) and 1(b), respectively. Note that they follow exponential distributions with the decay rate parameters of 0.020 ns and 0.103 ns, respectively.

(a) Excess delay   (b) Subpath excess delay

Figure A4.4.3.3-1: Probability density functions of excess delays and subpath delays for InH shopping mall NLoS scenarios in KAIST campus at 28 GHz.

Figure A4.4.3.3-2 shows the CDFs of the RMS delay and subpath delay spreads along with log-normal distributions as their best fits. The average value of the RMS delay spread and the subpath delay spread from the measurements in Daejeon are 18.91 ns and 3.90 ns, respectively.
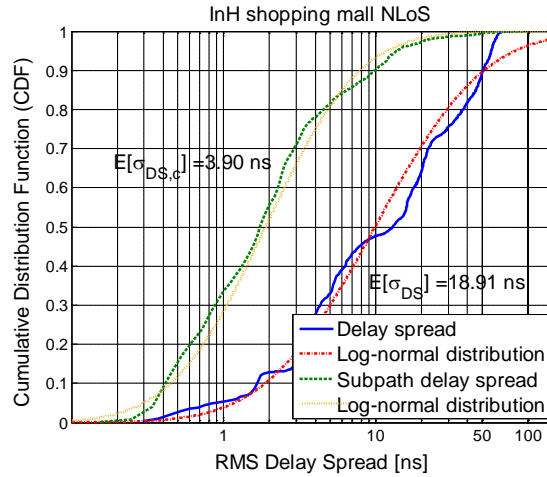
Figure A4.4.3.3-2: Cumulative distribution functions of RMS delay and subpath delay spreads for InH shopping mall NLoS scenarios in KAIST campus at 28 GHz.

2) Spatial analysis

The spatial characteristics for channel modeling can be analyzed through the distributions of the cluster AoD and AoA, and their corresponding circular angle spreads. In Figs. A.4.4.3.3-3(a) and 3(b), PDFs of the measured cluster AoD and AoA in InH shopping mall NLoS scenario are shown, and a Laplacian distribution is also plotted as the best fit. Note that the best-fit distribution for 28 GHz is different from the distribution for the cellular bands, which is the wrapped Gaussian distribution.

(a) Cluster AoD   (b) Cluster AoA
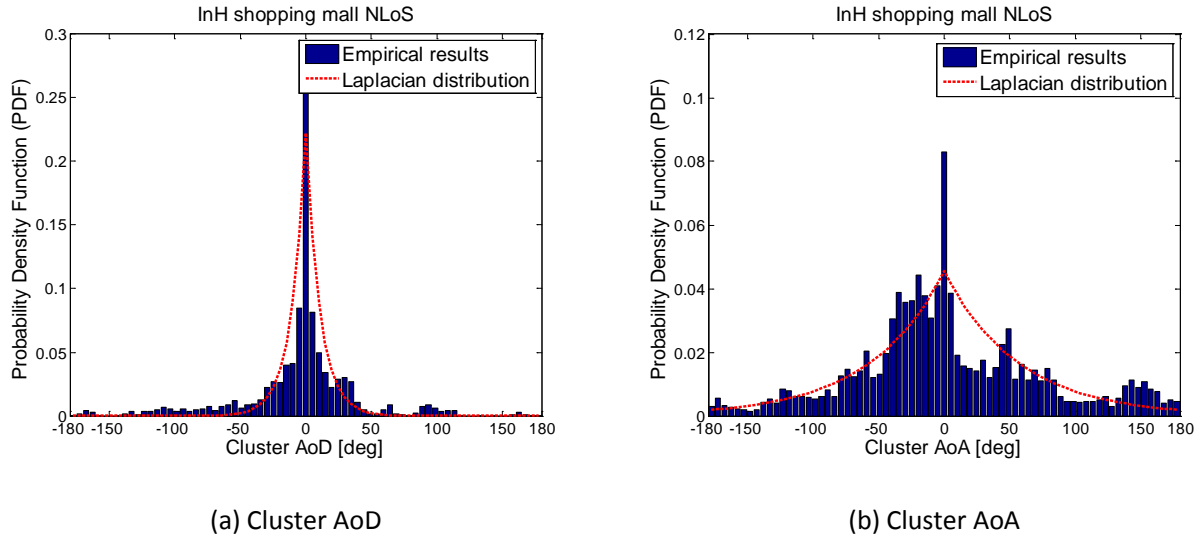
Figure A4.4.3.3-3: Probability density functions of cluster AoD and AoA for InH shopping mall NLoS scenarios in KAIST campus at 28 GHz.

The AoD and the AoA spreads (ASD and ASA) from the measurements in the building are illustrated with their CDFs in Fig. A.4.4.3.3-4. The average values of the AoD and AoA spreads are 15.02° and 32.16°, respectively. In addition, the measured intra-cluster AoD/AoA spreads of the in-building environments in campus have the mean values of {4.33°, 5.94°}, respectively. Note that the intra-cluster angular spreads smaller than the beam width of the horn antennas on the Tx and Rx sides were roughly calculated and based on subpaths which appear across several adjacent angular bins; the subpaths were resolved in the delay domain thanks to the large bandwidth of the sounder. If highly precise intra-cluster angular spread values are required for any specific application, it should be considered that the limited angular resolution of the channel sounder have an impact on the intra-cluster spreads. Thus, ray-tracing analysis and/or measurements with narrower beam width for our measurement scenarios would be needed to obtain more reliable intra-cluster spread values.

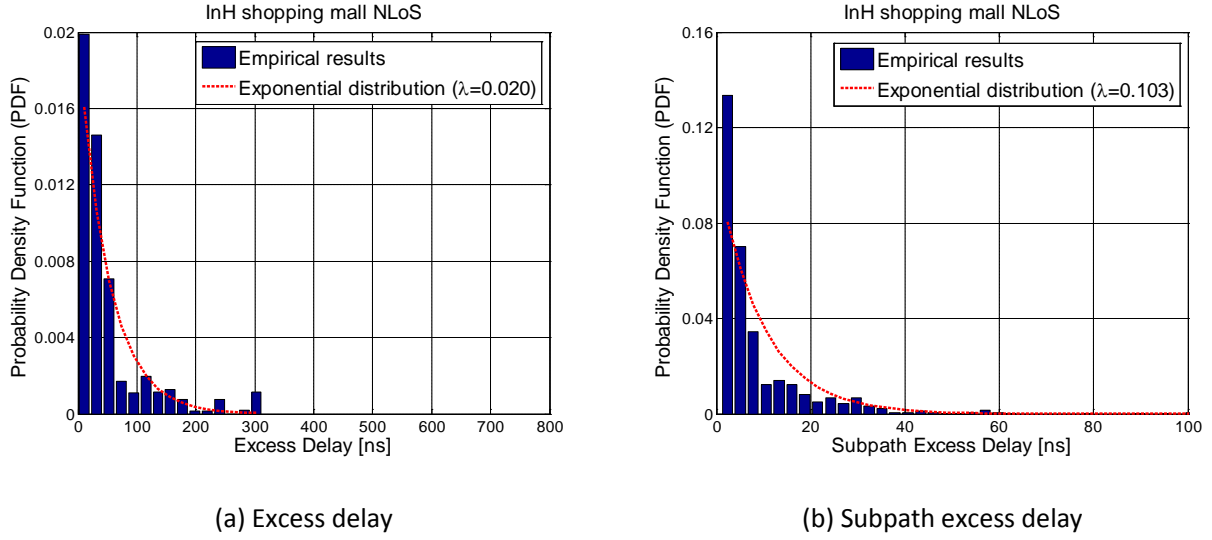
Figure A4.4.3.3-4: Cumulative distribution functions of the AoD and AoA spreads for InH shopping mall NLoS scenarios in KAIST campus at 28 GHz.

A.4.4.3.4 Cross correlation properties between the large scale parameters

The large scale parameters, i.e., the inter-cluster AoD and AoA spreads, RDS and shadow fading are generally correlated with each other. The cross correlation coefficients of the in-building scenarios are listed in Table A.4.4.3.4-1. Based on our 28 GHz measurements, usually there exists a dominant reflector near the Tx site,

which illuminates wide spatial areas and influences the inter-cluster AoD spread and the shadow fading, while indirectly affects the inter-cluster AoA spread and the RDS; radio wave propagation mechanisms are mainly dominated by reflections due to the weak diffraction effect at 28 GHz.

Table A4.4.3.4-1. Cross correlation coefficient of large scale parameters.

Parameters	InH shopping mall NLoS
DS vs SF	-0.0995
ASD vs SF	-0.1569
ASA vs SF	-0.0195
ASD vs DS	0.7926
ASA vs DS	0.8795
ASD vs ASA	0.6596

A.5 Urban macrocellular scenarios

A.5.1 China Mobile & Beijing University of Posts and Telecommunications

A.5.1.1 Channel sounder

Please refer to Section A.1.2.1.

A.5.1.2 Channel sounding

The channel measurement campaign is carried out in BUPT Hong Fu campus of Beijing, which can be categorized as a typical urban macrocellular scenario (UMa). The base station (as the transmitter) is installed on the top of a 7-floor teaching building. The base station antenna height is 31m. Surrounding buildings are relatively lower than base station. The measurement routes are mainly planned on the surrounding roads, as showed Fig.A5.1.2-1. Some of the routes are LoS whereas others are NLoS. The mobile terminal (as the receiver) is placed on the trolley with the height of 1.8m. The trolley moves at a pedestrian speed of about 3km/h. Table A5.1.2-1 shows the parameters of measurement.
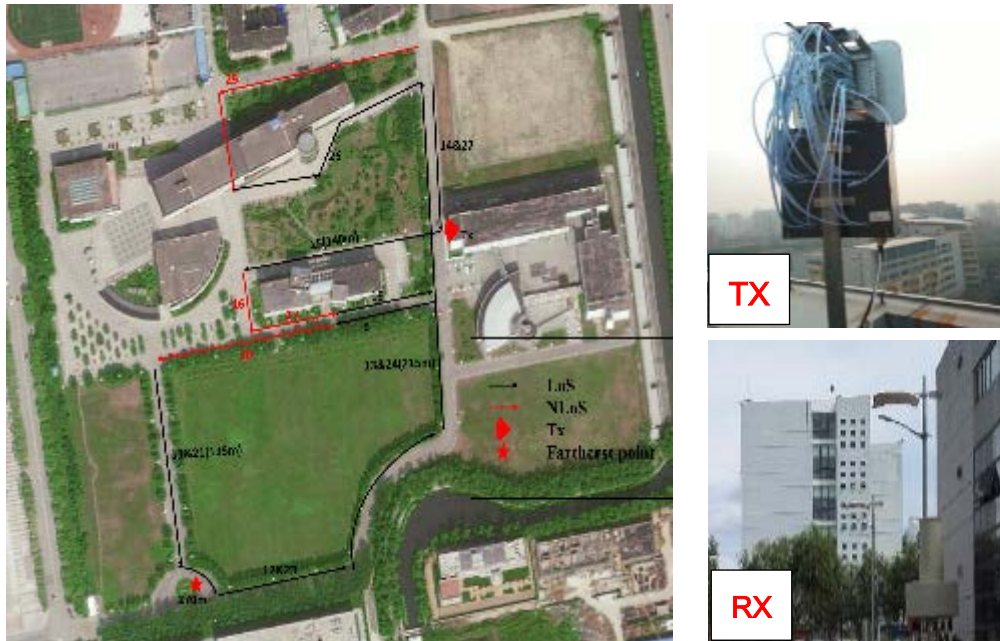
Figure A5.1.2-1: UMa measurements scenario.

Table A5.1.2-1: Parameters of measurement.

Item	Value
Tx height	31 m
Rx height	1.8 m
Length of PN sequence	254
Time of one chip	10 ns
Time of one cycle	4.63 ms
Transmitting power (fed to the Tx)	23 dBm

A.5.1.3   Findings and observations

A.5.1.3.1 EoA and EoD follows the Laplacian distribution in LoS and NLoS at 3.5 GHz and 6 GHz

Fig. A5.1.3.1-1 shows the EoD(Elevation angle of departure) and EoA(Elevation angle of arrival) distribution in UMa LoS and NLoS cases from field channel measurement results. Laplace distribution is considered for elevation angle distribution. In Figure A5.1.3.1-1, the mean value of EoD/EoA is normalized to 0. Laplace distribution is used to model EoD and EoA.
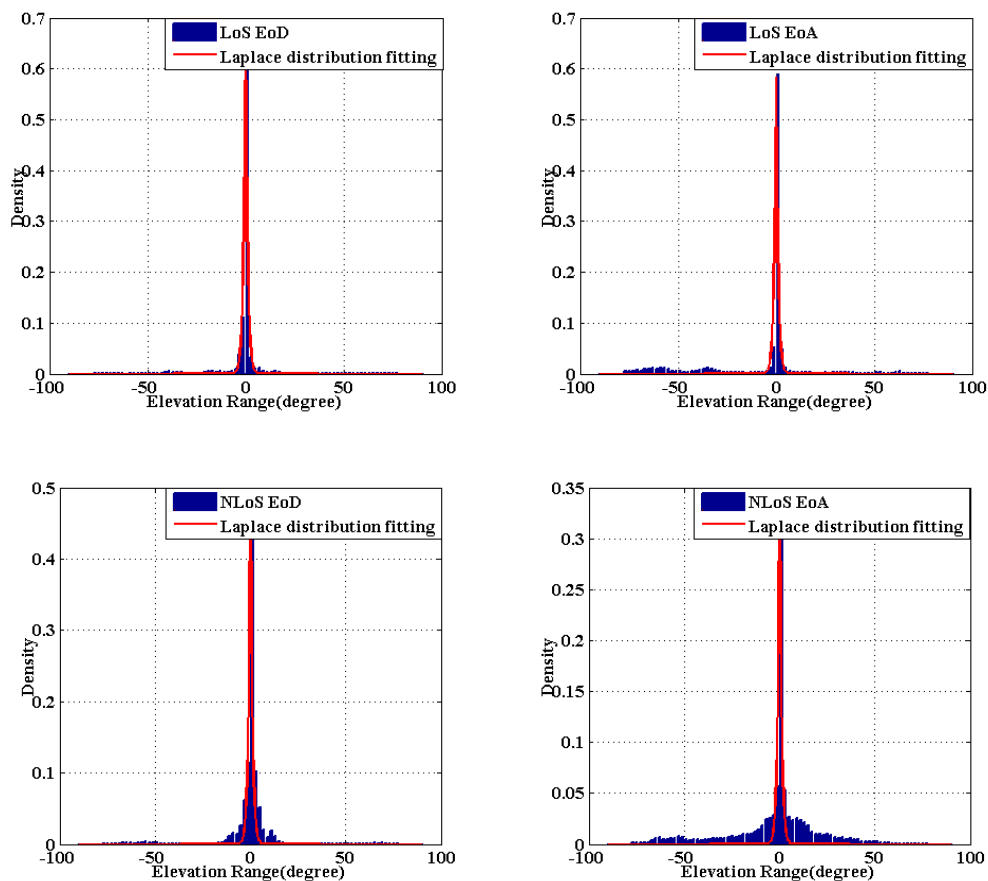
Figure A5.1.3.1-1 The EoD and EoA distribution in UMa LoS and NLoS.

The Laplacian distribution fits the EoD and EoA well. The multi-path energy concentrates on a specified angel in the LoS situation, while is dispersed over different angles in the NLoS situation.

A.5.1.3.2 ESA, ESD, ASA, ASD follows log-normal distribution both in LoS and NLoS. Angular spread in 6 GHz is larger than that in 3.5 GHz in general.

Table. A5.1.3.2-1shows the statistics of angular parameters including ESD (elevation angle spread of departure), ESA (elevation angle spread of arrival), ASD (azimuth angle spread of departure) and ASA (azimuth angle spread of arrival) in UMa LoS and NLoS from field channel measurement results. A larger angle dispersion can be observed for 6 GHz compared with 3.5 GHz.

Table A5.1.3.2-1: ESD, ESA,ASA and ASD in UMa LoS/NLoS.

Frequency		3.5GHz		6 GHz	
Situation		LoS	NLoS	LoS	NLoS
ESD[*]	μ	0.85	0.92	1.12	1.24
log10 ([degree])	σ	0.04	0.14	0.21	0.40
ESA[*]	μ	0.95	1.26	1.36	1.37
log10 ([degree])	σ	0.16	0.16	0.11	0.14
ASD[*]	μ	1.15	1.41	1.36	1.37
log10 ([degree])	σ	0.28	0.28	0.11	0.14
ASA[*]	μ	1.81	1.87	1.36	1.37
log10 ([degree])	σ	0.20	0.11	0.11	0.14

[*] The values of ESA, ASD and ASA in 3.5GHz are referred to 3GPP TR 36.873. The values of ESD are refer to 3GPP TSG-RAN WG1 #73 R1-132543.

A.5.1.3.3 Cross-correlations

Table A5.1.3.3-1: Cross-correlation with other LS parameters in UMa LOS/NLOS.

Frequency	3.5GHz		6 GHz	
Situation	LoS	NLoS	LoS	NLoS
ASD VS DS	0.4	0.4	0.06	0.12
ASA VS DS	0.8	0.6	0.02	0.07
ASD VS ASA	0	0.4	-0.06	0.6
ASD VS K	0	N/A	0.34	N/A
ASA VS K	-0.2	N/A	0.21	N/A
DS VS K	-0.4	N/A	0.28	N/A
ESD VS K	0	N/A	-0.23	N/A
ESA VS K	0	N/A	-0.07	N/A
ESD VS DS	-0.2	-0.5	0	0.13
ESA VS DS	0	0	-0.03	-0.03
ESD VS ASD	0.5	0.5	0.47	0.84
ESA VS ASD	0	-0.1	-0.24	0.51
ESD VS ASA	-0.3	0	-0.03	0.56
ESA VS ASA	0.4	0	0.13	0.51
ESD VS ESA	0	0	-0.19	0.60

A.5.2 Ericsson

A.5.2.1 Channel sounder

The high angular resolved measurements conducted are based on a standard and a software and hardware modified commercial radio. The Tx radio is a commercially available radio at 28 GHz with a maximum output power of 22 dBm. The antenna can either be a sector antenna ore a low gain 'open waveguide' solution. The Rx side is built up by a similar but SW and HW modified radio for high speed Rx power read out. The Rx site is mounted on a rotating table. The elevation and azimuth sweep can be set arbitrarily but are usually set to 360

degrees in azmuth with over 30000 samples per full 360 degree sweep, and -10 to +40 degrees in elevation with 1 degrees resolution, which gives rise to an extensive oversampling of the Rx levels, i.e. the angular resolution is set by the radiation lobe of the Rx antenna. The Rx antenna can be changed but are here a 34dBi, 3.3 degrees FWHM, reflector antenna that can be either vertical or horizontally polarized. In these measurements the vertical polarization has been used. The maximum link margin for the system is 173 dB depending on the antennas used.

Table A5.2.1-1: Measurement setup info.

	Lindholmen	**Mölndal**
Date	2015 Aug	2015 June
No of Rx positions	9 LOS 67 NLOS	9 LOS 51 NLOS
Height of Tx position	25 m	36 m
Height of Rx position	1.5 m	1.5 m
Antenna gain Tx	10 dBi	10 dBi
Antenna gain Rx	34 dBi	34 dBi
Tx power	22 dBm	18 dBm
Link margin	162 dB	158 dB
Polarization	Vertical	Vertical

A.5.2.2   Channel sounding

In this study two urban macro scenarios was investigated. The scenarios are based in/around Gothenburg Sweden; photos from the Tx position of the two sites are shown in Figures A5.2.2-1 and A5.2.2-2 together with a street map with the Rx positons marked. Both scenarios are common for the area in sense of building heights and building material. Both campaigns were conducted during daytime with people available but not within one meter from the Rx.

A.5.2.2.1 Lindholmen

At the Lindholmen site 76 positions were measured out of which 67 were in NLOS. The transmitted signal was detected in every position, with the maximum excess loss for any given point being 55 dB in this scenario. After inspecting the elevation and azimuth angle of all NLOS positions it can be concluded that the strongest paths never were a pure diffraction path, but rather single/multiple reflections or scattering. The path loss verses distance are shown in Figure A5.2.2.1-1.

A.5.2.2.2 Mölndal

At the Mölndal site 60 positions were measured out of which 51 were in NLOS. At all positions a clear signal was received, the maximum excess loss for any given point were 45 dB in this scenario. After inspecting the elevation and azimuth angle of all NLOS positions it can be concluded that the strongest paths were due to single/multiple reflections or scattering except for a single position where a pure diffracted path was dominant. The path loss verses distance are shown in Figure A5.2.2.1-1.

(a) Photo from the Tx position.
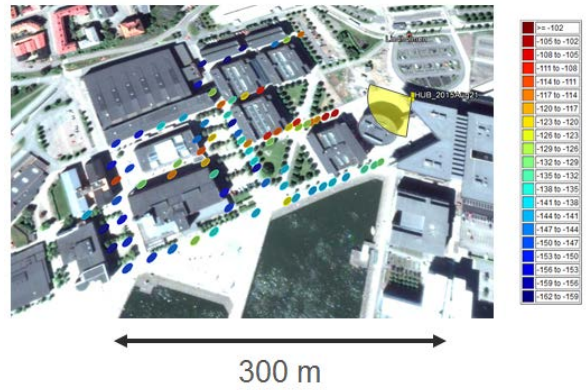
(b) Measured positions marked with circles, color identifying the total path gain in the given position. Tx is marked with yellow

Figure A5.2.2-1: Lindholmen scenario: photo and street plan.

(a) Photo from the Tx position.
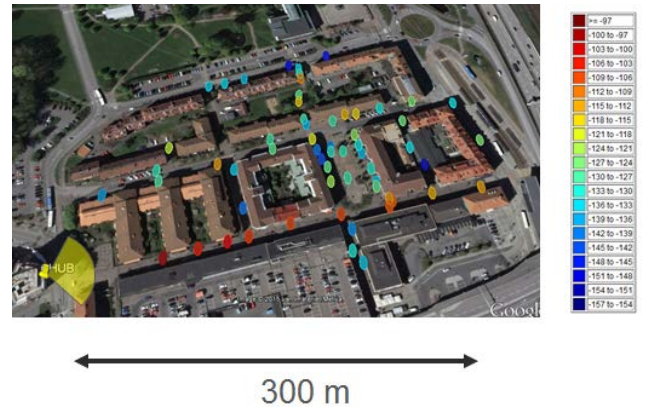
(b) Measured positions marked with circles, color identifying the total path gain in the given position. Tx is marked with yellow.

Figure A5.2.2-2: Mölndal scenario: photo and street plan.
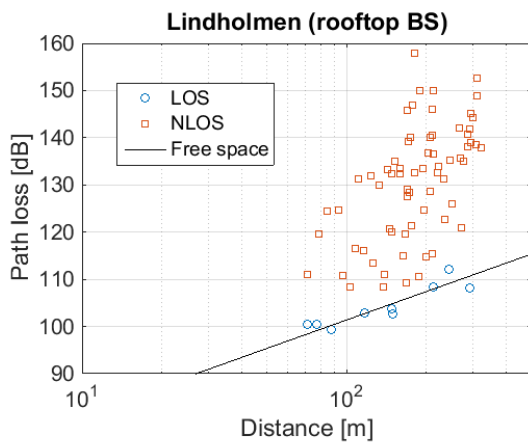
(a) Path loss verses distance for the Lindholmen scenario.
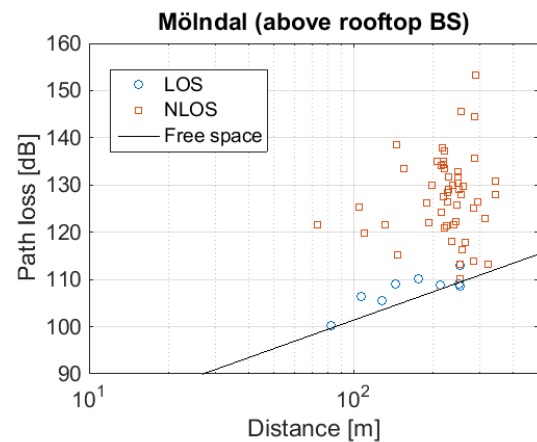
(b) Path loss verses distance for the Mölndal scenario.

Figure A5.2.2.1-1: Path loss vs distance.
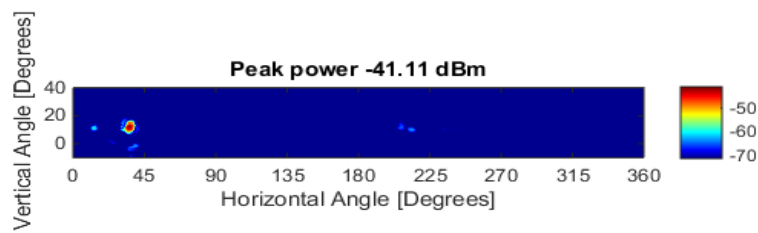
(a) Typical LOS scenario with strong LOS, a backscattering reflection 180 degrees from LOS and a ground reflection with negative vertical angle.
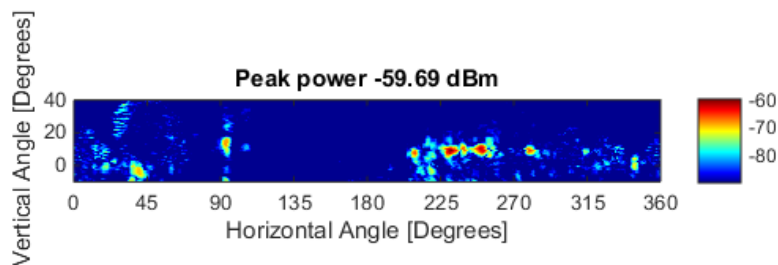
(b) A very rich NLOS channel
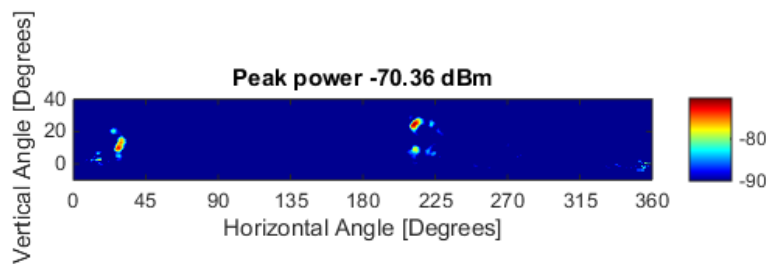
(c) A relatively poor NLOS channel

Figure A5.2.3-1

A.5.2.3 Findings and observations

Figure A5.2.3-1 shows that the majority of the energy was contained either in a LOS path or in specular reflections or reflections off smaller objects such as scaffolding, drain pipes, light poles, bikes, balconies and other objects that are typically not available in a building database. Only one location had a clearly identifiable diffraction path as the strongest. In urban macro environments at higher frequencies scattering and reflections will be the dominant paths in NLOS.

Excess loss above free space path loss up to 55 dB were observed for the rooftop BS (Lindholmen), and up to 45 dB for the above rooftop BS (Mölndal). Cross-polar scattering was also measured for one location, here the co-polar components had similar power while the cross-polar components were suppressed by 8-14 dB.

In NLOS locations there were quite many paths with similar power leading to significant richness and angular spread at the terminal side of the link.

A.5.3 New York University

A.5.3.1   Channel sounder

Please refer to section A.1.8.1 for the channel sounder specification regarding the 38 GHz UMa measurements.

A.5.3.2   Channel sounding

38 GHz cellular UMa measurements were conducted with three TX location chosen on two buildings at the UTA campus in the summer of 2011 at heights of 23 m and 36m, with a maximum measurable dynamic range of 160 dB, for various RX locations in the surrounding campus using narrowbeam TX antennas (7.8-degree Az. HPBW) and narrowbeam (7.8-degree Az. HPBW) or widebeam (49.4-degree Az. HPBW) RX antennas. A total of 33 TX-RX location combinations were measured for narrowbeam measurements (with T-R separation distances ranging from 61 m to 930 m) and 16 TX-RX location combinations were measured for widebeam measurements (with T-R separation distances between 70 m and 728 m) [RQTM+12, RGBD+13, RMCS+15, XRBS00, XRBS99].

A.5.3.3   Findings and observations

A.5.3.3.1 UMa omnidirectional path loss models

The 38 GHz UMa measurements show that LOS environments model yields a PLE very close to the Friis' free space PLE (n = 1.9). Additionally, the NLOS PLE is comparable to current microwave path loss with n = 2.7, showing that propagating signals attenuate by 27 dB per decade of distance using a 1 meter close-in free space path loss reference distance.

Please refer to section A.1.8.3 and Table A1.8.3.1-1 for UMa omnidirectional path loss models and for directional models in [RBDM+12, STRN+15, Sun16-2].
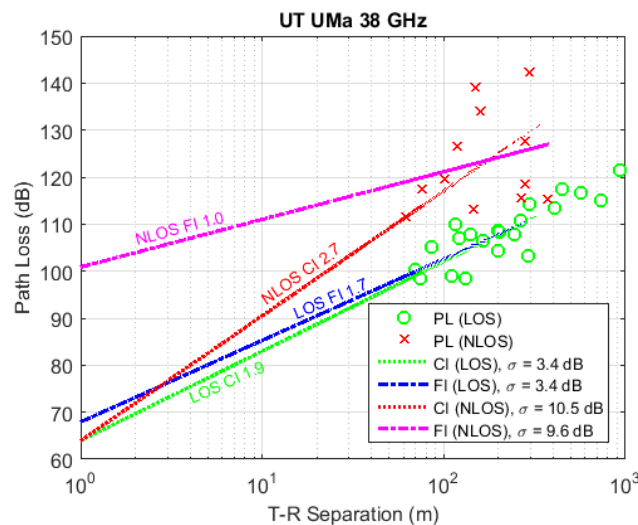
Figure A5.3.3.1-1: 38 GHz omnidirectional path loss models for the UMa scenario.

A.5.4 Nokia/Aalborg University

A.5.4.1   Channel sounding

To study the urban macro's propagation characteristics at the cmWave band, a drive-test measurement campaign was carried out between March and July 2015 in Aalborg, Denmark [Nguy16]. This experimental area represents a typical European medium city's residential district, in which the building height and street width are relatively homogeneous and measured at 17 and 20 meter, respectively. The measurement setup consists of a stationary Tx and a Rx mounted on a moving van. Figure A5.4.1-1 shows six locations of the Tx carefully chosen to cover the experimental area. At location 1a, 1b, 2, and 3 the Tx is elevated to different heights by the usage of a boom lift, while at location 4a and 4b it is placed on top of a tall hospital building. The combinations of

frequency, Tx height, location, measured range (minimum and maximum Tx-Rx separation) and number of measured samples are given in Table A5.4.1-1.

At the Tx, a narrowband continuous wave (CW) signal with the carrier frequency of interest, i.e. 10, 18 and 28 GHz, is fed to the Tx antenna with 35-39 dBm output power, depending on the frequency. Each frequency uses a separate horn antenna, but they all have similar characteristics of 55 degree half-power beamwidth (HPBW) in both elevation and azimuth plane and 10 dBi gain. No tilting is applied, except for the location 4a and 4b, where 11° mechanical down-tilt is added to ensure that the elevation HPBW of the Tx antenna covers the entire experimental area. Another narrowband CW signal at 2 GHz is always transmitted and recorded in parallel to serve as a reference. The 2 GHz band horn antenna is slightly wider, i.e. 60 degree HPBW in both planes, and lower gain, only 7 dBi. The output power for this branch is 36 dBm.

The Rx is placed on a van, which is driven around in the experimental area at average speed of 20 km/h. The driving routes are chosen so that they are confined within the HPBW of the Tx antennas. Two Rx antennas are mounted on top of the van, which is 2.5 m height. One dipole antenna is used at 2 GHz, while another biconical antenna is for all other frequencies. The dipole has 2 dBi gain and 35 degree HPBW in elevation, while the biconical antenna has typically 0 dBi gain and 45, 20 and 20 degree elevation HPBW at 10, 18 and 28 GHz, respectively. Received signal strength and GPS location are recorded at rate of 10 samples/s using the R&S TSMW Universal Radio Network Analyzer for extracting the corresponding path loss and 3-dimension (3D) Tx-Rx separation later. The measurement points are visually identified as LOS and NLOS on Google map during the post-processing stage. It is worth noticing that there are almost line-of-sight (ALOS) points, e.g. LOS direction being partially blocked by building corners or trees, present in both LOS and NLOS data sets.

Table A5.4.1-1: Frequencies and Measured Routes.

Frequency	Tx Height	Location (s)	Meas. Range	# of Samples
10 GHz	15 m	2, 3	54.5-793.5 m	8,765
10 GHz	20 m	1a	60.5-880.3 m	3,022
10 GHz	25 m	2, 3	60.2-1239.3 m	19,723
10 GHz	54 m	4a, 4b	68.4-1425.5 m	28,123
18 GHz	15 m	3	52.8-926.8 m	5,296
18 GHz	20 m	1a	60.2-870.6 m	3,328
18 GHz	25 m	2, 3	60.8-1032.3 m	10,285
18 GHz	54 m	4a, 4b	52.2-1429.1 m	31,064
28 GHz	15 m	1b, 3	50.7-539.8 m	5,841
28 GHz	20 m	1a, 1b	60.4-539.8 m	3,328
28 GHz	25 m	1b, 2, 3	50.7-876.7 m	10,285
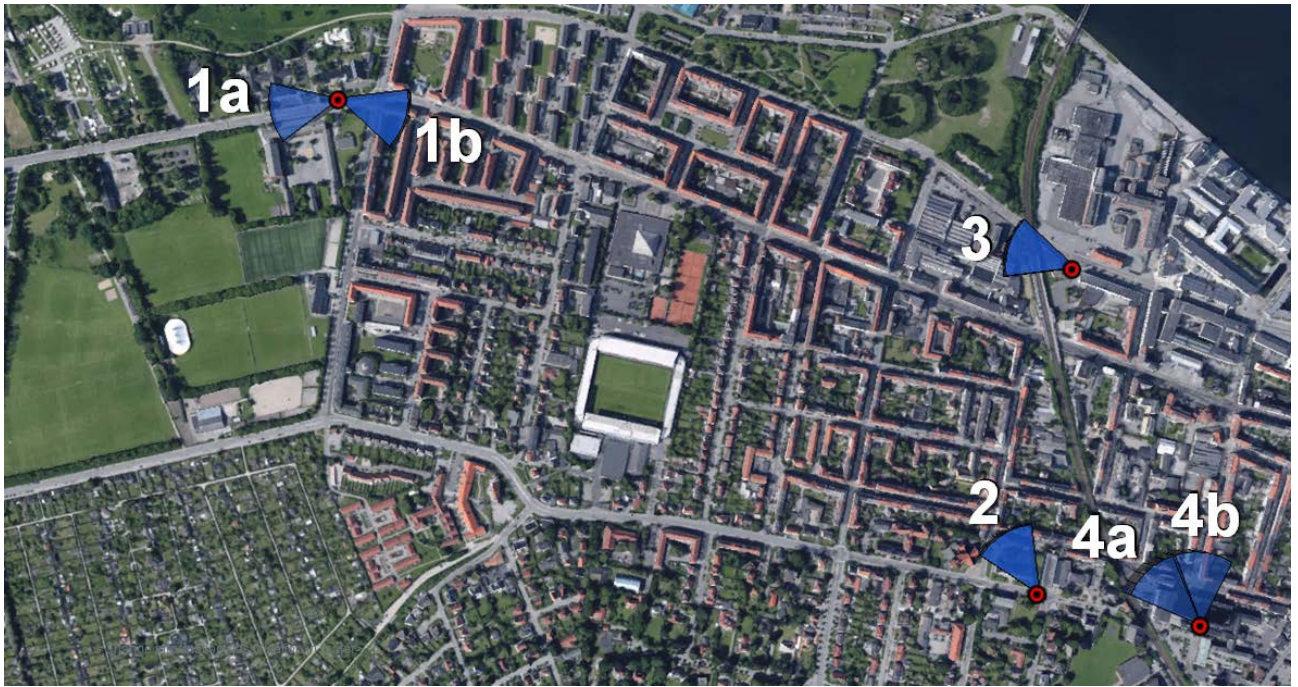
Figure A5.4.1-1: Measurement location in Aalborg, Denmark.

A.5.4.2   Channel simulations

The ray-tracing simulation was performed for TX2 and TX3 shown on the Figure A5.4.2-1 below using the WinProp v.13 ray-tracing simulator [AWEC] with the 3D Standard Ray Tracing model. The interaction models are based on Fresnel model for reflection and transmission prediction and GTD (Geometrical Theory of Diffraction) or UTD (Uniform Theory of Diffraction) for diffraction prediction, scattering model is based on single-lobe scattering pattern model described in [DEFV+07]. The electrical parameters of materials are from Recommendation ITU-R P.2040. The scattering coefficients for low frequency bands (<10GHz) are based on literature [FMKW06, VMDE+12]. The scattering coefficients for large frequency bands (>10GHz) are scaled accordingly to changes in Rayleigh roughness factor. The ray-tracing simulation parameters are the following:

- TX antenna height: 25m (for TX2 and TX3)

- RX antenna height: 1.5m

- Isotropic antennas in TX and RX

- Vertical polarization

- Walls: brick, roughness 0.2 mm

- Ground: medium dry ground, roughness 0.2 mm

- Resolution: 10m (TX3) , 20m (TX2)

- Max. Transmission = 0, Max. Reflections = 2, Max, Diffraction = 2

- Max. Reflections and Diffraction = 2

- Max. Path Loss of ray = 200dB

- Max. Number of rays = 20

Figure A5.4.2-1: The view on the Aalborg city map with indication of transmitters location used in ray-tracing simulation.

A.6 Outdoor-to-indoor scenarios

A.6.1 China Mobile (CMCC) & Beijing University of Posts and Telecommunications (BUPT)

A.6.1.1 Channel sounder

Please refer to Section A.1.2.1. The antenna used in the O2I measurements is vertical polarized dipole.

A.6.1.2 Channel sounding

A.6.1.2.1 BUPT campus

The measurements were performed at the center frequency of 3.5 GHz with 100 MHz bandwidth in the main building BUPT campus. The main building a 14 floor building with the height of 66 m. The measurement spots are deployed along the corridor of each measured floor. The walls of the building are made of concrete and the doors wood. Outside the western wall of the main building is large open area with only a few trees of approximately 10m high, 90-100m away from the main building.

The TX antenna was located at different distances to the western wall of the main building (9m, 19m, 64m, 95m, 215m respectively, shown in Fig. A6.1.2.1-2). The TX antenna height is 5 m. The RX antenna is 1.7 m high to the indoor floor. The RX antenna heights of measured floors to the ground are 10.8 m, 18 m, 32.5 m, and 46.8m. The detailed parameters of this measurement is showed in Table A6.1.2.1-1.

Figure A6.1.2.1-1: BUPT campus measurement campaign.

Table A6.1.2.1-1: Parameters of measurement.

Item	Value
Channel Sounder	Propsound
Center Frequency	3.5GHz
Chip Rate	25M Chips/s
Channel Sample Rate	1968.5Hz
Code Length	127
Power	30.8dBm
Antennanumber	1×1
Bandewidth（MHz）	100
Antenna type	Dipole

A.6.1.2.2 CMCC Innovation Building

The measurement campaign was performed in the CMCC Innovation Building. The building is 120m high with 30 floors. The measurement spots are deployed on the western corridor of each measured floor. The surface of the building is covered by the IRR glass. The TX antenna was set up at 9 m and 19 m, two different distances to the southern wall of the main building as shown in Fig. A6.1.2.2-1. The RX is deployed on different floors with the antenna height to the ground ranged from 14 m to 68 m. Two different antenna heights of 5 m and 10 m are considered during the measurement. The detailed measurement parameters are the same with the measurement of BUPT campus.
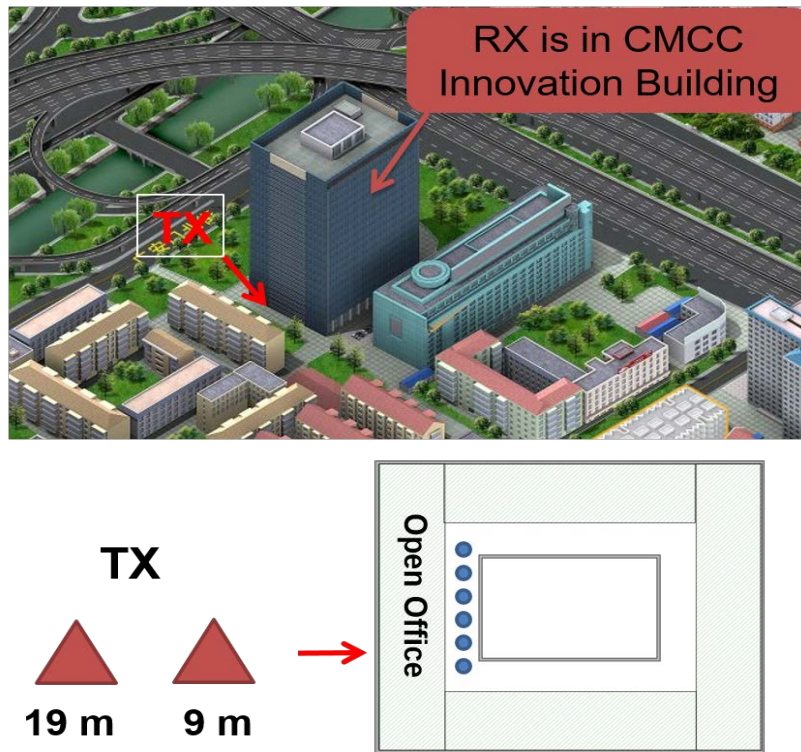
Figure A6.1.2.2-1: CMCC Innovation Building measurement campaign.

A.6.1.3   Findings and observations

As shown in Fig. A6.1.3-1, in BUPT campus measurement, penetration loss ranges from 13 dB to 37 dB with the mean value of 25 dB. For CMCC measurement, penetration loss ranges from 24 dB to 44 dB with the mean value of 37 dB. The building type. of the two measurement is so much different that results in about 12 dB gap in penetration loss. Fig. A6.1.3-2 shows the penetration loss is increasing with the tangent of the elevation angle from TX.
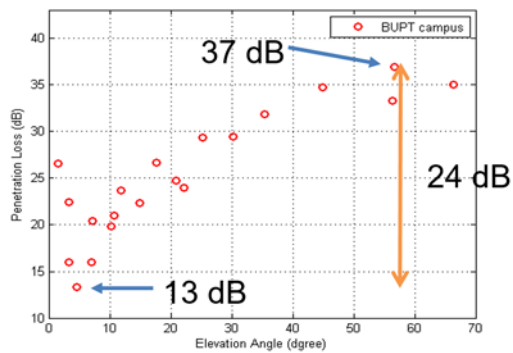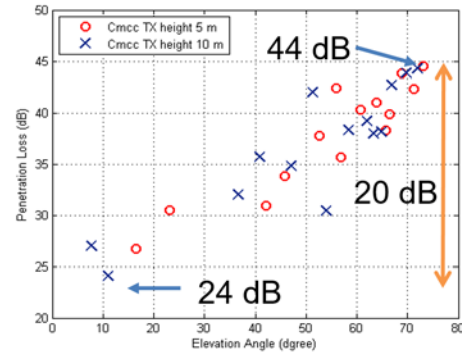
(a) BUPT campus   (b) CMCC Innovation Building

Figure A6.1.3-1: Penetration loss vs. elevation angle from TX.
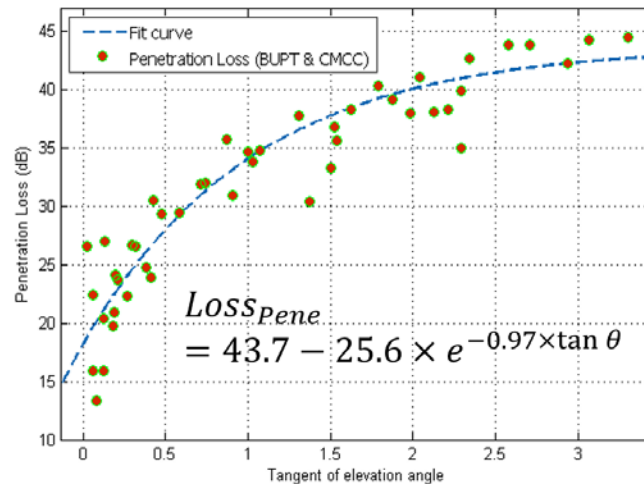
Figure A6.1.3-2: Modeling of Penetration loss vs. tangent of elevation angle.

A.6.2 Ericsson

A.6.2.1   28 GHz measurements

A.6.2.1.1 Channel sounder

The same channel sounder as described in Section A.5.2.1 was used also for the outdoor to indoor measurements. This channel sounder and some earlier measurements are also described in [LHOB14].

A.6.2.1.2 Channel sounding

The measurements have been done in four different office buildings during 2014 and 2015. These buildings represent somewhat different building styles and ages. In particular, in the two older buildings only very few windows have IRR coating while all windows have such coating in the two more modern constructions. Photos of these building can be found in Figure A6.2.1.2-1.

The outdoor wide beam antenna was placed with LOS to the building in a direction roughly perpendicular to the external wall. The indoor narrow beam antenna was moved to different positions close to the external wall and deeper into the building. In each position azimuth and elevation scans were performed and the received power was recorded for each pointing direction.

Figure A6.2.1.2-1: Office buildings for which outdoor to indoor measurements at 28 GHz have been performed. The two upper buildings are more modern constructions with 100% IRR glass

windows, while the two lower buildings are older constructions with predominantly regular window glass.

Table A6.2.1.2-1: Outdoor to indoor measurements.

	Old office building 1	Modern office building 1	Old office building 2	Modern office building 2
Date	May 2015	May 2015	2013	2015
No of Rx positions	12	15	44	28
Height of Tx position	On 8th floor	2 m above ground	12 m above ground	2m above ground
Distance from Tx to external wall	65 m	40 m	70 m	110 m
Height of Rx position	On 8th floor	On 3rd floor	On 3rd floor	On 3rd floor
Antenna gain Tx	22 dBi	22 dBi	22 dBi	22 dBi
Antenna gain Rx	34.6 dBi	34.6 dBi	34 dBi	34 dBi
Tx power	18 dBm	18 dBm	18 dBm	22 dBm
Link margin			169 dBi	173 dBi

A.6.2.1.3 Findings and observations

Non-coated windows as in older buildings lead to penetration losses in the order of 3-5 dB at 28 GHz, while coated windows cause penetration losses in the range 30-40 dB. When the external wall is composed of multiple materials with different loss characteristics (e.g. glass and brick/concrete) the penetration loss just inside the external wall varies quite strongly with position. However, further into the building the loss characteristics assume an average of the different materials characteristics. The loss as a function of distance into the building grows quite slowly in open areas while it can be highly variable when the interior contains walls and corridors. The range appears to be in the order of 0.5-2 dB/m.

A.6.2.2   15 GHz measurements

A.6.2.2.1 Measurement setup

The same measurement setup as described in A1.3.1.1 was used also for the outdoor to indoor measurements. Naturally, in the indoor environment, the mobile terminal carried by the electric scooter was used for data collection.

A.6.2.2.2 Measurement

Ericsson's outdoor-to-indoor measurement was conducted in an 8-floor office building in Kista; more specifically lower-right building in Figure A6.2.2.2-1, i.e. an older constructions with predominantly regular window glass.

Measurements were done during business hours with people occasionally blocking Rx-Tx paths.

Figure A6.2.2.2-1 shows typical variation of indoor received signal strength as a result of building window structure. At about 5 m distance from windows, there is an 8-10 dB variation in signal strength, which become more averaged deeper into the building.
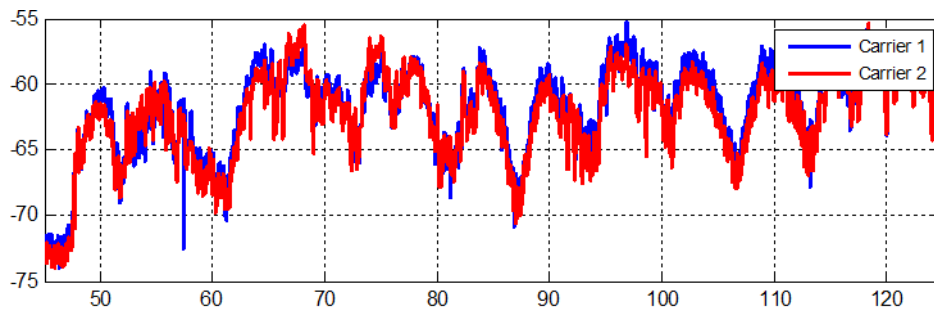
Figure A6.2.2.2-1: signal strength variation following building (window) structure about 5 m from windows.

Figure A6.2.2.2-2 illustrates two indoor walk routes where the "inner walk" is behind a second row of cubicle desks about 5 m further into the building, suggesting an additional propagation loss within this open office area to be in the order of 1 dB/m. Given building geometry in relation to position of used transmission point in that LoS between mobile terminal's and said transmission point antennas becomes blocked by horizontal window frames, an additional loss due to diffraction seems plausible.
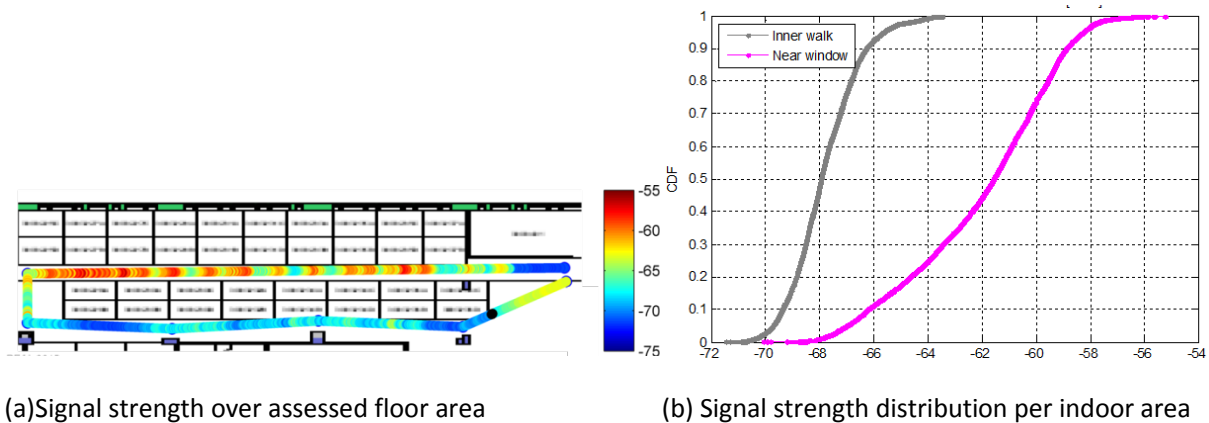
(a)Signal strength over assessed floor area

(b) Signal strength distribution per indoor area

Figure A6.2.2.2-2: signal strength variation with respect to in-building depth.

Measured penetration loss for different window configurations and blocking objects are listed in Table A6.2.2.2-1. Penetration loss from built-in metallic blinds was also considered; with blinds down but not closed, no additional loss was observed plausibly due to a blind separation in the order of the wavelength and due to the use of dual-polarized transmit and receive antennas. With blinds shut close, additional 8 dB signal loss was observed.

Table A6.2.2.2-1: Outdoor to indoor measurements, observed window and obstacle blocking losses.

Blocking Object	Measured loss	Model [ref]
3-glass ordinary window	6 dB	7.5 dB
3-glass ordinary window, closed blind	14 dB	N/A
3-glass IRR coated window	24 dB	27.5 dB
Human body at 30 cm from mobile terminal antenna	10 dB	N/A
2x1 m metallic whiteboard 3 m from mobile terminal antenna	10 dB	N/A
0.5 m wide concrete pillar 5 m from mobile terminal antenna	8 dB	

A.6.2.2.3 Findings and observations

- Path loss characteristics at 15 GHz seem rather similar to those experienced at cellular frequencies;
- Penetration loss through external wall with non-coated ordinary windows shows a typical penetration loss of 6 dB; closing built-in blinds may add 8 dB penetration loss. Windows with after-mounted coating show a penetration loss of 24 dB;
- It seems typical that indoor shadowing follows building façade structure, more specifically the structure of windows and concrete pillars, with 8-10 dB variation typically is observed at 5 m distance from windows. Variations observed to decrease deeper into the building;
- Typical and ordinary indoor objects such as whiteboards and human bodies attenuates received signal strength in the order of 6-10 dB;
- Additional indoor loss of 1 dB/m is observed and is likely due to impact from diffraction.

A.6.2.3　Multi-frequency measurements

A.6.2.3.1 Channel sounder

The channel sounder described in section A.1.3.2.1 have been used also for indoor measurements.

A.6.2.3.2 Channel sounding

The measurements are described in [R1-161688].

A.6.2.3.3 Findings and observations

The findings and observations are described in [R1-161688].

A.6.3 NTT DOCOMO, INC.

A.6.3.1　Measurement of path loss

A.6.3.1.1 Measurement system

Table A6.3.1.1-1 shows specifications of measurement equipment. Transmitter sends continuous wave (CW) and received power is recorded at receiver.

Table A6.3.1.1-1: Specifications of measurement equipment and parameters.

Parameters		Values					
Tx (BS)	Frequency (GHz)	0.81	2.2	4.7	8.45	26.4	37.1
	Power (dBm)	43	41	41	38	39	33
	Signal	CW					
	Antenna	Sleeve antenna					
	Antenna height	2.5 or 11.5 m					
Rx (MS)	Antenna	Sleeve antenna					
	Antenna height	1.5 m					
	Floor number of measurement	1, 2, 4, 6, 8					

A.6.3.1.2 Measurement campaign and data processing

Measurement was conducted in the campus of Niigata University, Japan. Measurement environment is illustrated in Fig. A6.3.1.2-1. Frequencies used for measurement were 0.81, 2.2, 4.7, 8.45, 26.4 and 37.1 GHz. Six sleeve antennas for each frequency were installed on a car roof (at B1 – B6) or roof of building (at A1 –A3) as BS with transmission of CW signal simultaneously. The antenna heights were 2.5 or 11.5 m. Measurement was conducted with two receiver units of hand trucks. Each one installed three different sleeve antennas on it with the interval of 1.5 m between floor and the antennas. Measurement was repeated on the floors of 1st, 2nd, 4th,

6th and 8th (namely, 1F, 2F, 4F 6Fand 8F). Note that vertically polarized waves were transmitted and received in the measurement.

The measured data of received power were post-processed in the following manner: (1) reference points were established every meter. (2) The data at the reference point and other data acquired within 0.5 m before/after the reference point were considered as a data set belonging to the reference point. (3) The median of the data set was determined as the received power at the reference point. (4) Finally, the power was converted to path loss.

(H)

(b)
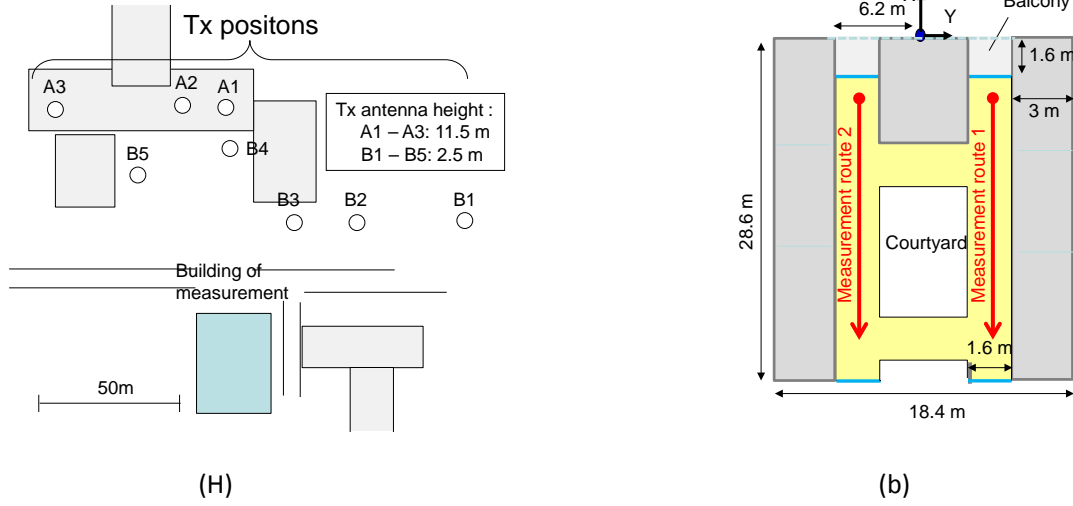
Figure A6.3.1.2-1: Measurement site. (a) Tx positions and building of measurement, (b) Layout of building and measurement routes.

In conventional model [3GPP15], O2I path loss in dB can be basically modeled by,

$$PL = PL_b + PL_{tw} + PL_{in} . \tag{A6.3.1.2-1}$$

Here, PL_b is "basic path loss" which represents loss in outdoor scenario, PL_{tw} is penetration loss into building, and PL_{in} is loss inside. Here, PL_b is assumed as free space loss;

$$PL_b = 20\log(d_{3D-out} + d_{3D-in}) + 20\log f_{GHz} + 32.4 , \tag{A6.3.1.2-2}$$

and PL_{in} is assumed as

$$PL_{in} = 0.5 d_{2D-in} . \tag{A6.3.1.2-3}$$

Equations (2) and (3) are same as that in 3GPP 3D channel model [3GPP15], f_{GHz} is frequency in GHz and definitions of other parameters are shown in the figure A6.3.1.2-2. The normalized measured data by calculated PL_b and PL_{in} are regarded as PL_{tw}.
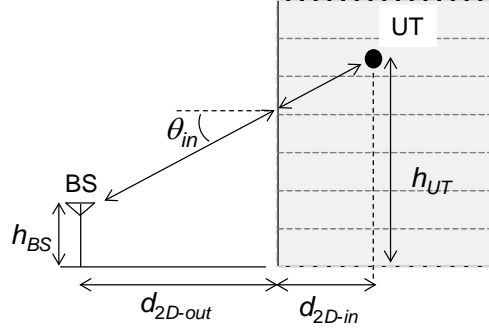
Figure A6.3.1.2-2: Definitions of parameters.

A.6.3.1.3 Findings and observations

Figure A6.3.1.3-1 shows the penetration loss characteristic, all measured data are plotted here. In this figure, the horizontal axis represents incident angle, θ_{in}, and vertical axis represents penetration loss, PL_{tw}. We find that PL_{tw} increases when θ_{in}, becomes large and there are upper limit and lower limit. This means that the characteristic can be modeled as sigmoidal function. The blue line is a regression result based on sigmoidal function, and it is expressed by

$$PL_{tw} = 6.8 + \frac{21.9 - 6.8}{1 + \exp\{-0.453(\theta_{in} - 19.4)\}} \cdot \qquad \text{(A6.3.1.3-1)}$$

Here, the values of 21.9 and 6.8 represent upper limit and lower limit, respectively. RMS value of residual error is 6.8 dB. And correlation coefficient between the residual error and incident angle is lower than 0.001. This means that the penetration loss, PL_{tw}, is randomized by our proposed model with regard to the incident angle, enough. Note that we have confirmed that frequency dependent of PL_{tw}, is very little.
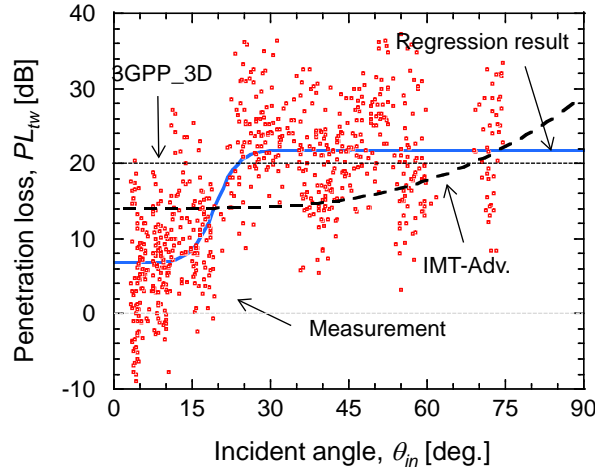
Figure A6.3.1.3-1: Penetration loss characteristics.

A.6.3.2   Measurement of channel model parameters

A.6.3.2.1 Channel sounder

Please refer to Section A.3.4.2.1.

A.6.3.2.2 Channel sounding

The channel sounding for Outdoor-to-Indoor (O2I) scenario was performed in the campus of Niigata University, Niigata, Japan as shown in Figure A6.3.2.2-1. In measurement, we located the Tx of the channel sounder at

points B2, B3 with the antenna height of 2.5 m. On the other hand, we located the Rx of the channel sounder in the building. Measurement data was acquired in corridors on 1st , 2nd, 4th, 6th, 8th floors (namely, 1F, 2F, 4F 6F and 8F) with the positions of 2 m, 9 m, 16 m from glass windows. The height of the horn antenna was 1.5 m. Here, at each Rx position, we rotated the horn antenna and measured PDPs. The ranges of rotation were from -180 degrees to +180 degrees with a 1 degree step for azimuth angle, and from -50 degrees to +50 degrees in a 10 degree step for elevation angle.
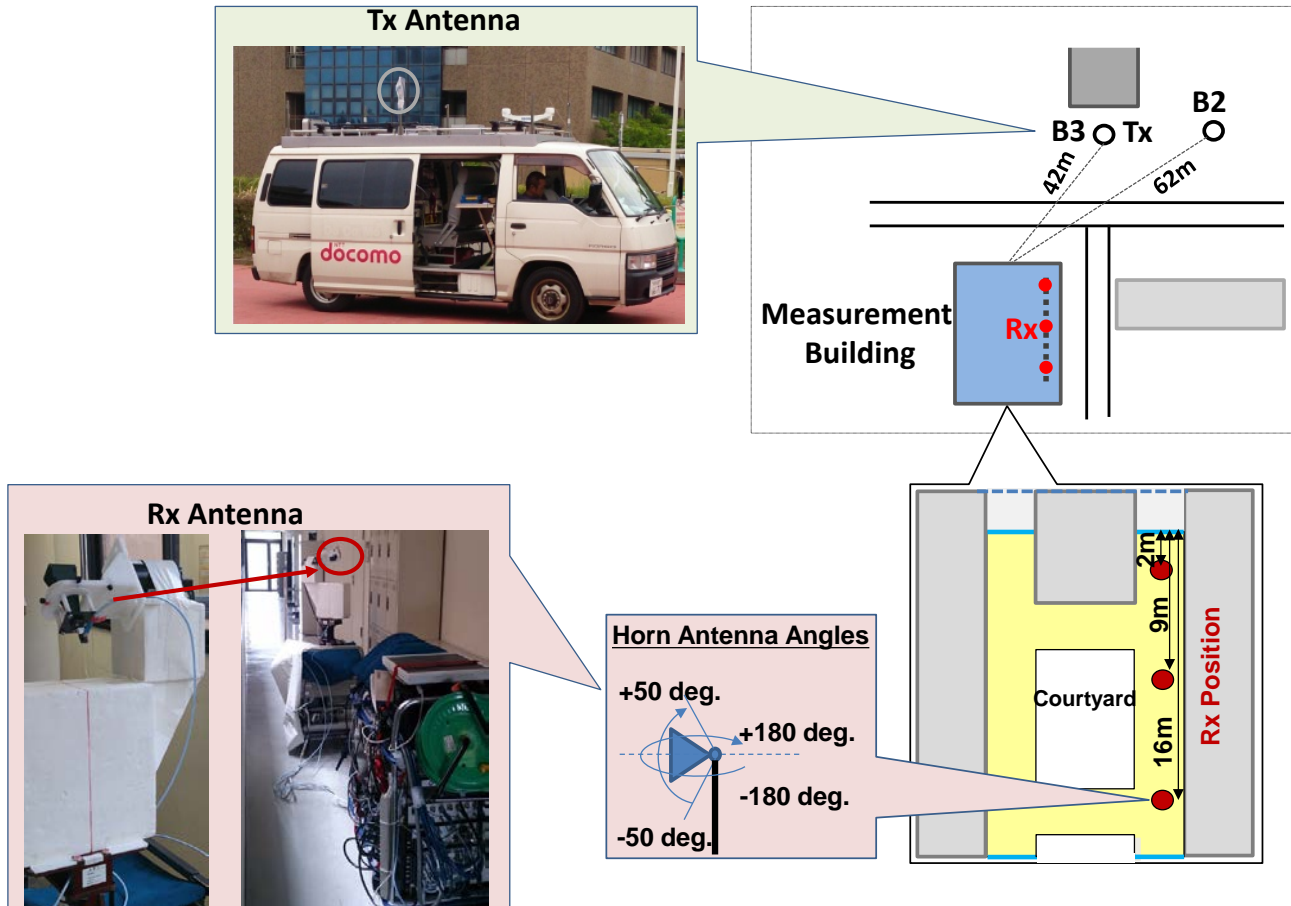
Figure A6.3.2.2-1: Channel sounding setups for Outdoor-to-Indoor scenario.

A.6.3.2.3 Findings and observations

Table A6.3.2.3-1 shows the measurement results for Outdoor-to-Indoor (O2I) scenario. Here, the K-Power-Mean method was used to cluster multipath. The delay times, azimuth angles, elevation angles of cluster centroids were used to obtain DS, ASA, ZSA at each position.

Floor	TX Positions	RX Positions	DS [ns]	ASA [deg.]	ZSA [deg.]	# of Paths	# of Clusters	# of rays per Cluster	Cluster DS [ns]	Cluster ASA [deg.]	Cluster ZSA [deg.]
1F	A1	2m	45.7	96.6	3.6	82.0	11.0	7.5	39.9	20.3	3.3
		9m	40.2	30.7	0.7	58.0	5.0	11.6	47.6	36.5	2.5
		16m	43.7	33.6	2.7	36.0	12.0	3.0	22.0	8.8	2.8
	A2	2m	56.4	52.2	1.7	61.0	4.0	15.3	53.8	37.4	3.9
		9m	51.7	21.6	1.1	60.0	3.0	20.0	61.7	69.2	3.5
		16m	52.7	52.7	1.9	68.0	6.0	11.3	23.5	55.2	4.0
2F	A1	2m	35.0	45.3	1.8	47.0	3.0	15.7	32.6	102.0	6.7
		9m	52.3	87.9	2.7	68.0	9.0	7.6	36.8	19.9	4.2
		16m	11.0	26.0	1.1	19.0	8.0	2.4	10.3	10.7	1.0
	A2	2m	82.2	64.1	2.7	75.0	9.0	8.3	35.6	16.3	3.4
		9m	64.2	25.6	0.8	64.0	3.0	21.3	71.7	63.5	4.7
		16m	62.4	26.2	2.0	54.0	3.0	18.0	62.3	56.9	6.2
4F	A1	2m	47.0	7.3	12.8	18.0	3.0	6.0	19.9	55.6	4.4
		9m	55.4	46.3	2.2	82.0	3.0	27.3	61.1	66.3	7.0
		16m	77.1	25.7	0.4	72.0	4.0	18.0	57.3	56.3	6.1
	A2	2m	3.5	50.2	6.7	43.0	3.0	14.3	50.1	40.4	10.5
		9m	12.9	64.8	3.4	71.0	3.0	23.7	91.5	45.9	5.1
		16m	104.8	32.6	1.2	50.0	3.0	16.7	40.1	50.2	6.2
6F	A1	2m	32.6	43.9	16.1	43.0	8.0	5.4	36.3	15.3	4.6
		9m	53.0	32.8	4.4	45.0	5.0	9.0	65.9	37.1	7.6
		16m	151.6	70.9	8.5	37.0	12.0	3.1	27.6	7.7	3.8
	A2	2m	77.9	43.0	18.0	45.0	10.0	4.5	49.1	12.2	6.5
		9m	77.8	20.0	5.5	16.0	8.0	2.0	5.5	6.7	3.7
8F	A1	2m	47.4	50.7	25.2	47.0	4.0	11.8	43.2	38.4	9.3
		9m	98.1	39.1	3.4	33.0	8.0	4.1	32.1	18.1	6.4
		16m	129.0	67.0	2.3	16.0	9.0	1.8	10.4	2.3	1.2
	A2	2m	123.6	81.0	21.6	58.0	8.0	7.3	58.6	29.9	8.0
		9m	98.3	63.0	3.1	17.0	5.0	3.4	18.7	17.1	6.0
		Mea	63.8	46.5	5.6	49.5	6.1	10.7	41.6	35.6	5.1
		Std	34.7	21.5	6.6	19.8	3.0	7.1	20.2	23.8	2.2
	log10	μ	-7.29	1.62	0.5	-	-	-	-	-	-
		σ	0.34	0.24	0.46	-	-	-	-	-	-

Cross-correlations	
ASA vs DS	0.25
ZSA vs DS	0.12
ZSA vs ASA	0.15

Table A6.3.2.3-1: Measurement results for Outdoor-to-Indoor scenarios.

A.7   Indoor hotspot scenarios – Airport terminal

A.7.1 Electronics and Telecommunications Research Institute (ETRI)

A.7.1.1   Channel sounder

Please refer to Section A.1.3.1.

A.7.1.2   Channel sounding

An airport terminal is a representative indoor hotspot environment where mobile traffics are likely to be congested due to dense population. The layout of airport site (Passenger terminal at Incheon International Airport) is a larger hall. The size is about 650m x 82m x 20m (height). The measurements were collected in the departure floor (where the check-in booths are arranged in parallel). The construction techniques are similar to those of the railway station.

All the equipment setting parameters were the same with the indoor hotspot scenario – Railway station. Figure A7.1.2-1 shows the airport passenger terminal measurement site on which locations of TX and RX are marked.

Figure A7.1.2-1: Measurement scenarios (left) and campaign at Incheon Airport Terminal (right).

A.7.1.3 Findings and observations

A.7.1.3.1 Path Loss

Figure A7.1.3.1-1 shows the measured path loss using an omnidirectional antenna along with the CI model predictions in indoor hotspot – Airport terminal scenario at 28 and 38 GHz. Table A7.1.3.1-1 summarizes the resulting empirical path loss parameters. In the indoor hotspot – Airport terminal scenario, we can observe that the PLEs are similar at both frequencies in LoS and NloS environments.

(a) 28 GHz   (b) 38 GHz
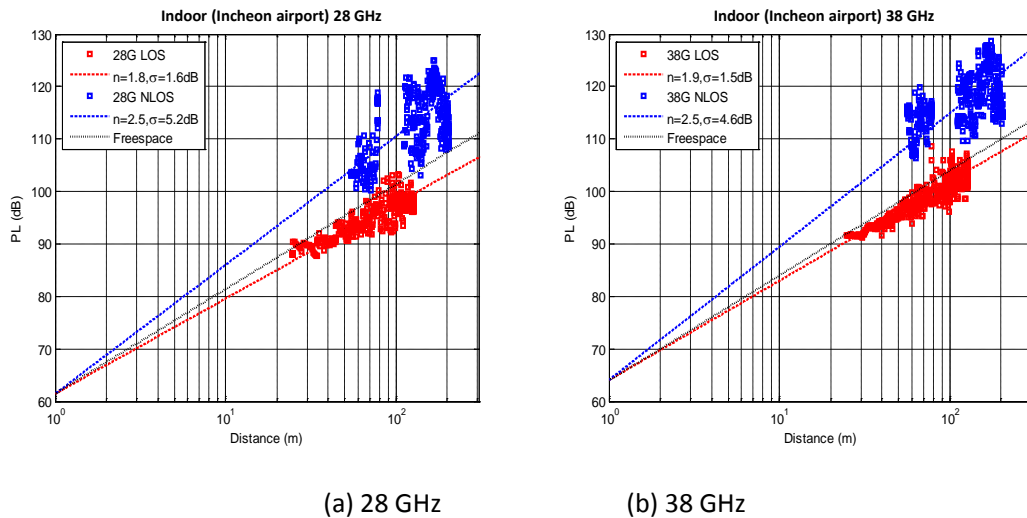
Figure A7.1.3.1-1: Measured path loss in Indoor hotspot scenario.

Table A7.1.3.1-1: Parameters in the CI path loss model in Indoor hotspot scenario.

Scenario	Model	28 GHz				38 GHz			
		LOS		NLOS		LOS		NLOS	
		PLE	σ[dB]	PLE	σ[dB]	PLE	σ[dB]	PLE	σ[dB]
Indoor Hotspot – Airport terminal	CI	1.8	1.6	2.5	5.2	1.9	1.5	2.5	4.6

A.7.1.3.2 Delay and angular spread

Please refer to Section A.1.3.4.2 for the detail calculation method of delay and angular spread. Cumulative distribution functions of delay spread (DS) and angular spread (AS) are shown in the below figures.
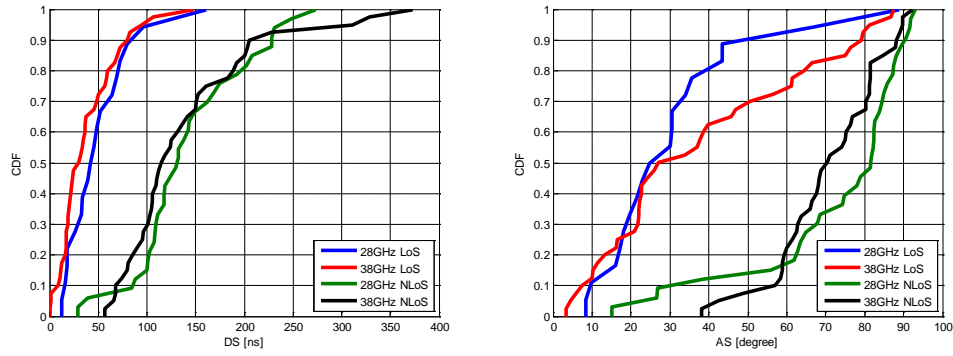
Figure A7.1.3.2-1: CDF of DS (left) and AS (right).

Table A7.1.3.2-1: Percentiles of DS and AS.

		Delay spread [nsec]		Angular spread [degree]	
		28 GHz	38 GHz	28 GHz	38 GHz
LOS	10%	15.1	8.3	9.6	7.5
	50%	42.2	30.0	24.8	27.1
	95%	102.8	94.3	69.4	81.2
NLOS	10%	85.6	68.1	30.3	57.0
	50%	130.6	115.1	81.6	70.3
	95%	236.8	311.4	91.6	89.8

A.7.1.3.3 Cluster parameters

For cluster-wise analysis, the K-PowerMeans algorithm is utilized for clustering of estimated MPCs from SAGE. Cumulative distribution functions of cluster parameters are shown in the below figures.
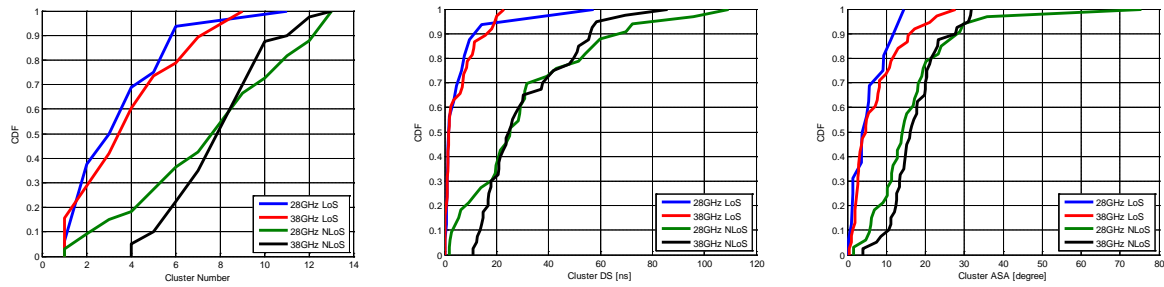
Figure A7.1.4.3-1: CDF of cluster number, DS and AS.

Table A7.1.4.3-1: Percentiles of cluster number, DS and AS.

		Cluster number		Cluster DS [nsec]		Cluster AS [degree]	
		28 GHz	38 GHz	28 GHz	38 GHz	28 GHz	38 GHz
LOS	10%	1.1	1.0	0.5	0.0	0.7	1.3
	50%	3.0	3.4	1.5	1.5	3.8	4.6
	95%	7.0	8.1	22.8	19.3	13.2	21.2
NLOS	10%	2.2	5.0	2.9	13.8	5.8	10.6
	50%	7.6	7.9	25.2	24.9	14.2	16.0
	95%	12.6	11.7	80.6	58.6	32.0	31.0

A.8 Indoor hotspot scenarios – Railway station

A.8.1 Electronics and Telecommunications Research Institute (ETRI)

A.8.1.1 Channel sounder

Please refer to A.1.4.1.

A.8.1.2 Channel sounding

A railway passenger terminal is a representative indoor hotspot environment where mobile traffics are likely to be congested due to dense population. The layout of railway site (Passenger terminal at Seoul Station) is a large hall with a dimension of 170m x 45m x 21m (height). The ceiling and walls are constructed with steel frames and thick tempered glasses. On the wall are mounted large TV screens that display train departure-and-arrival information.

Almost all the equipment setting parameters were the same with the outdoor measurement case except that we used a 60º (at 28 GHz) and a 40° (at 38 GHz) HPBW antenna at the TX side, respectively. To emulate typical hot-spot scenarios, we installed the TX antenna at a height of 8 m (ceiling level) from the floor and the RX antenna at 1.5 m (pedestrian level). Figure A8.1.2-1 shows the railway passenger terminal measurement site on which locations of TX and RX are marked. As can be seen, TX was held at a fixed position and its antenna was directed to measurement points as the shaded radial region in the figure.
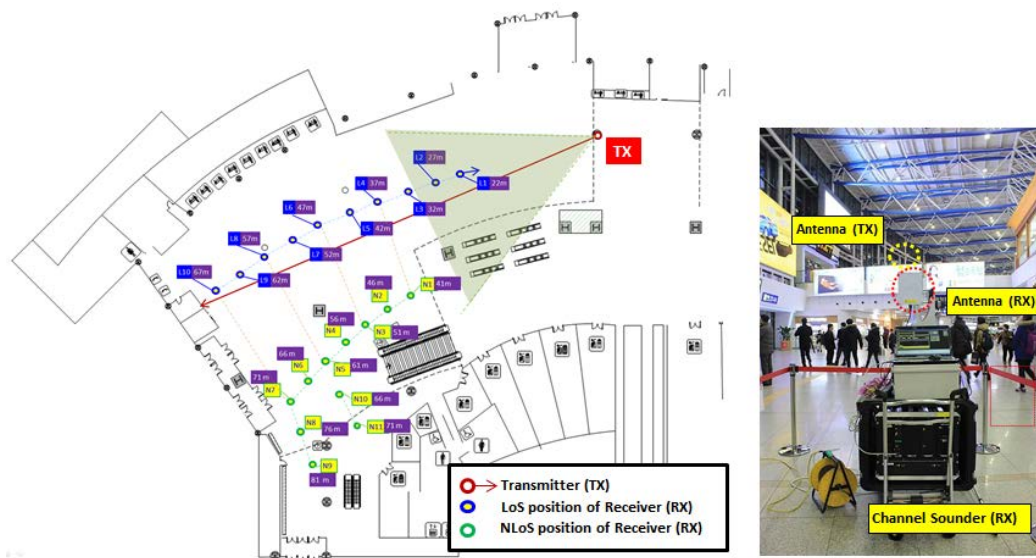
Figure A8.1.2-1: Measurement scenario (left) and campaign at Seoul Railway Station (right).

A.8.1.3 Findings and observations

A.8.1.3.1 Path Loss

Table A8.1.3.1-1 summarizes the resulting empirical path loss parameters. In the indoor hotspot – Railway station scenario, the PLEs of the CI model are 1.8 at LoS situations, which are smaller than the free space (PLE = 2). Comparing to the Umi scenario, we can also observe that the PLEs are similar at both frequencies in LoS and NloS environments. However, for NloS, the PLEs are smaller than those for the Umi environments. This can be explained that the indoor hotspot environments have richer scattering than the outdoor environments.

Table A8.1.3.1-1: Parameters in the CI path loss model in Indoor hotspot scenario.

Scenario	Model	28 GHz				38 GHz			
		LOS		NLOS		LOS		NLOS	
		PLE	σ[dB]	PLE	σ[dB]	PLE	σ[dB]	PLE	σ[dB]
Indoor Hotspot – Railway station	CI	1.8	0.7	2.6	7.9	1.8	1.2	2.7	6.4

A.8.1.3.2 Delay and angular spread

Please refer to Section A.1.3.4.2 for the detail calculation method of delay and angular spread. Cumulative distribution functions of delay spread (DS) and angular spread (AS) are shown in the below figures.
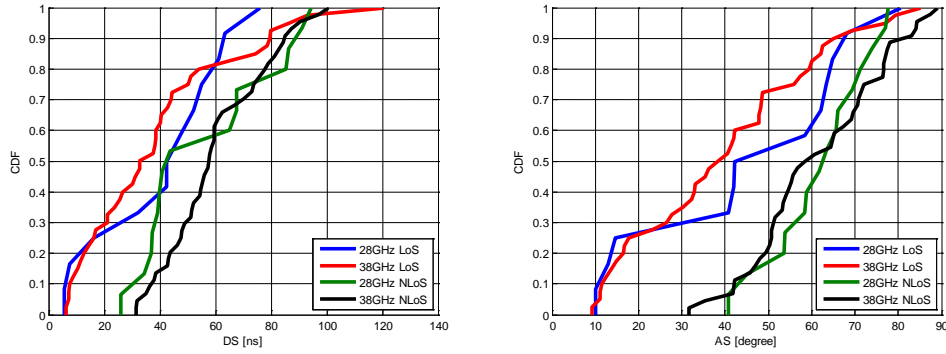
Figure A8.1.3.2-1: CDF of DS (left) and AS (right).

Table A8.1.3.2-1: Percentiles of DS and AS.

		Delay spread [nsec]		Angular spread [degree]	
		28 GHz	38 GHz	28 GHz	38 GHz
LOS	10%	6.0	7.6	10.6	11.4
	50%	42.5	32.7	42.3	38.5
	95%	68.5	86.3	73.1	77.0
NLOS	10%	30.2	36.9	43.0	42.0
	50%	42.2	57.5	62.5	58.4
	95%	91.9	89.9	77.3	84.2

A.8.1.3.3 Cluster parameters

For cluster-wise analysis, the K-PowerMeans algorithm is utilized for clustering of estimated MPCs from SAGE. Cumulative distribution functions of cluster parameters are shown in the below figures.
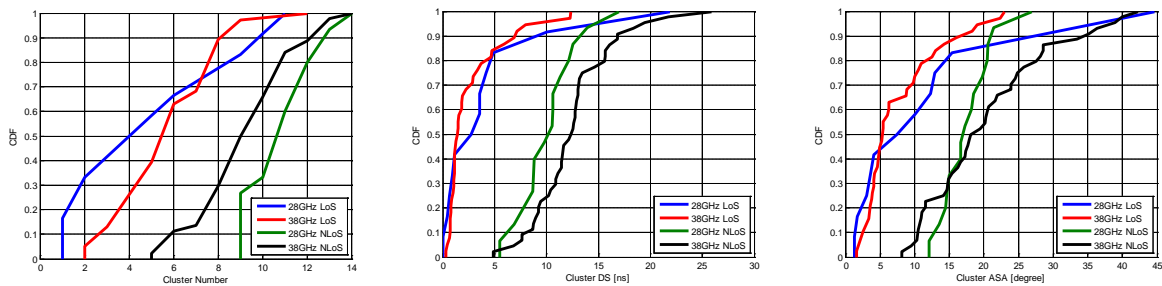
Figure A8.1.3.3-1: CDF of cluster number, DS and AS.

Table A8.1.3.3-1: Percentiles of cluster number, DS and AS.

		Cluster number		Cluster DS [nsec]		Cluster AS [degree]	
		28 GHz	38 GHz	28 GHz	38 GHz	28 GHz	38 GHz
LOS	10%	1.0	2.6	0.1	0.7	1.4	2.5
	50%	4.0	5.4	2.7	1.4	7.4	5.4
	95%	10.4	8.7	14.8	8.4	36.0	19.3
NLOS	10%	9.0	5.9	6.2	8.0	12.8	10.5
	50%	10.6	9.0	10.1	12.4	16.9	18.1
	95%	13.3	12.7	14.7	19.2	22.8	38.4

## A.9 Link blockage and penetration measurements

A.9.1 Ericsson

A.9.1.1 Measurement system

Please refer to Section A.1.3.1.1. An electric scooter carried the mobile terminal while maintaining a typical speed of 0.5 m/s. The mobile scooter is also equipped with a high definition action camera, with the recording sequences being time-aligned with radio terminal's data collection.

A.9.1.2 Findings and observations

Location of assessed test routes and corresponding stationary/mobile blocking objects are depicted in Figure A9.1.2-1. Assessed stationary blocking objects are road sign A, birch trees A-C and a van. Assessed mobile blocking objects are trucks A and B. A reflection path from road sign B is also identified.
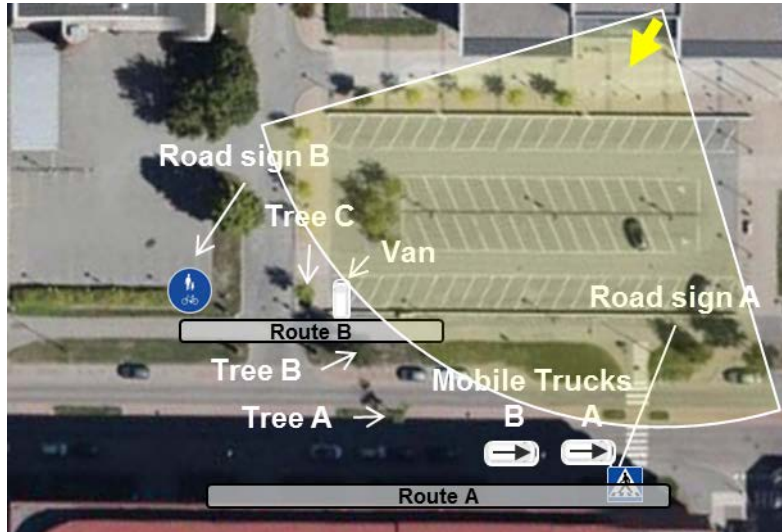
Figure A9.1.2-1: Ericsson 'Urban microcellular scenario – Overview outdoor blocking area.

A.9.1.2.1 Blocking due to a road sign pole and trees

Road sign A is located at approximately 1 m distance (50* wavelength) from the mobile terminal antenna. With used measurement setup, mobile terminal antennas are located below the sign itself, and observed signal blocking is only due to shadowing by the pole itself. It is observed that blocking of the LoS path decreases the received signal strength by about 3-4 dB, scattering is observed in areas slightly before/after the passage; see Figure A9.1.2.1-1.

(a)Mobile position behind blocking road sign pole　　　(b)Associated signal strength variation
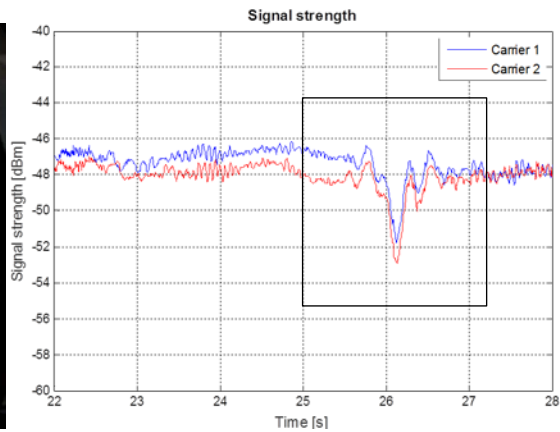
Figure A9.1.2.1-1: Ericsson 'Urban microcellular scenario – road sign blocking.

About 5 dB attenuation is observed due to smaller/medium size tree blocking LOS between TP and mobile terminal antenna; see Figure A9.1.2.1-1. Blocking by a somewhat wider tree (and partially a smaller truck) results in about 7 dB signal attenuation; see Figure A9.1.2.1-2.

(a)　Mobile position behind blocking mid-size tree(b) Associated signal strength variation

Figure A9.1.2.1-1: Ericsson 'Urban microcellular scenario – tree blocking.

(a)　Mobile position behind blocking larger tree　(b) Associated signal strength variation
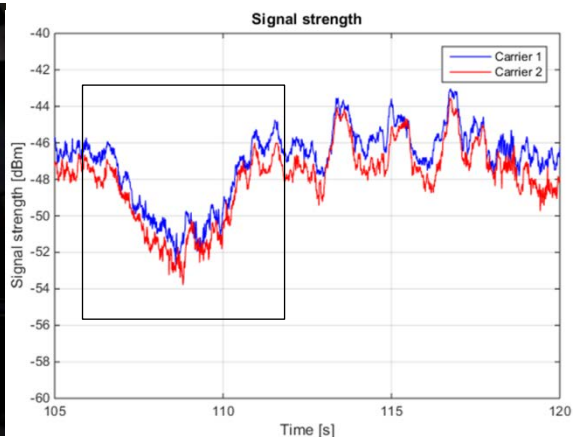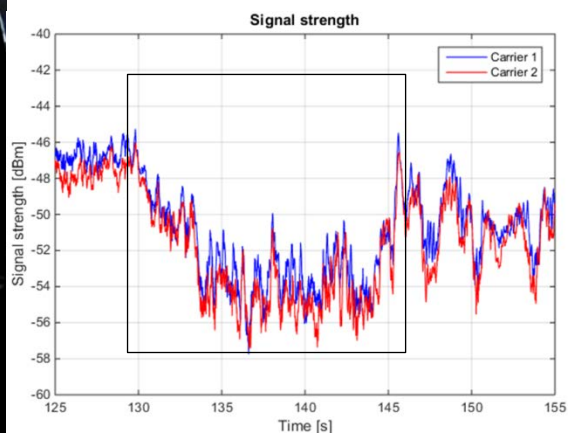
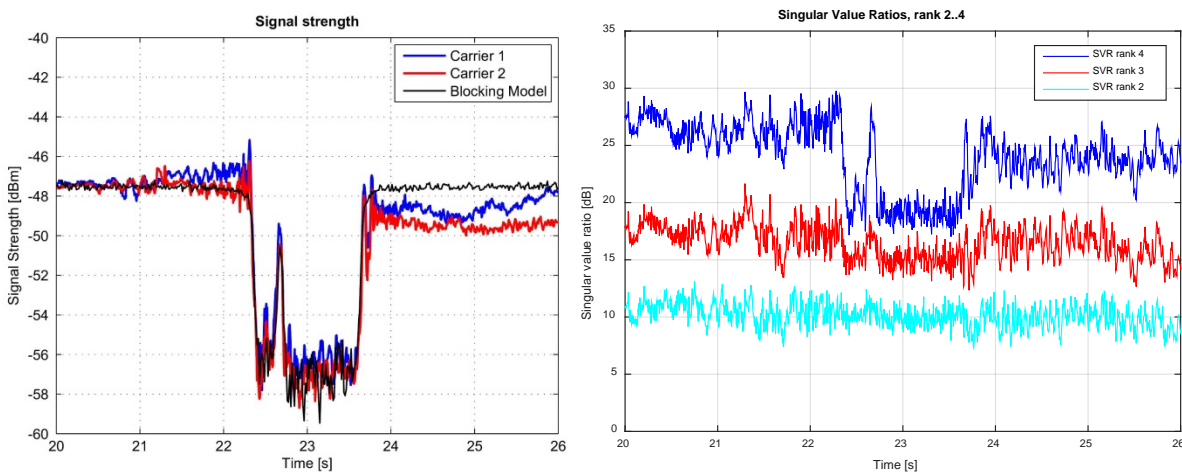**Figure A9.1.2.1-2: Ericsson 'Urban microcellular scenario – tree blocking.**

A.9.1.2.2 Blocking loss of around 10 dB for moving vehicles motivate that not only stationary obstacles but also mobile obstacles must be taken into account in blocking modelling

Figure A9.1.2.2-1 illustrates a snapshot when a three-axle truck, (moving to the right) blocks the LoS towards the TP. Figure A9.1.2.2-2(a) shows received signal strength associated with the passage of the truck in detail. Blocking of the LoS path decreases total received signal strength at the mobile terminal by typically 8-10 dB. The short LoS period between the driver's compartment and the container results in a sudden peak in the signal strength at ~22.7 s. Figure A9.1.2.2-2(b) shows singular value ratios (SVRs) during same period of time. SVR for rank r, r=2..4, is defined as the ratio of the first and the r-th ordered singular values of the MIMO channel; SVR is meant to represent the friendliness of the channel for r-layer MIMO transmission, where lower SVR indicates richer channel. As LoS path between the TP and the mobile terminal antennas are blocked, SVR for rank 4 is decreased by about 7-8 dB, which confirms that there is significant multipath in the channel and blocking only impacts some of this multipath.

Associated blocking loss by the truck is also simulated using two rectangular screens corresponding to the size of the truck (9 m length and 3 m height with a 0.4 m gap). Figure A9.1.2.2-2(a) shows that the METIS model predicts the blocking loss accurately.

Figure A9.1.2.2-1: Ericsson 'Urban microcellular scenario – Mobile terminal's position in relation to blocking garbage truck.

(a) Signal strength variation and METIS model

(b) Associated Singular Value Ratios

Figure A9.1.2.2-2: Ericsson 'Urban microcellular scenario – blocking from garbage truck.
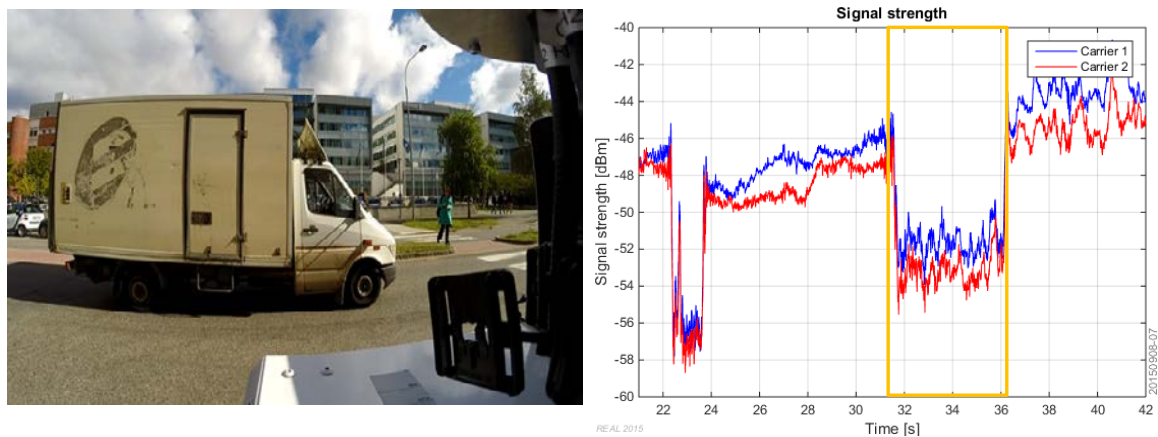
(a) Mobile terminal position in relation to the truck (b) Signal strength variation

Figure A9.1.2.2-3: Ericsson 'Urban microcellular scenario – blocking from truck.

Figure A9.1.2.2-3(a) illustrates a smaller truck (moving to the right, but temporally stopped at crosswalk) blocking LoS signal path towards the TP. By that received signals strength is attenuated by 6-7 dB. Similar trend as observed for the garbage truck.

A.9.1.2.3 Doppler analysis reveals that for some blocking objects such as cars and vans propagation happens only around the objects; for other objects such as trees, propagation happens through the object
Figure A9.1.2.3-1 shows Doppler power spectrum versus time for a measurement along route B in Figure A9.1.2-1, where the mobile terminal initially is stationary and then travels in the forward direction until the turning point where it is walked back along the same route to the initial position. As illustrated in Figure A9.1.2.3-1, there are two main blocking objects along the route, a stationary van and a birch tree, but also other objects such as e.g, road sign poles.

The Doppler spectrum shows that when the mobile terminal is stationary (area labeled "1"), the corresponding Doppler frequency is almost zero. During the walk along the LoS-like segments, a strong component with a negative Doppler frequency is observed when moving away from the TP (i.e. in the forward direction) and a positive Doppler frequency when moving in the opposite way (i.e. in the backward direction); see areas tagged as "2".

During transition from LoS to "behind the van" (areas tagged as "3"), the peak in the power spectrum becomes divided into two main paths with different Doppler frequencies (compared to LoS) suggesting that the van completely blocks the LoS propagation path.
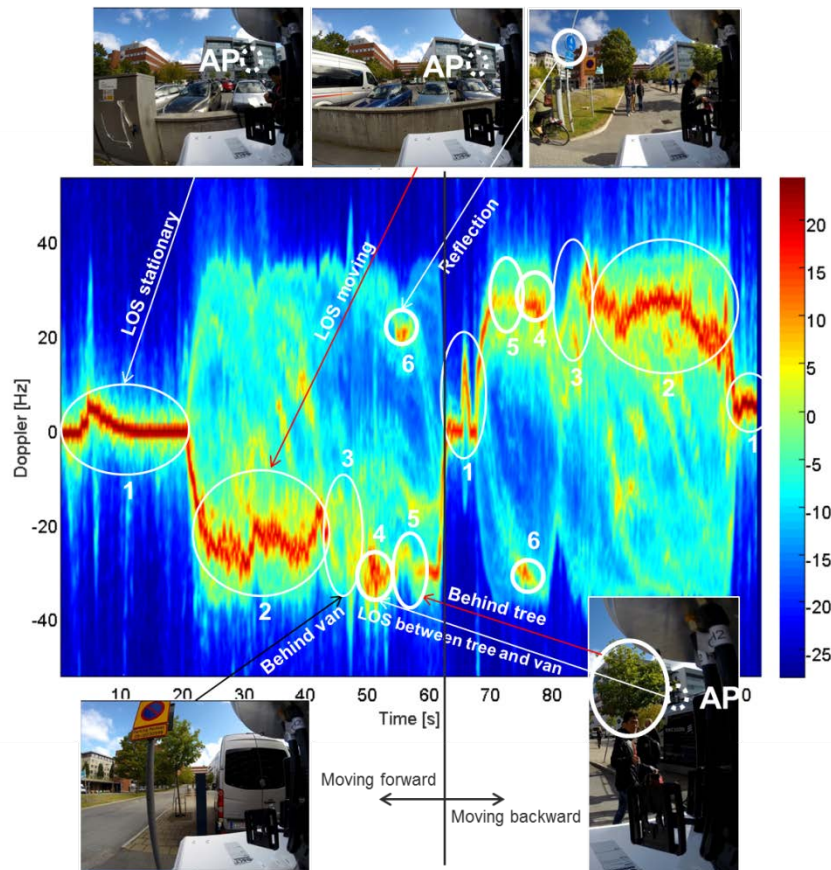
Figure A9.1.2.3-1: Ericsson 'Urban microcellular scenario – Doppler spectrum assessment.

After passing the stationary van, the mobile terminal arrives behind a birch tree (area tagged as "5"); in this area, the Doppler frequency is not significantly changed compared to LoS, but the received power becomes weaker indicating that the tree does not completely block the signal and the signal seems to propagate through the tree. In the transition from "behind van" to "behind tree", the terminal experiences LoS to the TP during a short period; see area labelled as "4". In that area, the power suddenly increases compared to the power "behind van" or "behind tree". Areas tagged as "6" illustrate a reflection in the road sign pole B.

A.9.2 Nokia

A.9.2.1 Channel sounder

The setup is shown in Figure A9.2.1-1 and consisted of continuous wave (CW) measurements at 28, 39, and 73 GHz. The Rx and Tx antennas were horn antennas with the setup given in Table A9.2.1-1. The penetration loss was calculated as power difference with and without material inserted between horn antennas. The penetration loss of various common residential building materials (as given in next section) were calculated.

Table A9.2.1-1: Measurement setup.

Frequency	Tx-Rx separation	Gain	Antenna dimension
28 GHz	17 cm	20 dBi	34.8 mm x 27.7 mm
39 GHz	23 cm	20 dBi	34.8 mm x 27.7 mm
73 GHz	41 cm	20 dBi	20 mm x 15 mm
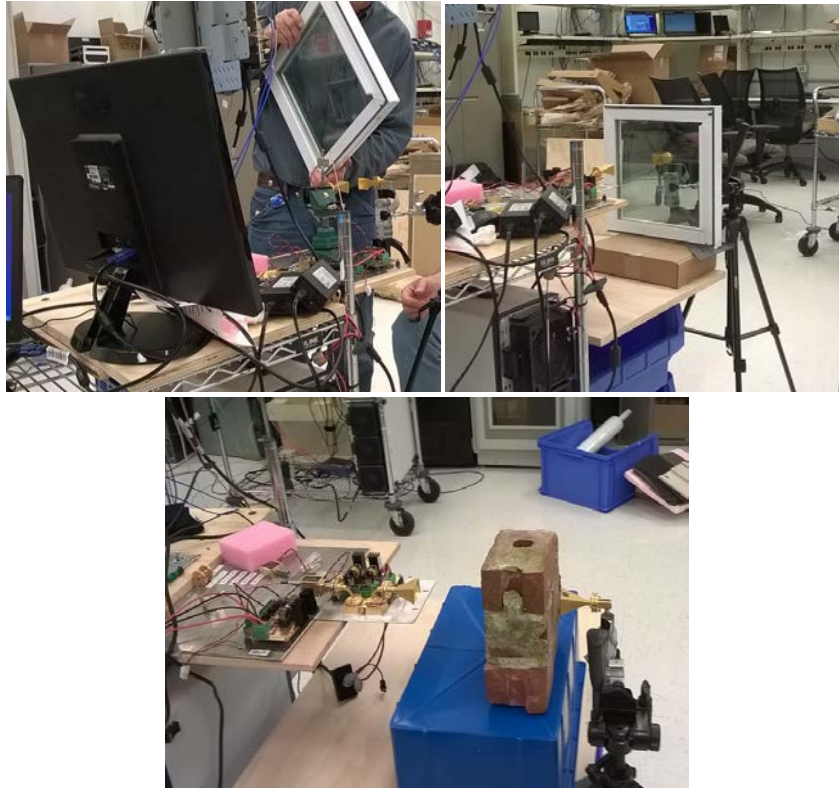
Figure A9.2.1-1: Penetration Loss Measurement Setup.

A.9.2.2   Channel sounding

Figure A9.2.2-1 and Figure A9.2.2-2 give the penetration loss measurements for the variety of residential building materials. The results in Figure A9.2.2-1 show the maximum loss at each frequency (note that the 73 GHz results for paver brick, cinderblock, and foil faced foam sheathing were beyond the measurement sensitivity and hence are not better than the other frequencies). Figure A9.2.2-2 provides a table of both the maximum loss and the nominal (minimum) loss at each frequency for all of the different building materials.

Figure A9.2.2-1: Penetration Loss Measurement Results.

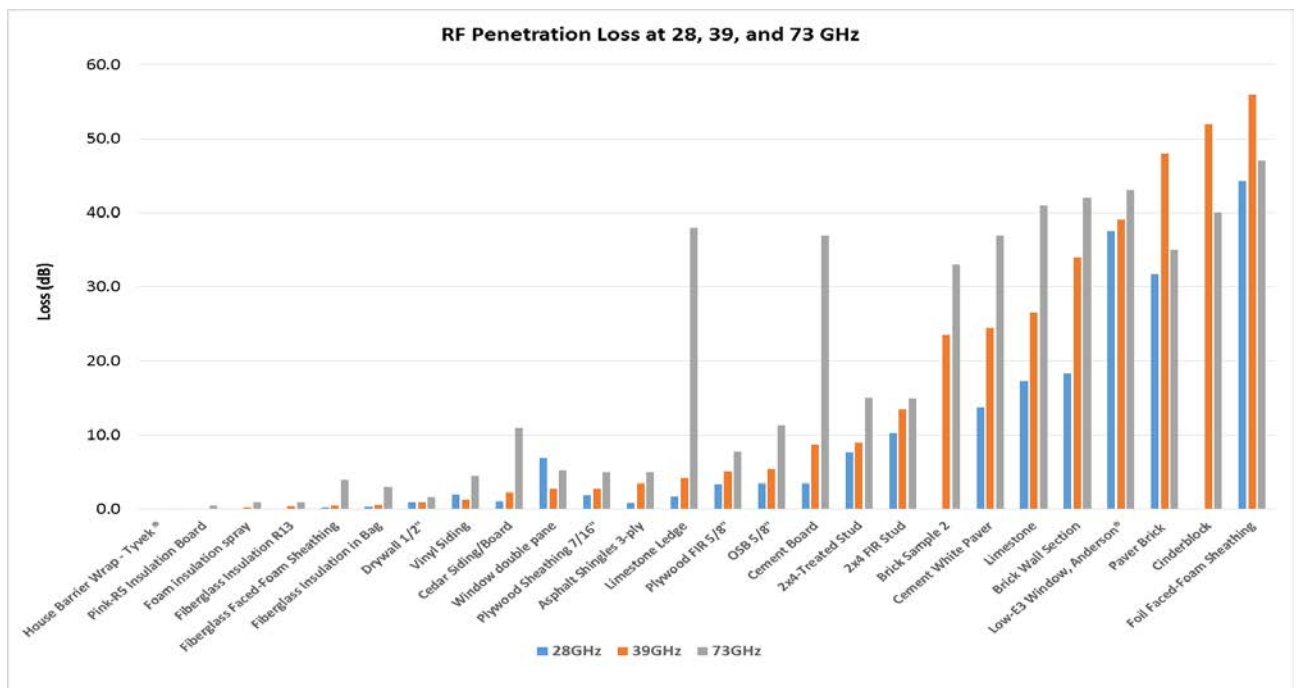| Material	28GHz		39GHz		73GHz	
	Nom Loss (dB)	Max Loss (dB)	Nom Loss (dB)	Max Loss (dB)	Nom Loss (dB)	Max Loss (dB)
OSB 5/8"	3.5	4.3	5.5	8.4	11.3	14.8
Plywood Sheathing 7/16"	1.9	2.3	2.8	3.7	5.0	
FiberGlassFaced-Foam sheathing	0.2	0.3	0.5	0.7	4.0	
Foil faced-foam sheathing	44.3	44.3	56.0	55.0	47.0	
Pink-R5 Insulation Board	0.0	0.0	0.1	0.1	0.5	
Vinyl Siding	2.1	3.8	1.3	1.7	4.5	8.8
Asphalt Shingles 3-ply	0.9	1.5	3.5	5.0	5.0	
2x4 FIR stud	10.3	11.3	13.5	15.0	15.0	
2x4-Treated stud	7.7	8.3	9.0	9.5	15.1	15.7
Cement board	3.5	4.5	8.8	9.5	37.0	39.0
Window doublepane	7.0	9.2	2.8	3.1	5.3	5.5
Drywall 1/2"	1.0	1.2	1.0	1.5	1.6	1.9
Cedar siding/Board	1.1	1.3	2.3	2.4	11.0	14.0
Plywood FIR 5/8"	3.4	4.1	5.1	6.2	7.8	8.9
Brick wall	18.4	25.3	34.0	47.0	42.0	44.0
Brick sample 2			23.5	37.0	33.0	34.0
Limestone	17.3	23.3	26.5	29.0	41.0	42.0
Limestone ledge	1.8	2.3	4.3	5.5	38.0	39.0
Cinder block			52.0	52.0	40.0	41.0
Cement white paver	13.8	18.3	24.5	32.0	37.0	38.0
Foam insulation spray	0.0	0.0	0.3	0.3	1.0	
Paver brick	31.8	32.3	48.0	48.0	35.0	
House Barrier Wrap - Tyvek ®	0.0	0.0	0.0	0.0	0.0	
Fiberglass insulation in bag	0.3	0.5	0.6	0.6	3.0	5.0
Fiberglass insulation R13	0.0	0.1	0.4	0.6	1.0	
Low-E3 Window, Anderson®	37.5	39.0	39.1	39.1	43.0	43.5

Figure A9.2.2-2: Penetration Loss Measurement Results.

A.10 References

[3GPP15]   3GPP, TR 36.873 (V12.2.0), "Study on 3D channel model for LTE," July 2015.

[Ande02]   C. R. Anderson, "Design and implementation of an ultrabroadband millimetre-wavelength vector sliding correlator channel sounder and in-building measurements at 2.5 & 60 GHz," M.S. dissertation, Virginia Polytechnic Inst. State Univ., Blacksburg, VA, May 2002.

[AnRa04]   C. R. Anderson, T. S. Rappaport, "In-Building Wideband Partition Loss Measurements at 2.5 and 60 GHz," IEEE Transactions on Wireless Communications, vol. 3, no. 3, May 2004, pp. 922-928.

[ARBV+02]   C. R. Anderson, T. S. Rappaport, K. Bae, A. Verstak, N. Ramakrishnan, W. H. Tranter, C. A. Shaffer and L. T. Watson, "In-building wideband multipath characteristics at 2.5 and 60 GHz," in Proc. IEEE 56th Vehicular Technology Conference, 2002 (VTC 2002-Fall), 2002, pp. 97-101.

[AWEC]   AWE Communications, www.awe-communication.com.

[BeBL92]   J. Berg, R. Bownds and F. Lotse, "Path loss and fading models for microcells at 900 MHz", IEEE Veh. Technol. Conf. (VTC), May 1992.

[CCSB+06]   N. Czink, P. Cera, J. Salo, E. Bonek, J. P. Nuutinen and J. Ylitalo, "A framework for automatic clustering of parametric MIMO channel data including path powers," in Proc. IEEE VTC-Fall 2006, September 2006.

[Czin07]   N. Czink, "The random-cluster model a stochastic MIMO channel model for broadband wireless communication systems of the 3rd generation and beyond," In Institut fur Nachrichtentechnik und Hochfrequenztechnik, Vienna, Technische Universitat Wien, December 2007, available at: http://publik.tuwien.ac.at/files/PubDat_112121.pdf

[DEFV+07]   V. Degli-Esposti, F. Fuschini, E. M. Vitucci, G. Falciasecca "Measurement and modelling of scattering from buildings," IEEE Trans. Ant. Prop., vol. 55 no. 1, pp. 143-153, Jan. 2007.

[DSMC+14]   S. Deng. C. J. Slezak, G. R. MacCartney, Jr., and T. S. Rappaport, "Small wavelengths – big potential: Millimetre wave propagation measurements for 5G," Microwave Journal, vol. 57, no. 11, pp. 4-12, Nov. 2014.

[DeSR15]   S. Deng, M. K. Samimi, and T. S. Rappaport, ''28 GHz and 73 GHz Millimetre-wave indoor propagation measurements and path loss models,'' in Proceedings of the IEEE International Conference on Communications Workshop (ICCW), June 2015, pp. 1244–1250.

[DuXR97]   G. D. Durgin, H. Xu, and T. S. Rappaport, "Path loss and penetration loss measurements in and around homes and trees at 5.85 GHz," Tech. Rep. MPRG TR-97-10, Virginia Tech, June 1997.

[DuRX02]   G. Durgin, T. S. Rappaport, H. Xu, "Measurements and models for radio path loss and penetration loss in and around homes and trees at 5.85 GHz," IEEE Transactions on Communications, vol. 46, no. 11, Aug. 2002, pp. 1484-1496.
[FMKW06] "Capability of 3-D Ray Tracing for Defining Parameter Sets for the Specification of Future Mobile Communications Systems", Thomas Fügen, Jürgen Maurer, Thorsten Kayser, Werner Wiesbeck, IEEE TRANSACTIONS ON ANTENNAS AND PROPAGATION, VOL. 54, NO. 11, NOVEMBER 2006

[FTHD+99] B. H. Fleury, M. Tschudin, R. Heddergott, D. Dahlhaus, and K. L. Pedersen, "Channel parameter estimation in mobile radio environments using the SAGE algorithm," IEEE Journal on Selected Areas in Communications, vol. 17, no. 3, pp. 434-450, Mar. 1999.

[HNJP16]   K. Haneda, S. L. H. Nguyen, J. Järveläinen and J. Putkonen, "Estimating omni-directional pathloss from directional channel sounding," in Proc. European Conf. Ant. Prop. (EuCAP2016), Davos, Switzerland, Mar. 2016.

[JaHa14]   J. Järveläinen and K. Haneda, "Sixty gigahertz indoor radio wave propagation prediction method based on full scattering model," Radio Science vol. 49, no. 4, pp. 293-305, Apr. 2014.

[JNHN+16] J. Järveläinen, S. L. H. Nguyen, K. Haneda, R. Naderpour and U. T. Virk, "Evaluation of Millimeter-wave Line-of-Sight Probability With Point Cloud Data," Wireless Commun. Lett., 2016.

[KITO+15] K. Kitao, T. Imai, N. Tran, N. Omaki, Y. Okumura, M. Inomata, M. Sasaki and W. Yamada, "Path loss prediction model for 800 MHz to 37 GHz in NLOS microcell environment," in Proc. Personal Indoor Mobile Radio Communications (PIMRC2015), Hong Kong, China, Sep. 2015.

[KJKH15]   A. Karttunen, J. Järveläinen, A. Khatun and K. Haneda, "Radio propagation measurements and WINNER II parametrization for a shopping mall at 61-65 GHz," in Proc. 81st Veh. Tech. Conf. (VTC2015-Spring), Glasgow, Scotland, May 2015.

[KiPP01]   D.-J. Kim, Y.-W. Park and D.-J. Park, "A novel validity index for determination of the optimal number of clusters," IEICE Transactions on Information & Systems, vol. 38, no. 2, pp. 281-285, Feb. 2001.

[KwKC15]   H.-K. Kwon, M.-D. Kim and Y.-J. Chong, "Implementation and performance evaluation of mmWave channel sounding system," in Proc. IEEE APS/URSI, 2015.

[Kyos07]   Kyosti, et al., "WINNER II Channel Models," D1.1.2 V1.1, IST-4-027756 WINNER II Deliverable, Sep. 2007. [Online]. Available: http://www.ist-winner.org/WINNER2-Deliverables/D1.1.2v1.1.pdf

[LHOB14]   C. Larsson, F. Harrysson, B.-E. Olsson and J.-E. Berg, "An outdoor-to-indoor propagation scenario at 28 GHz," in Proc. 8th European Conf. Ant. Prop. (EuCAP2016), Haag, Netherlands, Apr. 2014.

[MCDR16]   G. R. MacCartney, Jr., S. Deng, and T. S. Rappaport, ''Indoor Office Plan Environment and Layout-Based MmWave Path Loss Models for 28 GHz and 73 GHz,'' in Proc. 2016 IEEE 83rd Vehicular Technology Conference Spring (VTC 2016-Spring) 2016, May 2016.

[MCRS15]   G. R. MacCartney, Jr., T. S. Rappaport, and M. K. Samimi, "Exploiting directionality for millimeter-wave wireless system improvement," in Proc. 2015 IEEE International Conference on Communications (ICC), June 2015, pp. 2416-2422.

[MCRS+15] G. R. MacCartney, Jr., T. S. Rappaport, S. Sun, and S. Deng, "Indoor office wideband millimeter-wave propagation measurements and channel models at 28 GHz and 73 GHz for ultra-dense 5G wireless networks (Invited)," IEEE Access, vol. 3, pp. 2388-2424, Dec. 2015.

[MCZN+13] G. MacCartney, J. Zhang, S. Nie and T. Rappaport, "Path loss models for 5g millimeter wave propagation channels in urban microcells," in Proc. 2013 IEEE Global Communications Conference (GLOBECOM), Dec. 2013, pp. 3948–3953.

[MeAB15]   J. Medbo, H. Asplund and J.-E. Berg, "60 GHz channel directional characterization using extreme size virtual antenna array," in Proc. IEEE Int. Sym. Personal, Indoor, and Mobile Radio Commun. (PIMRC), Hong Kong, China, Aug. 30 -Sept. 2, 2015.

[Nguy16]   H. C. Nguyen, et al., "An empirical study of urban macro propagation at 10, 18, and 28 GHz," in Proc. IEEE VTC-Spring, 2016, May 2016.

[NMCS+13]   S. Nie, G. R. MacCartney, Jr., S. Sun, and T. S. Rappaport, "72 GHz millimeter wave indoor measurements for wireless and backhaul communications," in Proc. 2013 IEEE 24th International Symposium on Personal Indoor and Mobile Radio Communications (PIMRC), Sept. 2013, pp. 2429-2433.

[PLLK16]   J.-J. Park, J. Liang, J. Lee and M.-D. Kim, "Channel Model Parameters based on Measurements in Urban Micro Environment at 28 and 38 GHz," submitted to IEEE PIMRC'16, 2016.

[R1-161688] Ericsson, "Measurements of path and penetration losses at multiple carrier frequencies," Tech. Rep. 3GPP TSG RAN WG1 #AH Channel Model, R1-161688, Ljubljana, Slovenia, Mar. 2016.

[RBDM+12]   T. S. Rappaport, E. Ben-Dor, J. N. Murdock, and Y. Qiao, "38 GHz and 60 GHz Angle-dependent Propagation for Cellular & Peer-to-Peer Wireless Communications," in Proceedings the IEEE ICC 2012 – Wireless Communications Symposium, June 2012, pp. 4568-4573.

[RGBD+13]   T. S. Rappaport, F. Gutierrez, E. Ben-Dor, J. Murdock, Y. Qiao, and J. Tamir, "Broadband millimeter-wave propagation measurements and models using adaptive-beam antennas for outdoor urban cellular communications," IEEE Trans. Antennas Propag., vol. 61, no. 4, pp. 1850–1859, Apr. 2013.

[RMCS+15]   T. S. Rappaport, G. R. MacCartney, Jr., M. K. Samimi, and S. Sun, "Wideband millimeter-wave propagation measurements and channel models for future wireless communication system design (Invited Paper)," IEEE Transactions on Communications, vol. 63, no. 9, pp. 3029–3056, Sep. 2015.

[RQTM+12]   T. S. Rappaport, Y. Qiao, J. I. Tamir, J. N. Murdock, and E. Ben-Dor, "Cellular broadband millimeter wave propagation and angle of arrival for adaptive beam steering systems (invited paper)," in 2012 IEEE Radio and Wireless Symposium (RWS), pp. 151-154, Jan 2012.

[RSMZ+13]   T. S. Rappaport, S. Sun, R. Mayzus, H. Zhao, Y. Azar, K. Wang, G. N. Wong, J. K. Schulz, M. K. Samimi, and F. Gutierrez, "Millimeter wave mobile communications for 5G cellular: It will work!" IEEE Access, vol. 1, pp. 335-349, May 2013.

[SaRM15]   M. Samimi, T. Rappaport and G. MacCartney, "Probabilistic Omnidirectional Path Loss Models for Millimeter-Wave Outdoor Communications," Wireless Commun. Lett., vol. 4, no. 4, Aug 2015.

[STRN+15]   S. Sun, T. A. Thomas, T. S. Rappaport, H. Nguyen, I. Z. Kovacs and I. Rodriguez, "Path loss, shadow fading, and line-of-sight probability models for 5G urban macro-cellular scenarios," in 2015 IEEE Global Communications Conference Workshop (Globecom Workshop), Dec. 2015.

[SRRT+16]   S. Sun, T. S. Rappaport, S. Rangan, T. A. Thomas, A. Ghosh, I. Z. Kovacs, I. Rodriguez, O. Koymen, A. Partyka and J. Jarvelainen, "Propagation path loss models for 5G urban micro- and macro-cellular scenarios," IEEE VTC2016-Spring, 2016.

[Sun16]   S. Sun, et al., "Investigation of Prediction Accuracy and Parameter Stability of Large-Scale Propagation Path Loss Models for 5G Wireless Communications," submitted to IEEE Transactions on Vehicular Technology, Feb. 2016.

[Sun16-2]   S. Sun, et al., "Path loss models for 5G urban micro- and macro-cellular scenarios," 2016 IEEE 83rd Vehicular Technology Conference Spring (VTC 2016-Spring) 2016, May 2016.

[ViWH15]   U.-T. Virk, J.-F. Wagen and K. Haneda, "Simulating specular reflections for point cloud geometrical database of the environment," 2015 Loughborough Antennas and Propagation Conference, Loughborough, UK, Nov. 2015.

[VMDE+12]   E. M. Vitucci, F. Mani, V. Degli-Esposti and C. Oestges "Polarimetric properties of diffuse scattering from building walls: Experimental parameterization of a ray-tracing model", IEEE Trans. Ant. Prop., vol. 60, no. 6, June 2012.

[WZWG+15]   X. Wu, Y. Zhang, C.-X. Wang, G. Goussetis, el Hadi M. Aggoune, and M. M. Alwakeel, "28 GHz indoor channel measurements and modelling in laboratory environment using directional antennas," in Proceedings of European Conference on Antenna and Propagation (EuCAP), Lisbon, Portugal, Apr. 2015, pp. 1–5.

[XRBS99]   H. Xu, T. S. Rappaport, R. J. Boye, J. H. Schaffner, "38 GHz wideband point-to-multipoint radio wave propagation study for a campus environment," in Proceedings of the 1999 IEEE 49th Vehicular Technology Conference, Jul, 1999, vol. 2, pp. 1575-1579.

[XRBS00]   H. Xu, T. S. Rappaport, R. J. Boye, J. H. Schaffner, "Measurements and models for 38-GHz

point-to-multipoint radiowave propagation," IEEE Journal on Selected Areas in Communications, vol. 18, no. 3, Mar. 2000, pp. 310-321.

[XuKR02] H. Xu, V. Kukshya, and T. Rappaport, "Spatial and temporal characteristics of 60-GHz indoor channels," IEEE Journal on Selected Areas in Communications, vol. 20, no. 3, pp. 620–630, Apr 2002.

A.11 List of acronyms

ABG…………………………alpha beta gamma (path loss model)

ASA………………………..angle spread of arrival in azimuth (at the UE)

ASD………………………..angle spread of departure in azimuth (from the AP)

AP…………………………access point

BW…………………………bandwidth

CI…………………………..close in (reference-distance path loss model)

DS…………………………delay spread

ESA………………………..elevation angle spread of arrival (at the UE)

ESD………………………..elevation angle spread of departure (from the AP)

GHz………………………..Giga (billion) Hertz

InH…………………………indoor hotspot

LOS………………………..line of sight

MIMO……………………..multiple input/multiple output

NLOS……………………..non line of sight

O2I…………………………outdoor to indoor

O2O………………………..outdoor to outdoor

PL…………………………path loss

PLE………………………..path loss exponent

Rx…………………………receiver

SCM………………………..spatial channel model

SF…………………………shadow fading

Tx…………………………..transmitter

UE…………………………user equipment

UMa………………………..urban macro

UMi………………………..urban micro